University of South-Eastern Norway

www.usn.no

FMH606 Master's Thesis 2024

Energy and Environmental Technology (EET)

Monitoring a New Benchmark Solvent for CO_2 Capture: Pushing Technical Boundaries

Alamgir Alam

Faculty of Technology, Natural sciences and Maritime Sciences

Campus Porsgrunn

University of South-Eastern Norway

www.usn.no

Course: FMH606 Master's Thesis, 2024

Title: Monitoring a New Benchmark Solvent for CO2 Capture: Pushing Technical Boundaries

Number of pages: 84

Keywords: CO_2 capture, CESAR1, Multivariate data analysis, FTIR, Partial Least Squares Regression, RMSEP

Student: Alamgir Alam

Supervisor: Prof. Maths Halstensen,

Prof. Kjell-Arne Solli,

PhD fellow Peshalya Madhawi Kothalawala

External partner: Technology Centre Mongstad (TCM)

University of South-Eastern Norway

www.usn.no

Summary:

Global warming of the earth is increasing significantly due to the emission of greenhouse gases where CO_2 is the main influential gas for this adverse effect. To mitigate this problem CO_2 capture with aqueous amine solvent is a most promising technology for many years.

The study focuses on a new benchmark solvent for CO_2 capture, CESAR1, which consists of 2-amino-2-methylpropan-1-ol (AMP) and piperazine (PZ) blend. The objectives of this thesis are to prepare different CO_2 loading and unloading sample with various range of CESAR1 concentration and measured the physical properties of density, pH, conductivity of the prepared sample to predict the solvent performance. Using FTIR Spectroscopy spectral regions of interest for estimation of α-CO_2 loading, AMP, PZ, density, pH, and conductivity are identified as respectively, 1575-1213 cm^{-1}, 1095 - 877 cm^{-1}, 1213 - 1096 cm^{-1}, 1080 to 502 cm^{-1}, 1835 to 502 cm^{-1}, and 1810 to 502 cm^{-1}.

The methodology involves preparation of aqueous amine samples and estimation of density, pH, and conductivity of the amine solvents. To understand the solvent behaviour and correlation between the multivariable data partial least square regression (PLS-R) modelling has been conducted in this study.

The key finding investigates the effect of CO_2 loading in the CESAR1 blend samples. Different species concerned with CESAR1 blend (AMP+PZ) are identified through speciation of pre-processed FTIR spectra including some stretching band. Six PLS-R models are developed to predict α-CO2 loading, AMP, PZ, density, pH, and conductivity of the observed CESAR1 solvent. The model accurately predicts RMSEP values of 0.0234 mol/mol, 0.1338 mol/kg, 0.1611 mol/kg, 0.0048 g/cm^3, 0.1842, and 0.6321 mS/cm for α-CO_2 loading, AMP, PZ, density, pH, and conductivity respectively with a good fit performance.

From this study, it is quite evident that online monitoring integrated with FTIR spectroscopy analysis is an appropriate method for CO_2 capture.

Preface

I am thankful to Almighty God for gifting me with this life and continuously leading me on the road of truth and peace. This master thesis has been written during the semester of spring 2024 as a part of the master's program of "Energy and Environmental Technology" at the University of South-Eastern Norway.

This study focuses on preparation of CESAR1 blend samples with water and CO_2 by maintaining various range of concentration and to see the effects of CO_2 with amine compounds. Also, multivariate data analysis alongside FTIR spectra are measured to develop Partial Least Square Regression (PLS-R) model to predict the results for different components mainly α-CO_2 loading, AMP, PZ, density, pH, and conductivity during the CO_2 capture process.

During this thesis, I have received constant support, direction, supervision, and encouragement. I sincerely thank my supervisors, Prof. Maths Halstensen, Prof. Kjell-Arne Solli, and PhD fellow Peshalya Madhawi Kothalawala, for keeping patience with me and giving me the opportunity to learn about the CESAR1 solvent preparation and speciation using FTIR spectroscopy. It has been a great experience for me to work with you all. According to the decision on the meetings with all supervisors, the PLS-R models and spectral peak identification were done by PhD fellow Peshalya Madhawi Kothalawala which is reported on Appendix B. I sincerely appreciate her hard work and efforts on my thesis.

I also thank Prof. Klaus J Jens for his valuable guidance and direction during the first two meetings of initial stage. The work of previous academics and researchers has helped me understand the aqueous CESAR1 solvent mix for the CO_2 capture method.

Finally, I am grateful to my family and friends who have always supported me in my academic endeavours.

It is my immense wish that the findings of this study will stimulate additional research on the CESAR1 solvent mix and enhance the efficiency of the CO_2 capture process in a more environmentally friendly way.

Porsgrunn, 30th May 2024

Alamgir Alam

Contents

1 Introduction 9

1.1 Background of the Interest in CO_2 Removal 9
1.2 Scope of the Study 10
1.3 Objectives 10
1.4 Organization of the Report 10

2 Literature Review of CO_2 Capture 11

2.1 Carbon Capture Use and Storage (CCUS) 11
2.2 CO_2 Capture Technologies 11
2.2.1 Pre-Combustion Capture Process 12
2.2.2 Post-Combustion Capture Process 12
2.2.3 Oxy-fuel Carbon Capture Process 13
2.3 Overview of Post-Combustion Carbon Capture Methods 14
2.4 Different Solvents and Blends 15
2.4.1 Classification of Solvents 15
2.4.2 Characteristics of a Good Solvent 16
2.5 CESAR1: Characteristics and their Chemical Structure 17
2.6 CO_2 Capture using Amines and their Equilibrium Reactions 18
2.7 Important Parameters 19
2.8 Comparative Study on CESAR1 and Traditional Solvent 20

3 Theory 23

3.1 Physical Properties 23
3.1.1 Density 23
3.1.2 pH 23
3.1.3 Conductivity 24
3.2 Importance of Spectroscopy 25
3.2.1 Electromagnetic Spectrum 26
3.2.2 Fourier Transform Infrared Spectroscopy (FTIR) 26
3.2.3 ATR-Cell 27
3.2.4 Interpretation of Spectra 27
3.3 Multivariate Data Analysis 28
3.3.1 Data Pre-processing 28
3.3.2 Principal Component Analysis 29
3.3.3 Partial Least Squares 30
3.3.4 Average Prediction Errors in the Model 31
3.3.5 Partial Least Square-Regression 32

4 Materials and Methodology 33

4.1 Chemicals 33
4.2 Health, Safety and Environmental Assessment 33
4.3 Ternary Plot Design of Unloaded and Loaded Samples 34
4.4 Sample Preparation 35
4.4.1 Unloaded CO_2 Samples 35
4.4.2 CO_2 Loaded Samples 36
4.5 Instruments and Procedures 38
4.5.1 Density Measurement 38
4.5.2 pH Measurement 39
4.5.3 Conductivity Measurement 39
4.5.4 Spectrum One FTIR Spectrometer Measurement 40

5 Results 41

5.1 Precipitation Behavior of Unloaded and Loaded Solution 41
5.2 Assessment of Density Measurements 44
5.3 Analysis of pH Measurement 45
5.4 Conductivity Measurement Analysis 47
5.5 Summary of PLS-R Model for FTIR Spectra and Measured Physical Properties 49
5.5.1 Raw and Pre-processed FTIR Spectra for α - CO_2 Loading, AMP, and PZ Model 49
5.5.2 Predicted PLS-R Model with Speciation for 'α – CO_2 Loading' 49
5.5.3 Predicted PLS-R Model for 'AMP Concentration with Specition 50
5.5.4 Predicted PLS-R Model for 'PZ Concentration' with Speciation 51
5.5.5 Raw and Pre-processed FTIR Spectra used in Density, pH, and Conductivity Model 51
5.5.6 Predicted PLS-R Model for Density Measurement 51
5.5.7 Predicted PLS-R Model for pH Measurement 52
5.5.8 PLS-R Model for Conductivity Measurement 52
5.5.9 Identified Outliers for AMP and PZ Model 52

6 Discussion 53

7 Conclusion 56

8 References 57

9 Appendices 61

Appendix A – Signed final project topic description. 62
Appendix B – Prepared PLS-R model for measured FTIR spectra and physical properties (Density, pH, and Conductivity). 64
1. Raw and Pre-processed FTIR Spectra used in CO_2 Loading, AMP, and PZ Model 64
2. PLS-R Models, Identified and Corresponding Literature IR Bands, Variable Ranges of the Models 64
3. Predicted PLS-R Model with speciation for 'α – CO_2 Loading' 65
4. Predicted PLS-R Mode with speciation for 'AMP Concentration 67
5. Predicted PLS-R Model for 'PZ Concentration' 70
6. Raw and Pre-processed FTIR Spectra used in Density, pH, and Conductivity Model 72
7. Predicted vs. Measured PLS-R Model for 'Density' with T^2 vs. Q-Residual plot (1080-502 cm^{-1}, Cal/Val, 3-LV) 72
8. Predicted vs. Measured PLS-R Model for 'pH' with RMSEP plot, (1835-502 cm^{-1}, Cal/Val, 3-LV) 74
9. Predicted vs. Measured PLS-R Model for 'Conductivity' with RMSEP plot, (1810-502 cm^{-1}, Cal/Val, 4-LV) 77
10. Identified Outliers for AMP and PZ Model 79
Appendix C – Observation of precipitated samples. 81
Appendix D – Excel sheet record for the preparation of samples and estimated data of density, pH, and conductivity. 82

Nomenclature

CO_2	Carbon dioxide
NOAA	National oceanic and atmospheric administration
MEA	Monoethanolamine
AMP	2-amino-2-methyl-1-propanol
PZ	Piperazine
PLS-R	Partial least square regression
FTIR	Fourier transform infrared spectroscopy
WGS	Water gas shift
IR	Infrared radiation
PCA	Principal component analysis
RMSEC	Root mean square of calibration
PLS	Partial least squares
RMSEP	Root mean square error of prediction
CCUS	Carbon capture utilization and storage
HSE	Health, safety, and the environment
ASU	Air separation unit
LV	Latent variable
RMSECV	Root mean square error of cross validation
NMR	Nuclear magnetic resonance
TCM	Technology center Mongstad
wt%	Weight perctentage
mol	Mole
IPCC	Intergovernmental panel on climate change
PCC	Post-combustion carbon capture
ATR	Attenuated Total Reflectance
OPD	Optical path difference
CCS	Carbon capture and storage

MWe	Megawatt electrical
LHV	Lower heating value
GJ/ton CO_2	Giga joules energy required per ton of CO_2
MJ/ton CO_2	Mega joules energy required per ton of CO_2
CO_2SEPPL	CO_2 Separation plant
α	Loading capacity
AC	Absorption capacity
CC	Cyclic capacity
CL	Capacity Loading
Q_{reg}	Regeneration energy

1 Introduction

Global warming has a tremendous impact on the environment and poses a potential threat to human health and wildlife. The climate has changed significantly due to the escalation of global warming, which is primarily caused by greenhouse gas emissions. Carbon dioxide (CO_2) is considered the main influential gas for the increasing global temperature of the earth because of its high emission content. Therefore, advanced, applicable solutions to reduce the amount of greenhouse gases that cause global warming are the major concern today for governments worldwide as well as for the pollutant industries. To enhance the sustainability of the environment, mitigation of the adverse effects of greenhouse gas emissions is mandatory now. Around the world, industries and scientists have implemented various CO_2 capture plants, which are based on solvents to absorb CO_2. Researchers are more focused on chemical solvents, like the aqueous amine method for CO_2 capture, and their properties to ensure the most effective solvent for the absorption process. The recent interest is to reduce energy consumption and costs by using alternative amine solvents instead of traditional monoethanolamine (MEA).

1.1 Background of the Interest in CO_2 Removal

The annual report from NOAA worldwide monitoring lab show that the average global atmospheric carbon dioxide reached a new record of 417.06 parts per million (ppm) in 2022 [1]. Every year, an enormous amount of CO_2 is released by human activities into the atmosphere compared to natural processes. There has been a consistent increase in annual emissions from fossil fuel ingestion. More precisely, the Global Carbon Budget 2022 [2] reports that carbon dioxide emissions have increased from around 11 billion tons annually to an estimated 36.6 billion tons. The current atmospheric carbon dioxide level is 50% higher than during the Industrial Revolution [1].

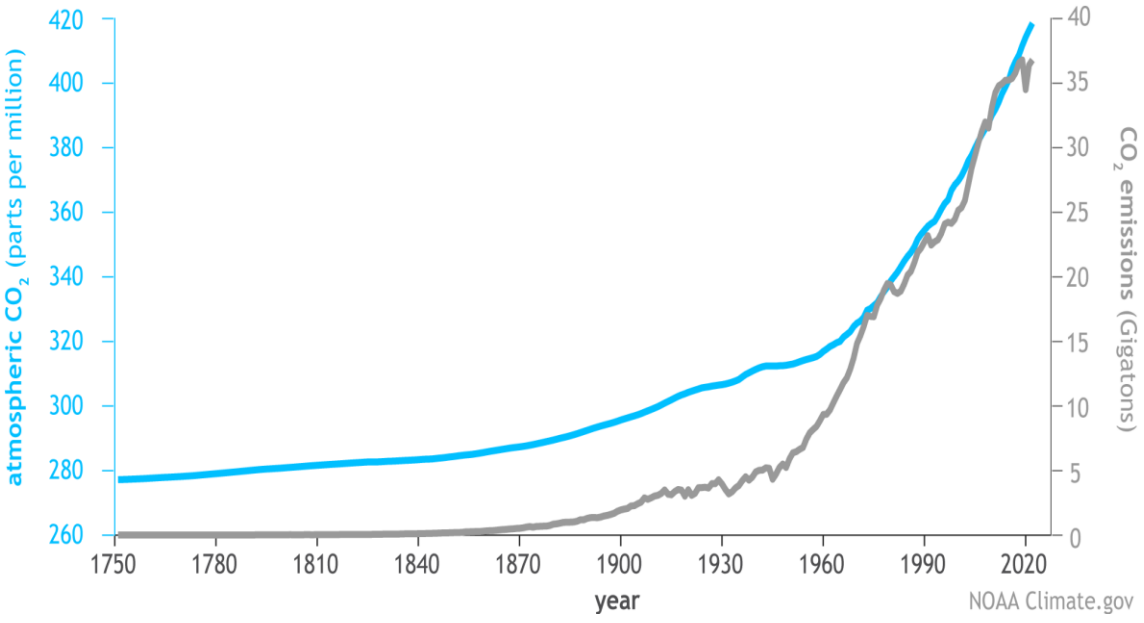

Figure 1.1: Global atmospheric carbon dioxide compared to annual emissions (1750-2020) [1].

1.2 Scope of the Study

The study focuses on a new benchmark solvent for CO_2 capture, CESAR1, which consists of aqueous 2-amino-2-methylpropan-1-ol (AMP) and piperazine (PZ) and has many benefits compared to MEA. The main advantages of using CESAR1 are low regeneration energy, slower rates of deterioration, a high capacity for CO_2 capture, and less corrosive effects. These essential characteristics make CESAR1 an excellent choice for general use in Post-Combustion Carbon Capture (PCC) systems. Firstly, various concentrations of the CO_2-loaded and unloaded samples are prepared using CESAR1 solvent for calibration and validation to see the effects of the AMP/PZ ratio with CO_2 in the capture process. Then, the physical properties like density, pH, and conductivity of the prepared blend samples are analyzed. Additionally, advanced spectroscopy methods like FTIR (Fourier Transform Infrared Spectroscopy) are used to identify the spectrum regions of interest for the speciation of the amine blend samples. Moreover, Partial Least Square Regression (PLS-R) modelling of spectra and physical properties is conducted using PLS Toolbox software in MATLAB for this study to enhance the CO_2 absorption process.

1.3 Objectives

The task background of this thesis is included Appendix A. Based on the task description the main objectives of this thesis are depicted below:

- To conduct experimental work and measure the physical properties of density, pH, and conductivity of the aqueous CO_2 loaded and unloaded solutions of CESAR1 blend to analyze the effect of various AMP/PZ ratios.
- Inline monitoring of CESAR1 solvent by identifying spectral regions of interest for the speciation by using FTIR spectroscopy.
- To conduct Partial Least Square Regression (PLS-R) modelling of FTIR spectra as well as estimated density, pH, and conductivity using PLS Toolbox software in MATLAB.

1.4 Organization of the Report

For this thesis, the organization of the report is as follows: The first chapter provides a detailed introduction with background information on CO_2 capture, the scope of the study, and the objectives. In addition, the second chapter gives a clear idea of the literature review by demonstrating carbon capture technologies with an overview of PCC systems, solvents, and characteristics of good solvent with comparative study of traditional and CESAR1 with some pilot plant studies. Next, chapter three indicates the important theory regarding FTIR spectroscopy and multivariate data analysis for the predicted PLS-R model and physical properties. Moreover, chapter four provides materials and methodology section used for sample preparation, instruments, and procedures. Then, chapter five presents the experimental outcomes with summary of the PLS-R model findings and explanation for pre-processed FTIR spectra as well as the physical properties. After that, chapter six provides the discussion of the conducted work and model with summary of findings, uncertainties, and recommendations. Chapter seven gives a brief conclusion to the conducted work. All the predicted PLS-R model are presented in appendices section.

2 Literature Review of CO_2 Capture

This chapter provides a detailed information about CO_2 capture technologies, and clear ideas about chemical solvents, CO_2 using amines with their equilibrium reaction as well as the CESAR1 characteristics and also in the end a brief idea of previous work on CESAR1 solvent with some pilot plant studies.

2.1 Carbon Capture Use and Storage (CCUS)

Carbon Capture Utilization and Storage (CCUS) is an optimal method for mitigating carbon emissions. Figure 2.1 depicts the CCUS procedure. Initially, CO_2 is collected from power plants or refineries. Subsequently, this CO_2 is conveyed by pipelines, ships, or trucks to an injection site, where it is stored in a geologically appropriate formation for a long period. In addition, the residual carbon dioxide is utilized by transforming it into valuable chemicals and fuels, among other applications, and is also used to improve oil extraction at the reservoir location. CO_2 capture is a well-established and liquid separation process used by industry or power plants which involves a large operating cost in the capture process. That is the main problem for industries. So, in terms of the economic point of view, it is not an interesting part to install it as it reduces the efficiency of the plant a lot.

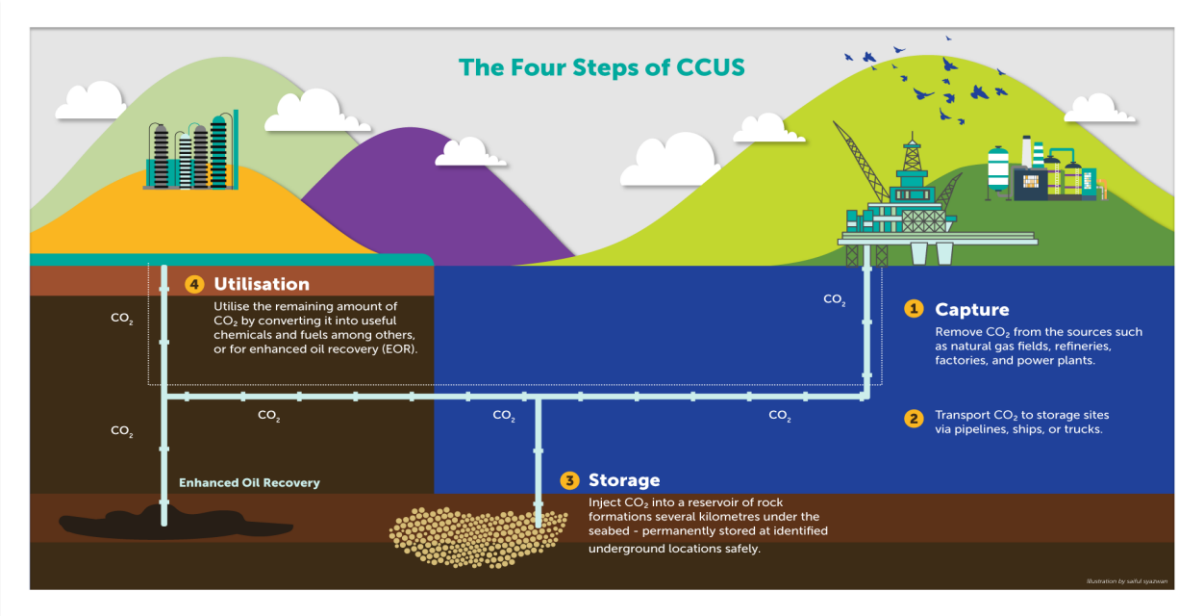

Figure 2.1: Process of CCUS [3].

2.2 CO_2 Capture Technologies

As per the IPCC, the most effective method for reducing carbon emissions is CCS [4]. Carbon dioxide (CO_2) is produced as a byproduct of combustion. Commercially available methods for capturing CO_2 tend to be costly, making up around 70-80% of the total expenses of a complete CCS system, which includes capture, transport, and storage [5]. There are three main CO_2

capture systems linked to different combustion processes, namely pre-combustion, post-combustion, and oxyfuel combustion [6]. These 3 processes are described in the below section.

2.2.1 Pre-Combustion Capture Process

In pre-combustion capture, CO_2 is removed before combustion. This can be accomplished by gasification of a fuel or by steam reforming gas, as seen in figure 2.2.

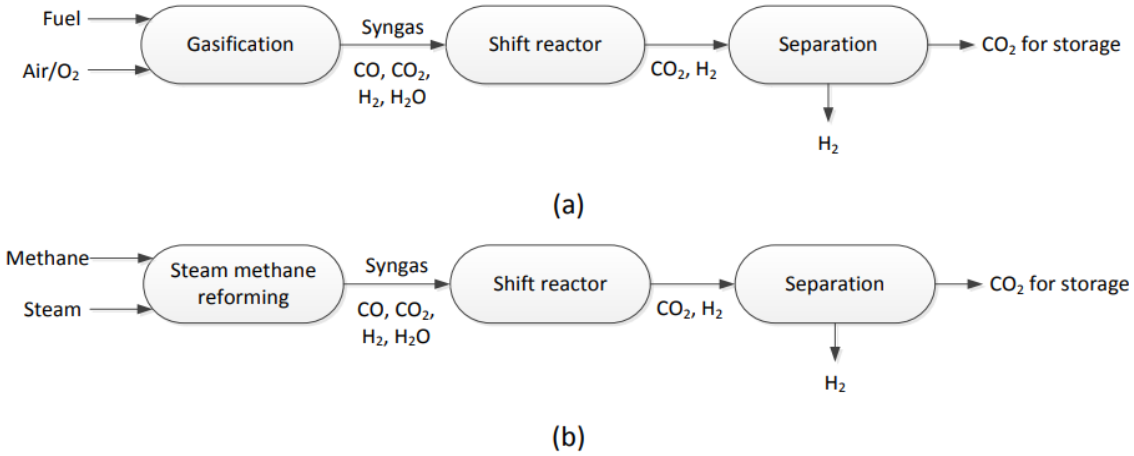

Figure 2.2: Pre-combustion process for CO_2 capture via (a) gasification and (b) steam methane reforming [7].

Equation (2.1) illustrates the coal gasification process, resulting in the formation of syngas consisting primarily of CO and H_2, with minimal presence of additional pollutants. Subsequently, the syngas will be subjected to a water-gas shift reaction in the presence of steam, resulting in the production of additional H_2, while the CO gas will be transformed into CO_2 according to equation (2.2). Most CO_2 removal comes from a syngas combination of CO_2 and H_2. The raw syngas contains CO, CO_2, H_2, CH_4, N_2, and H_2O, with trace pollutants varying by fuel source and technique [7].

$$Coal \rightarrow CO + H_2 \quad (Gasification) \tag{2.1}$$

$$CO + H_2O \rightarrow CO_2 + H_2 \quad (Water - gas\ shift) \tag{2.2}$$

$$CH_4 + H_2O \rightarrow CO + H_2O \quad (Reforming) \tag{2.3}$$

The gas mixture is cleaned to eliminate harmful contaminants and then shifted via the water-gas shift (WGS) process to produce CO_2 and H_2 [6]. Subsequently, the CO_2 and H_2 are separated by physical absorption, a process that is aided by the high pressure of the H_2/CO_2 gas mixture.

2.2.2 Post-Combustion Capture Process

Post-combustion carbon capture is the process of capturing CO_2 from flue gas after the combustion by absorbing it in a chemical solvent. This is often done by employing chemical absorption, physical adsorption, membrane separation, or a chemical loop [8]. Figure 2.3 represents the post-combustion carbon capture process with traditional MEA solvent.

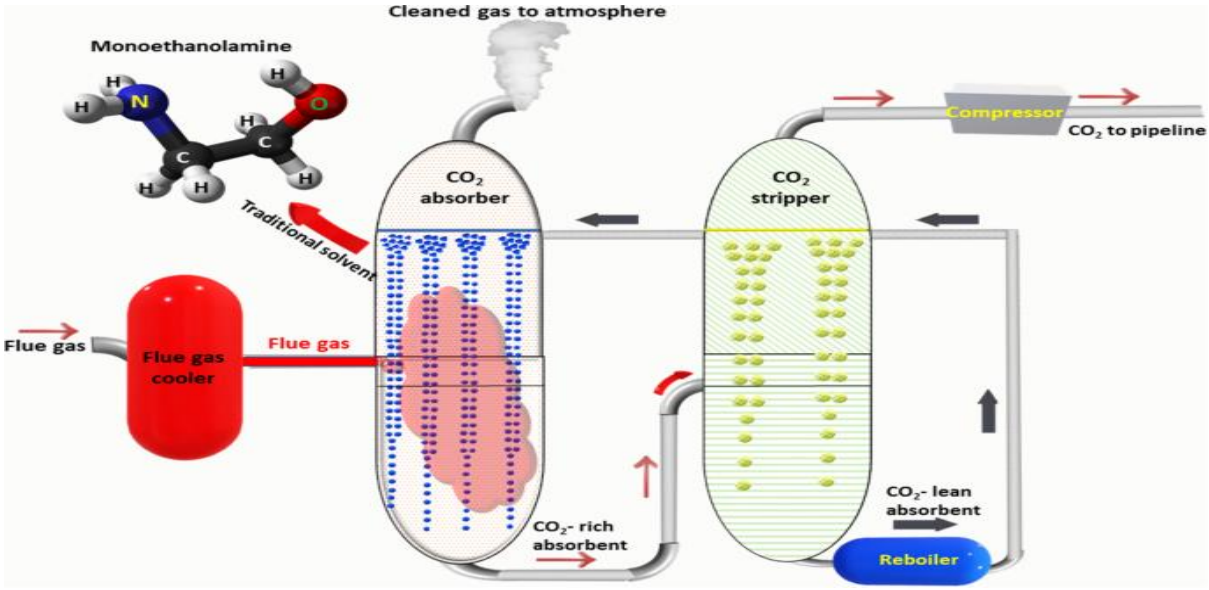

Figure 2.3: Post-combustion carbon capture process with MEA solvent [9].

The absorbent (solvent) reacts with CO_2, and CO_2 is transferred from the gas phase to the solvent, which is chemical or physical absorption. The solvent renews itself within the stripper by going through a reverse chemical reaction. Multiple investigations have verified that absorption is the most advanced post-combustion capture method. Regarding the evaluation of the post-combustion capture process, 57% of assessments utilize absorption, 14% depend on adsorption, 8% employ membranes, and 21% utilize mineralization or bio-fixation [10]. Since absorption gas separation is widely used in petrochemical industries, these findings are valuable for the implementation.

2.2.3 Oxy-fuel Carbon Capture Process

The oxy-fuel combustion process consists of three primary steps. Firstly, the air is separated to remove nitrogen before combustion. This oxygen-rich, nitrogen-free environment primarily composes the final flue gases of CO_2 and H_2O. Lastly, the CO_2 is compressed and purified. The CO_2 produced contains impurities such as SOx and NOx, which have a moisture content of 60-75%. These impurities can be eliminated using conventional methods, as illustrated in Figure 2.4. Water can be condensed to provide a CO_2-only flue gas stream from oxyfuel burning, reducing the need for gas separation depending on desired purity. Typically, a cryogenic air separation unit (ASU) is used to produce a significant amount of moderately pure (95%) oxygen by commercial technology. Large O_2 production requirements might be expensive.

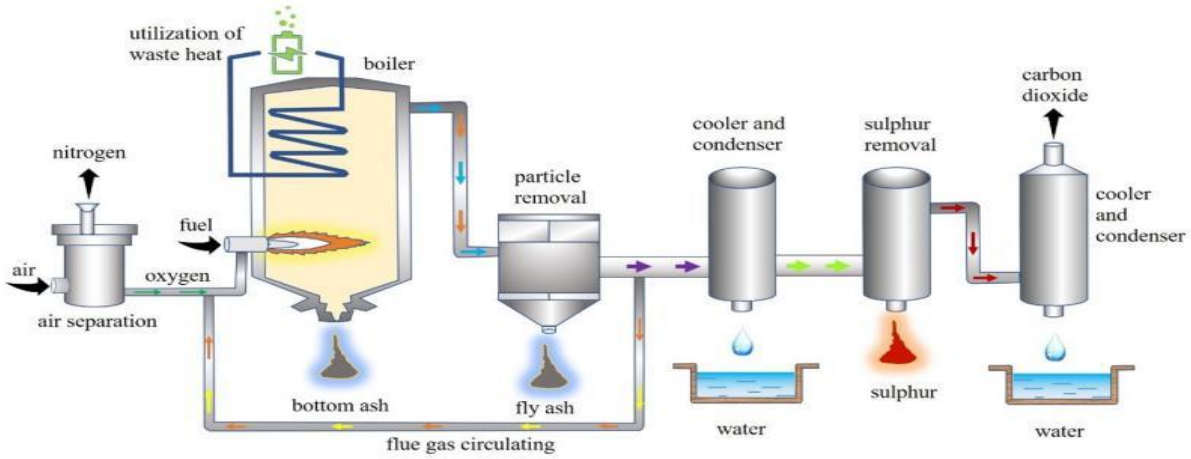

Figure 2.4: Oxy-fuel combustion carbon capture process [13].

2.3 Overview of Post-Combustion Carbon Capture Methods

Figure 2.5 summarizes the four most common post-combustion CO_2 collection methods: absorption, adsorption, membrane, and microalgae. These are more detailed in Osman et al. (2021) [9, 10] and Chao et al. (2021) [10], where absorption is the most mature technology for post-combustion carbon capture. Membrane and solid sorbents show potential as alternatives, but additional research is required to facilitate large-scale implementation. Micro-algae face a significant limitation in terms of its low capture rate.

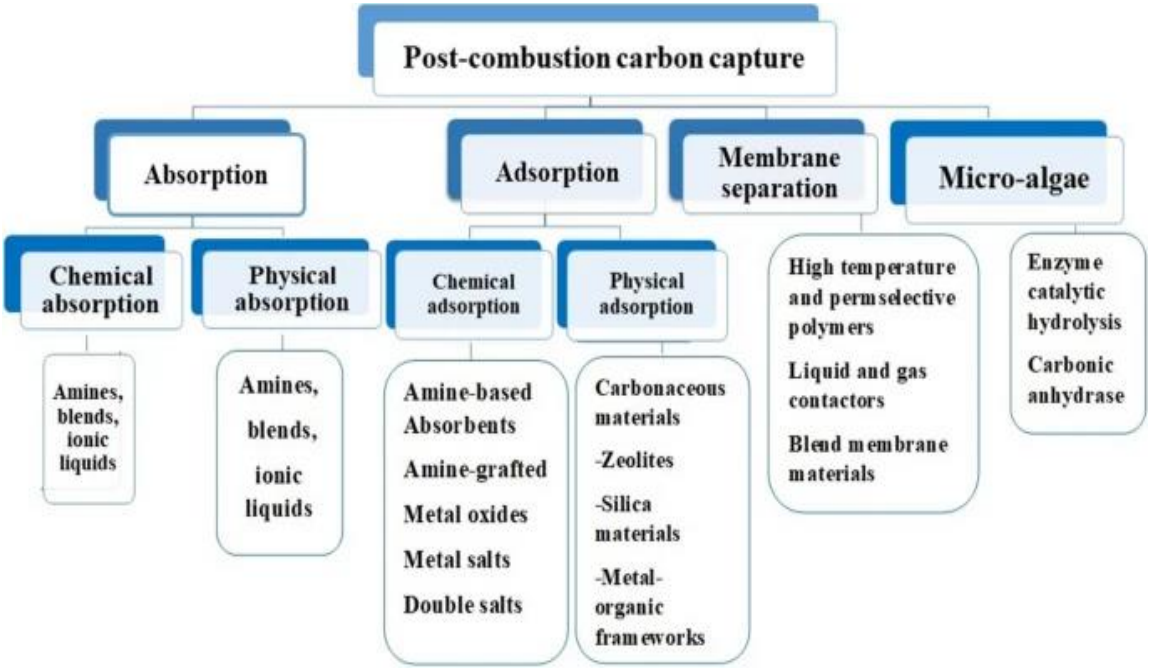

Figure 2.5: Commonly used technologies and methods in the separation post-combustion carbon capture [9].

2.4 Different Solvents and Blends

The choice of an appropriate solvent is important in the CO_2 capture process since it directly affects the efficiency and total cost by influencing aspects such as the capacity of CO_2 absorption, the size of equipment, and the energy required for solvent regeneration [12]. This section will focus on the use of various solvents or their blends for CO_2 removal with different properties.

2.4.1 Classification of Solvents

There are different types of solvents available for CO_2 absorption. Among them, chemical solvents, physical solvents, and mixture solvents are more common. A reversible reaction with a chemical solvent extracts carbon dioxide (CO_2) from the flue gas. The solvent is commonly amine-based but can also consist of salt solutions or ammonia. Chemical solvents have several key benefits. They are capable of handling low acid gas partial pressures, increasing high absorption and desorption mass transfer coefficients and capturing low acid gas levels as parts per million (ppm). A significant challenge in the absorption-desorption system is the energy needed for solvent regeneration, which can account for 20-30% of a power plants production [12].

Table 2.1 provides information on various chemical solvents and their respective properties.

Table 2.1: Physical Characteristics of chemical solvents [16].

Family	**Name**	**Chemical Formula**	**MW (g/mol)**	**Density (g/cm3)**	**Melting Point (°C)**	**Boiling Point (°C)**
Amine	MEA/Primary	C_2H_7NO	61.08	1.012	283.4	443
	DGA/Primary	$C_4H_{11}NO_2$	105.14	1.056	-12.5	221
	DEA/Secondary	$C_4H_{11}NO_2$	105.14	1.097	28	271.1
	DIPA/Secondary	$C_6H_{15}N$	133.19	0.722	-61	84
	TEA/Tertiary	$C_6H_{15}NO_3$	149.19	1.124	21.60	335.4
	MDEA/Tertiary	$C_{12}H_{17}NO_2$	119.16	1.038	-21	274.1
	AMP/Hindered	$C_4H_{11}NO$	89.140	0.934	25	165
	Morpholine/Cyclic	C_4H_9NO	87.12	0.996	-6	129
	PZ/Cyclic diamine	$C_4H_{10}N_2$	86.14	0.998	106	146
Ammonia	-	NH_3	17.031	0.769	−77.73	33.34
Salt solutions	Potassium carbonate	K_2CO_3	138.210	2.428	981	-

Salt solutions	Potassium bicarbonate	$KHCO_3$	100.120	2.170	292	-
	Sodium carbonate	Na_2CO_3	105.988	2.540	851	-
	Sodium bicarbonate	$NaHCO_3$	84.006	2.200	50	-
	Calcium hydroxide	$Ca(OH)_2$	74.093	2.211	580	-
	Potassium hydroxide	KOH	56.105	2.120	360	-

In the literature, the amine family is the most mature and widely utilized, and it is easy to mix the two solvents to mitigate their drawbacks. The use of ammonia is more complex and inefficient. Also, using salt solutions as solvents causes precipitation in the reboiler and pipelines. In this study, aqueous AMP+PZ blends with CO_2 are utilized; hence, it is essential to understand the characteristics of employing these amines.

2.4.2 Characteristics of a Good Solvent

The primary drawback of post-combustion CO_2 capture using chemical solvents is the significant energy demand for regenerating the solvent. Therefore, the key to achieving efficient energy performance in the plant lies in utilizing solvents that exhibit significant changes in CO_2 loading at different temperatures. Additionally, other limitations such as the corrosiveness of the solvent, the pace at which the solvent degrades, qualities linked to health, safety, and the environment (HSE), viscosity, and cost need to consider. Moreover, selecting an appropriate chemical solvent requires consideration of numerous other factors [13]. To facilitate regeneration, a good solvent should also have a very low absorption enthalpy. It should have a large loading capacity and react quickly with CO_2. It should also have a large loading cycle to enable the absorber to recover CO_2 at high rates.

A typical 500 MWe hard-coal power station has a power generation efficiency of 44% without the PCC process. Adding the carbon capture process can lower power generation efficiency by 9.4-10.6% [14]. The progress in capturing CO_2 since the 1980 is great. Current commercial technology indicates that the energy required has decreased by about 30% to around 2.6 GJ (or 1.2 tonnes of steam for every metric ton of CO_2 removed). Novel chemicals, when used in specifically blended solvents, could further reduce the energy demand of PCC to 2.0 GJ, equivalent to 1.0-0.8 tonnes of steam per tonne of CO_2 captured. Recent research indicates that it is possible to further decrease this energy need to around 1.1 GJ (equivalent to 0.6 tonnes of steam per tonne of CO_2) [15].

Figure 2.6 illustrates the energy needed to capture one tonne of CO_2 with the development of solvents.

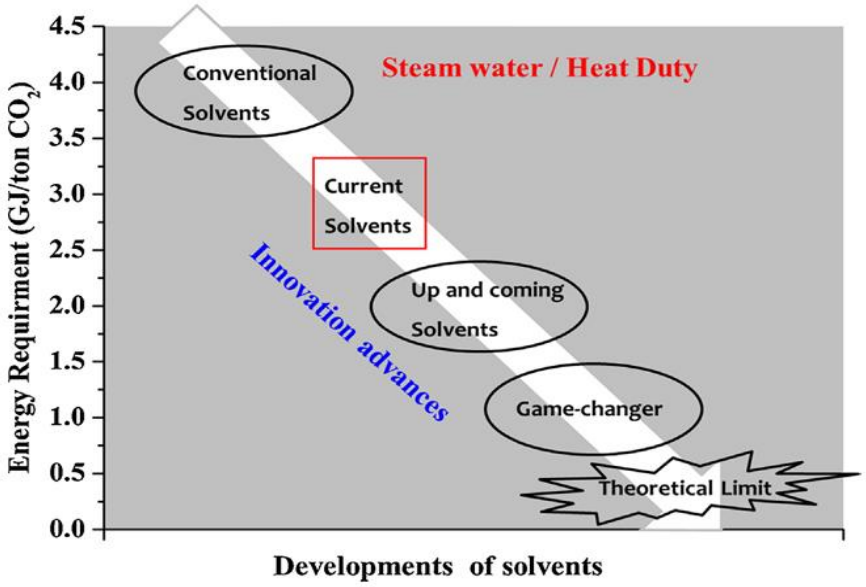

Figure 2.6: The energy requirement of post-combustion captures technologies from past, present, and future developments [15].

2.5 CESAR1: Characteristics and their Chemical Structure

Currently, CESAR 1 is known as the new standard solvent. CESAR1 is a blend of an aqueous solution of 2-amino-2-methylpropan-1-ol (AMP) and piperazine (PZ). While comparing MEA to CESAR 1, it demonstrates a notable reduction in the amount of energy required for regeneration, lower rates of deterioration, a greater capacity for capturing substances, and is less likely to cause corrosion. Figure 2.7 represents the molecular structure of AMP and PZ with water and carbon diode.

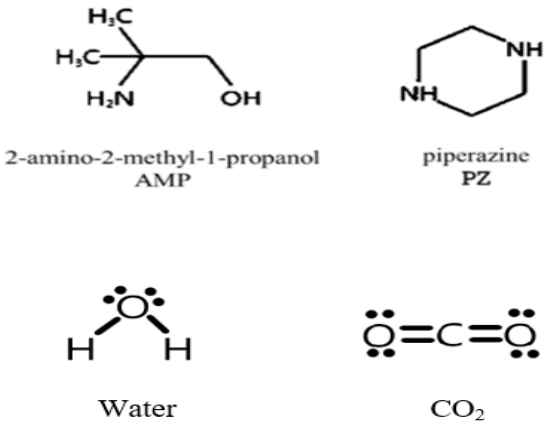

Figure 2.7: Molecular structure of CESAR 1 (AMP+PZ) with water and CO_2 [14].

AMP, a sterically hindered amine, comprises primary or secondary amines with alkyl groups connected to the amino group. This compound shares thermal characteristics with tertiary amines but reacts with CO_2 to form carbamate and bicarbonate/carbonate, lowering regeneration energy. Additionally, AMP enhances absorption by releasing free amine molecules to react with CO_2 [16]. However, the reaction kinetics of this system is slower compared to MEA.

PZ is a cyclic diamine containing two secondary amine nitrogen. Compared to MEA, it exhibits a quicker response rate, greater absorption capacity, and enhanced resistance to heat and oxidative degradation. PZ functions as an additive, sometimes referred to as an activator, which is employed to enhance the velocity of a reaction and counterbalance the sluggish reaction kinetics of AMP with CO_2 [16].

Studies have shown that AMP-PZ blends exhibit lower rates of corrosion in comparison to other amine solutions. According to reports, almost 25% of the maintenance expense is allocated specifically for corrosion management. The corrosivity order for blended amines is as follows MEA-PZ > MEA-AMP > MEA-MDEA > MDEA-PZ > AMP-PZ [17]. So, CESAR1 solvent is a good choice for CO_2 capture in terms of corrosivity.

2.6 CO_2 Capture using Amines and their Equilibrium Reactions

Figure 2.3 illustrates a general CO_2 capture process for post-combustion, where the flue gas enters from the bottom of the absorption column and a fresh or lean amine solution flow down from the top of the absorber column. Then the flue gas and amine solutions react with each other, forming a CO_2-rich solution that flows toward the mid-heat exchanger and stripper column. In the stripper column, heated steam removes CO_2 from the amine and regenerates it for reuse. High temperatures and oxygen exposure degrade amine, reducing its efficiency. About 55 °C and 1 atm are the standard temperatures and pressures in absorber columns. Maintaining the stripper column at temperatures between 100 and 120°C and pressures between 1.5 and 2 atm is crucial for generating rich solvent [18]. Continuous replenishment of fresh solvent represents a significant operational cost. The absorber column oxygen accelerates amine degradation through oxidative reactions.

The following equilibrium reactions for AMP-PZ-H_2O-CO_2 system are occurred in the CO_2 capture process [19].

1. Water Dissociation

$$2H_2O \leftrightarrow H_3O^+ + OH^- \tag{2.4}$$

2. Bicarbonate Formation

$$CO_2 + OH^- \leftrightarrow HCO_3^- \tag{2.5}$$

3. Carbonate Formation

$$HCO_3^- + H_2O \leftrightarrow CO_3^{2-} + H_3O^+ \tag{2.6}$$

4. AMP Protonation

$$AMP + H_3O^+ \leftrightarrow AMPH^+ + H_2O \tag{2.7}$$

5. AMP Carbamate Formation

$$AMP + CO_2 + H_2O \leftrightarrow AMPCOO^- + H_3O^+ \quad (2.8)$$

6. PZ Protonation

$$PZ + H_3O^+ \leftrightarrow PZH^+ + H_2O \quad (2.9)$$

7. PZ Carbamate Formation

$$PZ + CO_2 + H_2O \leftrightarrow PZCOO^- + H_3O^+ \quad (2.10)$$

8. PZ Carbamate Protonation

$$PZCOO^- + H_3O^+ \leftrightarrow PZH^+COO^- + H_2O \quad (2.11)$$

9. PZ Bi-Carbonate Formation

$$PZCOO^- + CO_2 + H_2O \leftrightarrow PZ(COO^-)_2 + H_3O^+ \quad (2.12)$$

2.7 Important Parameters

To better understanding the conducted work and literature study on the next section, some common definitions are needed to be explained.

- Loading capacity (α)

The amount of CO_2 that a particular amount of amine can absorb is known as its loading capacity. It is calculated as the ratio of the moles of CO_2 to the moles of amine.

$$\alpha = \frac{n_{co_2}}{n_{amine}} \quad (2.13)$$

Where n_{co_2} is the number of moles for CO_2 component and n_{amine} corresponds number of moles for amine [20]. This parameter is defined as rich and lean. Rich loading refers to the maximum amount of CO_2 that an amine solution can contain under equilibrium conditions. It is an indicator of the solutions CO_2 carrying capability. While lean loading represents the quantity of CO_2 remaining in an amine solution after it has undergone regeneration. This technique returns the amine solution to a condition that allows it to absorb more CO_2.

- Absorption capacity (AC)

This is the moles of CO_2 absorbed per litre of CO_2-loaded aqueous solution at equilibrium [21] conditions. It indicates the potential CO_2 carrying capacity of an amine and can be calculated by

$$AC = \alpha_{rich} * C \quad (2.14)$$

Where AC is absorption capacity, α_{rich} is the CO_2 equilibrium loading of an amine solution, and C is the molar concentration of the amine solution. Both AC and C have similar unit of [mol/L] and α_{rich} is unitless.

- Cyclic capacity (CC)

It refers to the amount of desorbed CO_2 from the amine solution, and can be calculated from the difference in CO_2 loading between the rich and lean states as

$$CC = (\alpha_{rich} - \alpha_{lean}) * C \quad (2.15)$$

In equation above, CC is cyclic capacity, α_{rich} shows CO_2 loading of the initial amine solution and α_{lean} is the CO_2 loading of amine solution after regeneration [22]. It is essential to determine the effectiveness of the CO_2 capture and regeneration cycle.

- Capacity loading (CL)

This term is defined as difference of rich and lean CO_2 loadings. So,

$$CL = (\alpha_{rich} - \alpha_{lean}) \tag{2.16}$$

Both defined parameters, absorption capacity and cyclic capacity, should be larger to reach an ideal solvent.

- Regeneration energy

The amount of energy needed to remove absorbed CO_2 from the amine solution in order to renew it is known as regeneration energy. The ratio of reboiler energy to stripper CO_2 mass rate called regeneration energy [23]. So,

$$Q_{reg} = \frac{H_{reboiler} - H_{loss}}{\dot{m}_{co_2}} \tag{2.17}$$

Where Q_{reg} is the regeneration energy, $H_{reboiler}$ is the heat duty of the reboiler, H_{loss} is the loss of energy from reboiler and $\dot{m}_{co_2}$ is mass flow rate of absorbed Carbon Dioxide which comes out from stripper. Commonly, H_{loss} is low comparing with heat of reboiler, so it can be neglected.

2.8 Comparative Study on CESAR1 and Traditional Solvent

Chemical absorption utilizing 30 wt% MEA was the benchmark technology for CO_2 capture applications for several years. This amine is suitable for removing low quantities of CO_2 from flue gasses. It has a high soluble capacity and reactivity with CO_2. However, it has some drawbacks, including strong corrosiveness, poor thermal stability, limited CO_2 absorption capacity, high reaction heat, and high energy consumption for regeneration. Furthermore, this kind of amine is not appropriate for high-pressure gas streams [12,14]. In comparison, CESAR1 (AMP and PZ blend) exhibit superior oxidative and thermal stability compared to MEA, which is a crucial factor in PCC applications.
The key findings and conclusions from several important research along with some pilot plant studies that directly examined the performances of MEA and AMP+PZ from various angles, are briefly summarized here:

- Bruder et al. (2011) [24], did an experiment and showed the results of a simplified model for the absorption of CO_2 into aqueous solutions of AMP and PZ. When comparing the maximum loading found in tests for AMP/PZ (3+1.5 M) and 30 wt% MEA systems, it is observed that the AMP/PZ system has a CO_2 partial pressure twice that of MEA, which is quite high at 120°C. Additionally, the AMP/PZ system has a specific cyclic capacity that is 128% higher when the operation temperature is between 40 and 80°C. The study investigated the relationship between the AMP/PZ ratio and the overall amine concentration. It is found that the highest AMP/PZ ratio, with a 40 wt% amine solution, prevents the production of solid precipitates during CO_2 absorption at 40°C.

- Another important comparison study was conducted by Sanchez Fernandez et al. (2014) [25]. This study analyses the efficiency and effectiveness of advanced supercritical pulverized coal (ASC) and natural gas combined cycle (NGCC) power plants equipped with two post-combustion CO_2 collection units. The capture units utilize chemical absorption using an enhanced amine solvent called CESAR1 as well as the traditional solvent monoethanolamine (MEA). The net electric efficiency for the power plants without capture is 45.25% and 58.3% for the ASC pulverized coal and NGCC, respectively. The MEA capture unit in the ASC power plant reduces efficiency by 11.7%, whereas the CESAR1 capture unit reduces efficiency by 9.4%. The NGCC power plant achieves reductions of 8.4% and 7.6% for the MEA and CESAR1 capture units, respectively [25].

- The results for another important study come from the process simulation model of Van Der Spek et al. (2016) [26] case study of post-combustion CO_2 capture from an Advanced Super Critical Pulverized Coal Power Plant. The results indicate that the AMP/PZ post-combustion technology surpasses the MEA technology in terms of various performance indicators. For instance, AMP/PZ reduces the Specific Reboiler Duty from 3.6 GJ/ton CO_2 for MEA to 2.9 GJ/ton CO_2. Additionally, the specific cooling water requirement has decreased from 4.1 to 3.4 GJ/ton CO_2. The use of AMP/PZ technology results in a significant increase in amine emissions to the environment, namely from 0.18 g/ton CO_2 to 15.3 g/t CO_2. The net efficiency of the coal power plant with AMP/PZ capture is 37.2%$_{LHV}$, whereas the efficiency without CCS is 46.1%$_{LHV}$. Using CCS with MEA reduces the efficiency to 36.2%$_{LHV}$.

For a significant period, MEA 30% has been the standard solvent for post-combustion CO_2 collection. Currently, AMP+PZ has emerged as the new benchmark or reference point. Although with many shortcomings, researchers have conducted several studies to identify a superior solvent to MEA. The many comparative investigations have demonstrated the need to prioritize AMP+PZ as a new standard solvent.

A. Pilot Plant Studies

There are so many pilot plant studies that have been conducted on CESAR1 solvent compared to the other conventional amine solvents. Some important studies are discussed below to understand the CESAR1 influence on CO_2 capture.

- Niderausseem

Over 18 months, Niederaussem conducted a highly intriguing pilot plant study. The study examined several crucial factors, including the energy required to regenerate the solvent, the quality of the flue gas, the rate of solvent recirculation, the plant design, its operational conditions, the emissions of vapours and aerosols, its analysis of transient behaviour, and the intricate chemistry of solvent degradation [27]. The ALIGN-CCUS project conducted the test, which lasted for 12,275 operating hours. Its objective was to expedite the transition of existing industry and power sectors towards a future characterized by sustained economic sustainability and reduced carbon emissions. Furthermore, in 2011, the post combustion capture pilot plant in Niederaussem conducted long-term testing with 30 wt% aqueous MEA for a total of 13,000 hours. This trial yielded valuable data that not only advanced solvent management but also improved models for solvent degradation in amine-based CO_2 capture.

A comparison between the 2 tests is possible. While MEA had a higher specific solvent regeneration heat demand (3,450 MJ/ton CO_2), CESAR1 had two major advantages: it was more stable against degradation, and its specific solvent regeneration heat demand was much lower (2,970 MJ/ton CO_2). During the testing period, CESAR1 only degraded linearly. However, after 220 days, the MEA-based solvent went from degrading linearly to degrading exponentially, causing rapid increases in solvent consumption. CESAR1 had to be refilled four times (after 79 (1,896 h), 280 (6,720 h), 315 (7,560 h) and 458 days (10,992 h)) during the testing period to make up for losses. MEA, on the other hand, had to be replaced after only 334 days because it was losing its effectiveness so quickly [27]. In summary, CESAR 1 does not exhibit self-accelerating degradation behaviour but rather undergoes a gradual linear degradation over time. CESAR1 is known for its lower corrosiveness compared to MEA because of its higher amine resistance to oxidation, ammonia emissions are lower than MEA.

- Dürnrohr, Austria

A comprehensive pilot plant research study was conducted in Dürnrohr, Austria, to examine the use of aqueous piperazine (PIP) activated 2-amino-2-methyl-1-propanol (AMP) (with a concentration of 28/17 wt% AMP/PIP) as a solvent in a PCC. The solvent regeneration process may achieve a specific energy consumption of 3.15 GJ/ton CO_2. This results in a 10% energy reduction when compared to using 30 wt% MEA. The solvent flow rate is 38% lower than the 30 wt% MEA flow rates, resulting in reduced pumping requirements. Compared to using 30 wt% MEA, the energy consumption increases significantly less while reducing the height of the absorber column. Using shorter absorber columns can lead to a substantial decrease in investment expenses. Unlike the MEA process, energy consumption does not change when the desorber pressure is varied [28]. Figure 2.8 shows the measurement results generated at the CO_2SEPPL pilot plant for 28/17 wt% AMP/PIP, in comparison to results from the Kaiserslautern pilot plant.

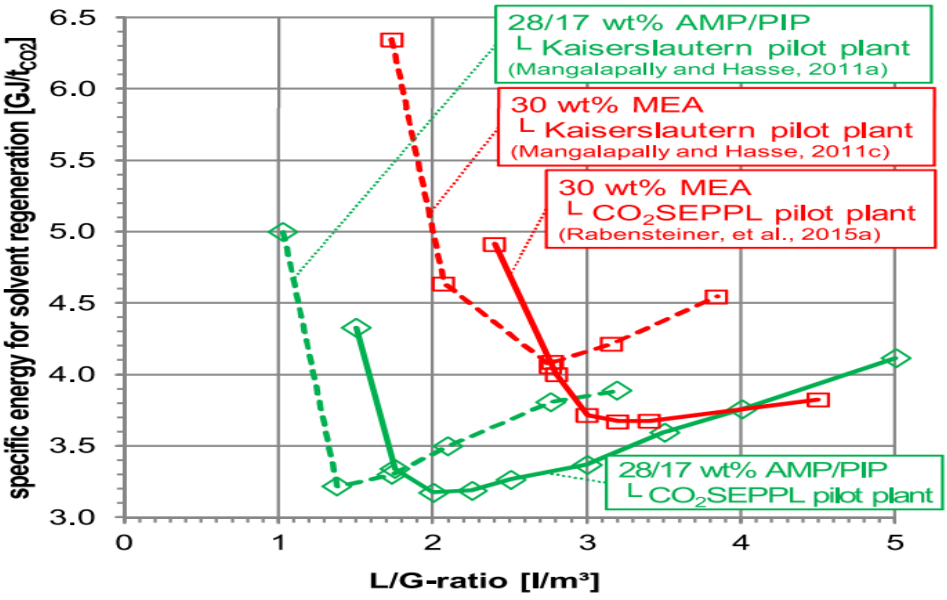

Figure 2.8: Specific energy for solvent regeneration as a function of the L/G-ratio. Experimental data for 28/17 wt% AMP/PIP ◇ and 30 wt% MEA ▭ generated at the CO_2SEPPL (solid line) and Kaiserslautern pilot plant (dashed line) [28].

3 Theory

In this chapter important theories related to this work are explained properly. For example, the importance of spectroscopy with their electromagnetic radiation, FTIR spectroscopy, multivariate data analysis consisting of PCA, data pre-processing, scores, outliers, average prediction error, partial least square regression etc. are discussed. Physical properties of pH, density and conductivity were also demonstrated properly with respect to amine solutions.

3.1 Physical Properties

The theory related to the physical properties of pH, density and conductivity of amine solutions are discussed below. To optimize the CO_2 capture process, these three parameters are important to understand the CESAR1 solvent effectiveness.

3.1.1 Density

Density is the mass per unit volume of a substance, typically expressed in g/cm³. Density can be measured using an oscillating U-tube principles based on the vibration frequency of the tube filled with the sample, which changes with the mass of the sample inside. The density of an unloaded CESAR 1 solvent depends on the concentration and composition of the AMP and PZ. As CO_2 loading increases, the formation of heavier bicarbonate and carbonate ions increases the overall mass of the solution, resulting in a higher density. A significant increase in density indicates that more CO_2 has been absorbed, as the dissolution of CO_2 causes an increase in the mass of the solution per unit volume.

$$\rho = \frac{m}{V} \tag{3.1}$$

Density is temperature-dependent, with higher temperatures generally decreasing the density of a liquid due to volume expansion while mass remains constant.

3.1.2 pH

pH is a measure of the concentration of hydrogen ions in a solution, indicating whether it is acidic or basic. It can be measured as

$$pH = -log[H^+] \tag{3.2}$$

Where [H+] is the concentration of hydrogen ions. pH can be determined with pH meters, which generally use a glass electrode that is sensitive to hydrogen ions. The amine solution absorbs CO_2, which reacts with water to generate carbonic acid (H_2CO_3), which then dissociates into bicarbonate and $HCO_3^-$and hydrogen ions H^+.

$$CO_2 + H_2O \leftrightarrow H_2CO_3 \leftrightarrow HCO_3^- + H^+ \tag{3.3}$$

The pH of the solution is lowered by the presence of these additional hydrogen ions. As a result, the degree of CO_2 absorption and conversion to bicarbonate and carbonate species is indicated by a decreased pH in a sample loaded with CO_2. For unloaded amines, pH is determined by itself. Furthermore, as amines are basic due to free amine, which can accept protons (H^+) from

water, forming ammonium ions (RNH_3^+) and hydroxide ions (OH^-). This results in a high pH [29].

On the other hand, the logarithmic constant (pK_a) reflects a compounds acid dissociation constant (K_a). It represents the strength of an acid, precisely the pH at which half of the acid is dissociated into its conjugate base, which can be referred to as follows.

$$pK_a = -logK_a \tag{3.4}$$

The pK_a value is significant for understanding how an amine substance behaves in solution at different pH levels. When the pH of the solution equals the acids pK_a, the protonated and deprotonated forms are equally concentrated. The Henderson-Hasselbalch equation governs this connection [30].

$$pH = pK_a + \log\left(\frac{[A^-]}{[HA]}\right) \tag{3.5}$$

Where $[A^-]$ is the concentration of the deprotonated form and [HA] is the concentration of the protonated form. Those amines have high pK_a value, they are stronger bases and result in a higher pH in the unloaded samples. So, to efficient and stable operation in the CO_2 capture process, monitoring of pH changes with pKa of the amine is an important property.

3.1.3 Conductivity

Conductivity here means the ability to conduct current in a medium, which depends on the presence of an ion in the solution. A conductivity meter is usually used for measuring conductivity. The device measures the current produced by applying an electrical voltage to electrodes immersed in the solution. The conductivity meter converts this measurement into a conductivity value, often stated in µS/cm or mS/cm. In terms of unloaded samples of CESAR1 solvent, AMP and PZ can ionize with water to some degree, generating $AMPH^+$, PZH^+, and OH^- that add to the solution's overall strength. Furthermore, various chemical reactions that result in the formation of HCO_3^-, H^+, $AMPH^+$, PZH^+, occur during the absorption of CO_2. This significantly increases the ionic concentration. That means increasing the conductivity of the samples as well [30].

There are so many factors that can affect conductivity. As the amount of CO_2 absorbed increases, the concentration of ionic species increases, which also enhances the conductivity. Adding to that, the ratio of AMP/PZ has a significant impact on the conductivity. Different amines have different ionic behaviour and capacities for CO_2 absorption, influencing the overall ionic strength of the solution. Also, higher concentrations of AMP and PZ result in more ions in solution upon CO_2 absorption, leading to higher conductivity. In addition, the mobility of ions increases with higher temperatures, leading to higher conductivity. Therefore, control of temperature is crucial for accurate conductivity measurements. So, to optimize the process of CO_2 capture, solvent performance, and quality control, measurement and interpretation of conductivity are essential parameters.

3.2 Importance of Spectroscopy

Spectroscopy is a technique used to extract precise quantitative data from the electromagnetic spectrum by measuring the absorption or emission of photons at various wavelengths. When electromagnetic radiation interacts with matter, it may be seen as a collection of discrete units of energy known as photons. Electromagnetic radiation exhibits both wave and particle characteristics. Certain lights pass through the substance, while others are reflected, absorbed, or dispersed.

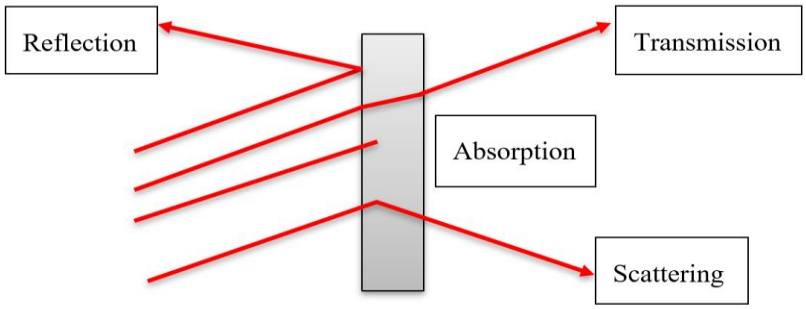

Figure 3.1: Light behaviours during interaction with material.

In spectroscopy, Beer's Law is used to relate the amount of light absorbed by a sample to the concentration of the absorbing species. The Beer's law known as (Beer-Lambert law) is a linear relationship between the absorbance and the concentration, molar absorption coefficient and optical path length of a solution [31]. This law is fundamental in various types of spectroscopies, particularly for diluted solutions. The mathematical expression of Beer's Law is:

$$A = \varepsilon \cdot c \cdot l \tag{3.6}$$

Where A is the absorbance (a unitless measure of the amount of light absorbed); ε is the molar absorption coefficient (L/mol cm); which is a measure of how strongly the substance absorbs light at a particular wavelength; c is the concentration of the solute (mol/L), l is the optical path length of the light through the solution (cm).

The law is most accurate for diluted solutions where the relationship between absorbance and concentration remains linear. The limited range of validity to linear response for high concentrations (like CO_2-loaded amine solutions), which is overcome by multivariate data analysis like PLS-R including pre-processing of absorbance spectra. At higher concentrations, several factors can cause deviations. These can be molecular interactions due to high concentrations, refractive index changes can also affect light absorption, high chemical equilibrium shifts.

3.2.1 Electromagnetic Spectrum

The range of all types of electromagnetic radiation is electromagnetic spectrum.

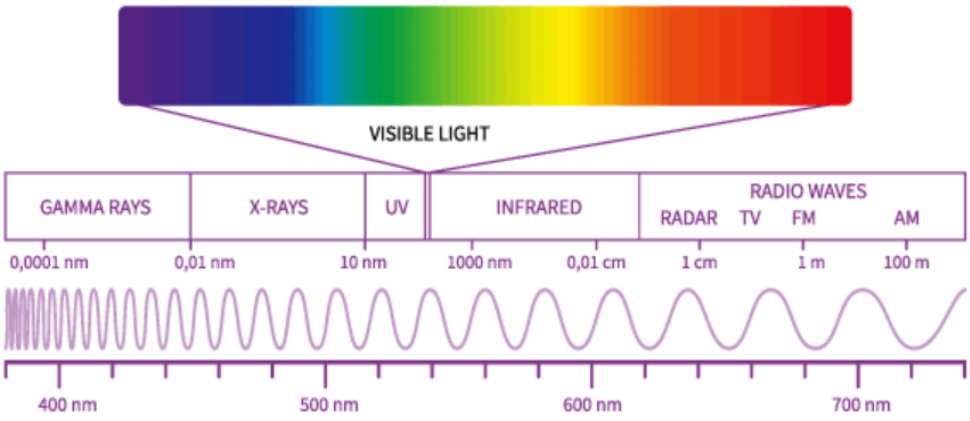

Figure 3.2: Electromagnetic spectrum [32].

As seen in Figure 3.2, the spectrum is separated into distinct areas according on wavelength and frequency. Infrared radiation comes before radio waves and after UV radiation. On the other hand, the visible light falls inside the 400 nm to about 700 nm infrared area.

3.2.2 Fourier Transform Infrared Spectroscopy (FTIR)

Fourier Transform Infrared Spectroscopy (FTIR) is a technique employed for the identification of different chemicals and molecules. The optical apparatus known as an interferometer is made up of two moving and one stationary mirrors, a beam splitter, and an infrared source [33]. The incident light from the source is split by the beam splitter, and one half is sent to each of the two mirrors. Before the beam passes through the sample and arrives at the detector, it is first reflected by the mirrors and then recombined at the beam splitter. This principle is displayed in Figure 3.3.

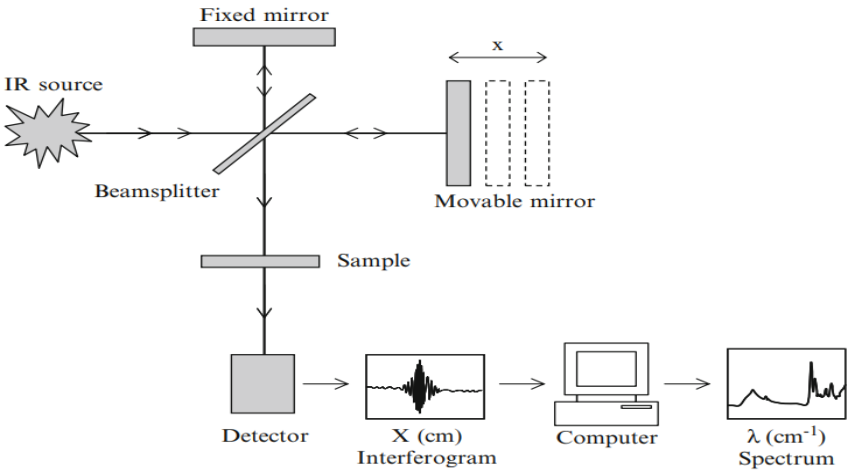

Figure 3.3: FTIR spectrometer [34].

Because one of the mirrors is moving, the distance the beam travel must be changed; this difference is referred to as the optical path difference. The interferogram displays a visualization of the intensity of the beams over the OPD. The interferogram acquired with an interferometer must be converted into a readable spectrum. The spectrum is a representation of the intensity over wavenumber or frequency, and to do this Fourier transform (FT) can be used. The Fourier Transform allows rapid acquisition at acceptable signal-to-noise ratios and resolution, but the information content of the spectra remains the same as traditional IR. The Fourier Transformation is a mathematical method that transforms the interferogram to a spectrum. The Fourier Transform component in modern FTIR instruments is crucial for enhancing the efficiency, speed, and quality of spectra acquisition [33].

3.2.3 ATR-Cell

An Attenuated Total Reflectance cell, a component of an FTIR spectrometer built for the ATR sampling technique, is an excellent choice for studying water-containing materials. It is often made of a high-refractive-index crystal (such as diamond, zinc selenide, or germanium) upon which the sample is placed. This crystal provides attenuated total reflectance of the IR beam inside the crystal. The crystal is in contact with the sample and provides internal reflections of the IR beam. From these internal reflections, evanescent waves that penetrate the sample are formed. The sample is place directly on the crystal. ATR-FTIR can be used to study the surface of a sample, and the penetration depth can be changed by adjusting the reflection angle. The amount of sample needed for this spectroscopic method is minimal, and there is no need to destroy a sample [35].

There are two common modes for FTIR measurements: standard transmission mode (using salt windows or KBr disks) and Attenuated Total Reflectance (ATR) mode. ATR-cell offers major advantages in terms of ease of use, minimal sample preparation, and suitability for surface and thin film analysis and provides good signal-to-noise ratio due to the multiple reflections within the ATR crystal. When non-destructive examination is needed or samples that are challenging to prepare for transmission measurements, it is very helpful. Standard FTIR (Transmission Mode) remains the preferred method for analysing bulk materials and gaseous samples where path length and resolution are critical [36].

3.2.4 Interpretation of Spectra

The large absorption of O-H from water in IR spectroscopy might possibly hide signals from other molecules in the aqueous solution, which is a drawback. If the samples contain water, ATR-cell for FTIR spectroscopy is a good choice. The most significant region of the IR-spectrum is from 4000-665 cm^{-1} [37]. The stretching vibrations of the most significant functional groups are in the high frequency range. Amines exhibit broad, moderate absorption in the low-frequency range, particularly in the area surrounding 950 cm^{-1}, as seen by the C-NH_2 absorption in figure 3.4. The stretching of the inorganic compounds in the aqueous amine solutions are found in the region from 2000 to 900 cm^{-1}. The peaks related to carbonate, bicarbonate, carbamate and dissolved CO_2 fall in the region of 900-1600 cm^{-1}. This region has unique absorption for every molecular specie and can be used to identify which compounds are present in the samples. O-H is one for the most important functional groups, and the stretching of O-H produces a broad band in the region 3700 to 3400 cm^{-1}. The organic carbons, in form of C-H stretching are identified in the region enclosing 2900 cm^{-1}, these are often buried by the

O-H peak, making it hard to identify them [38]. The result is typically overlapping absorption bands that are challenging to analyse analytically; however, information can be extracted by using multivariate data analysis on the variation in spectra from various compositions. Figure 3.4 shows the ATR-FTIR spectrum of a sample of aqueous MEA solution, loaded with CO_2, displaying the most important stretching vibrations.

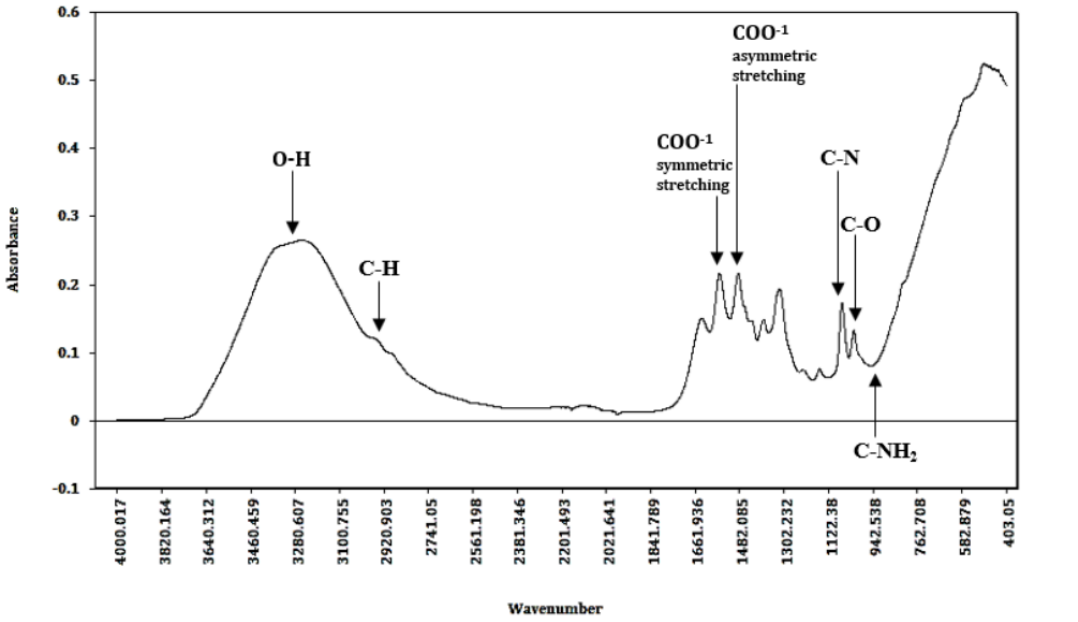

Figure 3.4: ATR-FTIR spectrum of a sample of aqueous MEA solution, fully loaded with CO_2, displaying the most important stretching vibrations based on [37, 38].

3.3 Multivariate Data Analysis

Multivariate data analysis is a type of statistical analysis that involves more than two dependent variables, resulting in a single results [39]. Multivariate data analysis is a commonly used method for examining datasets that contain many variables. Understanding the relation between variables and predicting their behaviour based on observations is important in multivariate data analysis. This method is very suitable for obtaining precise information from large datasets, such as Spectroscopy. Before interpretation, data pre-processing is required to convert the FTIR spectra into chemical information. In this project, the PLS Toolbox is used to perform Partial Least Squares Regression (PLS-R) on the measured sample data and FTIR spectra.

3.3.1 Data Pre-processing

The data obtained from the instrument, such as FTIR spectra, may contain noise and scattering, as well as common and flat offsets to each other, which may have a negative impact on extracting the required information for analysis. The baseline correction helps to subtract the common offset and causes data to overlay better. So, data pre-processing is very important to get a reliable dataset and use multivariate calibration models, the pre-processing of the data is

very important. There are many automatic baseline correction methods utilized to do the estimations and remove baseline offsets from the raw data. The baseline correction automatically identifies the position of variables against a baseline reference for each spectrum (above or below the baseline). Lastly, when the baseline references are determined, the common offsets will be removed. A proper correction of the baseline reduces the number of variables and makes the data interpretation easier. In this work, automatic Whittaker filtering and Mean Centering using the MATLAB PLS Toolbox have been used to perform baseline correction.

3.3.2 Principal Component Analysis

Principal Component Analysis is a method that uses mathematical principles and transforms correlated variables by reducing them into a smaller number of variables, or principal components. Generally, PCA is used to find the hidden information (latent variables) in the multivariate data matrix. PCA is also used to compress the large data. PCA is the first stage to analyse larger datasets, which simplifies the data by reducing multi-dimensional datasets into a new dataset of low dimensions that are orthogonal and independent. An important feature of PCA is the simultaneous interpretation of score plots and loading plots. The PCA outcome is graphs, which are easy to interpret but have a lot of information [40].

$$X = TP^T + E \tag{3.7}$$

$$X = T_1P_1^T + T_2P_2^T + \cdots + T_nP_n^T + E \tag{3.8}$$

X: indicates the multivariate data matrix (variables), P_i (i=1, 2, 3, …, n) indicates number of components containing the orthogonal loadings, E: indicates noise (residual matrix) containing the information not explained by T and P, T: is simply the score matrix, P^T: indicates the transpose of the loading matrix. The first principal component (PC1) and second principal component (PC2) are orthogonal. Also, PC1 and PC3, PC1 and PC4, … are orthogonal. Figure 3.5 presents scores as PC-coordinate.

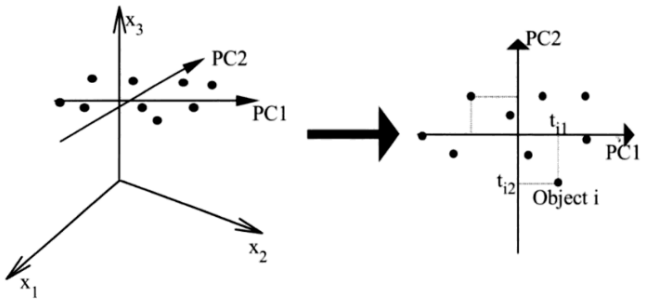

Figure 3.5: Scores as PC-coordinate [40].

A. Scores

In the score plots for LV1-LV2 and LV1-LV3, where scores correspond to samples. PCA utilizes latent variables as principal components to reduce dataset dimensionality by transforming the original variables into fewer variables that represent most of the variance. To do principal component analysis, it is required to check the all-score plots for LV1- LV2, LV1-

LV3, etc. Figure 3.6 shows example of a score plots for PLS components 1 vs. 2 representing calibration and test samples.

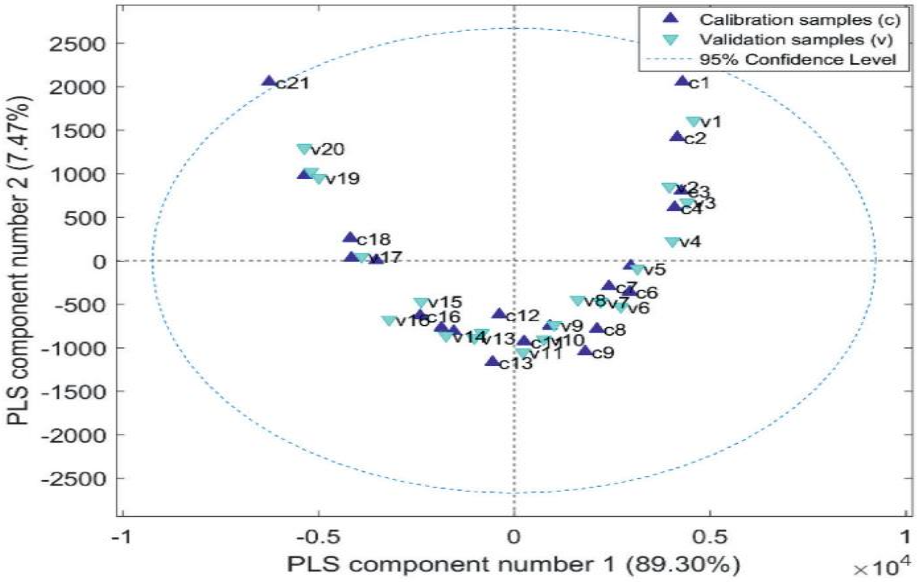

Figure 3.6: Score plot of PLS components 1 vs. 2 showing calibration and validation samples for PLS-R model of MEA [41].

B. Outliers

Outliers are samples or objects that deviate significantly from the rest for reasons that are difficult to identify. This could be an operator mistake, noise in the instrument, the wrong measurement, and so on. For any reason, the outliers have a negative effect on our models, outcomes, and extracting required information simultaneously. To mitigate this problem, the possible outliers should be identified and even corrected or removed if necessary. In PLS, the outliers can be seen in the regression model. It is essential to evaluate the impact of the identified outlier on the data. Removing a decided outlier that has a significant effect on the data might result in an inaccurate and unreliable model.

3.3.3 Partial Least Squares

Partial least squares (PLS) is a regression method which is used to find the most suitable model for prediction of Y (the parameter) from multiple X measurements or raw data. The model translates the multivariate X measurements into Y parameters[40]. Equation (3.9) describes the best model for PLS.

$$\hat{Y} = X.b + a \tag{3.9}$$

Where, $\hat{Y}$= predicted value, X= multivariate measurement, b = regression coefficient and a = constant.

3.3.4 Average Prediction Errors in the Model

The definition of the root mean square error of prediction (RMSEP) is given in equation (3.10). This is the average of squared differences between measured and predicted values. To find the accuracy of the model, root mean square error of prediction (RMSEP) should be checked. For the same measurement units, the RMSEP estimates the average prediction error in the prepared model. Figure 3.7 shows an example of predicted vs. measured plot in PLS-R model of CO_2 loading for MEA.

$$RMSEP = \sqrt{\frac{\sum_{i=1}^{n}\left(y_{predicted} - y_{reference}\right)^2}{n}} \tag{3.10}$$

Here, $y_{predicted}$ = the predicted values, $y_{reference}$ = the measured values and n = total number of samples.

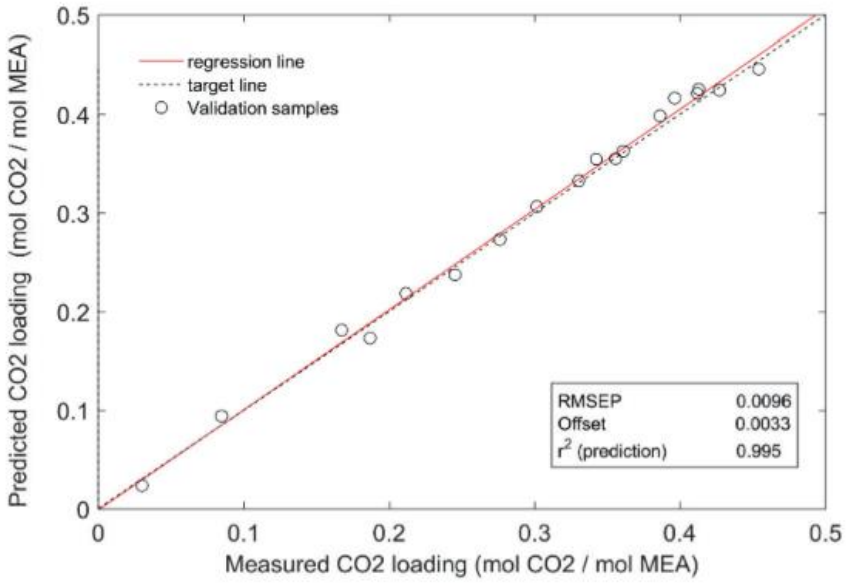

Figure 3.7: RMSEP in predicted vs. measured plot CO2 loading of MEA [41].

The definition of important statistical parameters which is used in this study in the predicted vs. measured plot are below -

LV: Latent Variables in PLS are determined to maximize the correlation with the response variable.
RMSEP: Root Mean Square Error of Prediction**.**
RMSEC: Root Mean Square Error of Calibration.
RMSECV: Root Mean Square Error of Cross Validation.
R^2 (Pred): represents the squared correlation between observed outcomes and predictions made by the PLS model on new data.

3.3.5 Partial Least Square-Regression

The Partial Least Squares Regression (PLS-R) method aims to determine the correlation between two matrices, X (predictors) and Y (responses), by identifying a group of latent variables (LVs) that exhibit the highest covariance with the response.
The basic steps and equations in PLS-R include:

$$X = \sum_{A} TP^T + E \tag{3.11}$$

$$Y = \sum_{A} UQ^T + F \tag{3.12}$$

Here, X is the matrix of predictors, and Y is the matrix of responses. T and U are scores matrices for X and Y respectively; P and Q are the loadings matrices for X and Y, and E and F are residual matrices for X and Y.
The decomposition is finalized to maximize the covariance between T and U. So, the covariance between the scores in the X part and the score in the Y part needs to be maximized.

4 Materials and Methodology

This chapter describes a detailed explanation of all the tools, chemicals, procedures, and how CO_2-loaded and unloaded solutions were prepared during the experiment and the experimental outcomes.

4.1 Chemicals

The chemical used for this work are shown in Table 4.1 with their purity, molecular formula, weight, and sources. Figure 2.7 shows the chemical structures of the chemicals used for this study.

Table 4.1: Chemical used in this work.

Chemicals	CAS No.	Sources	Purity	Molecular weight	Molecular formula
AMP	110-85-0	Sigma Aldrich	99%	89.14	$C_4H_{11}NO$
PZ	124-68-5	Sigma Aldrich	98%	86.14	$C_4H_{10}N_2$
Distilled water	-	E-building, USN	-	18.015	H_2O
Carbon dioxide (gas)	-	CO_2 lab, USN	-	44	CO_2

4.2 Health, Safety and Environmental Assessment

Health, safety and environmental information regarding chemical risk assessment and precautions in the lab for personal safety are discussed below.

- Chemical Risk Assessment

Before conducting experimental work, a comprehensive chemical risk assessment should be conducted. This process includes identifying potential hazards associated with each chemical, evaluating the risks of exposure, and implementing measures to mitigate these risks. As AMP and PZ are identified as hazardous chemicals and corrosive to skin and eyes, PZ can cause respiratory irritation, and both are harmful if inhaled too much. AMP and PZ pose moderate to high risk if proper precautions are not taken. During the loading of CO_2 in amine solutions, the pressure valve and flow rate control valve should be open in such a way that a balanced flow of CO_2 get mixed with the amines.

- Control Measures and Precautions

Before starting to work, proper training regarding chemicals handling and personal care should be taken. To prepare samples with amines fume hoods must be used to manage the vapours and dust. Proper ventilation in the lab is mandatory. For Personal protective care lab coats, gloves, safety goggles, and face shields must be used when handling chemicals. Also, standard operating procedures for handling chemicals should be available in the lab. In case of any

spillage of amines or chemicals, for small spills, appropriate absorbent materials should be used and dispose them according to local regulations. For large spills, evacuation, and ventilation of the area is needed. Usage of spill kits designed for hazardous chemicals must be used. First aid station should be covered all the required materials for immediate actions. If any symptoms persist seeking medical attention should be taken.

- Handling, Storage and Disposal

Proper tools with care must be used for handling the chemicals to avoid spill and contamination. All the prepared and used amines samples should be labelled with their date of open and preparation with contents and hazard warnings. Prepared AMP and PZ samples should be stored in a cool, dry cabinet away from strong oxidizers. For disposal, appropriate regulations chemical waste must be followed. It is not wise to pour chemicals down the drain. Also, Labelling waste containers with the contents and associated hazards is a good way to protect the environment from contamination.

4.3 Ternary Plot Design of Unloaded and Loaded Samples

The CESAR1 solvent is a mixture of 2-amino-2-methyl-1-propanol (AMP) and piperazine (PZ) dissolved in distilled water, with concentrations of approximately 3.21 mol/kg and 1.5 mol/kg, respectively. This refers to an aqueous solution containing roughly 27 wt% of AMP and 13 wt% PZ, as stated in reference [27]. The aim is to investigate the impact of varying weight percentages of loaded and unloaded CO_2 by considering various parameters, such as density, pH, conductivity, and identifying chemical species region of the samples by FTIR Spectroscopy. To achieve a diverse range of recipes for the samples, the following ranges are decided: AMP (14-40 wt%), PZ (>0-20 wt%), and H_2O (50-70 wt%) for the preparation of unloaded solution. The ranges of AMP (15 and 40 wt%) and PZ (2 and 12 wt%) for 6 mixtures design is planned to use for loaded samples. Prior to sample preparation, the wt% concentration of all samples was randomly computed using a Python code to introduce variety, rather than being determined manually. These values were then recorded in an Excel sheet for easy management and preparation.

Figure 4.1 displays the design of the ternary plot of unloaded and loaded sample weight percentage concentrations. The red square represents the actual referenced CESAR1 solvent, while the green and blue squares represent the unloaded and loaded samples with different AMP, PZ, and water concentrations, respectively. Different CESAR1 blends are planned to prepare to identify the variations of the AMP/PZ ratios with CO_2 loading and its impact on the physical properties of pH, density and conductivity. This plot is generated utilizing a website ternaryplot.com for proper visualization.

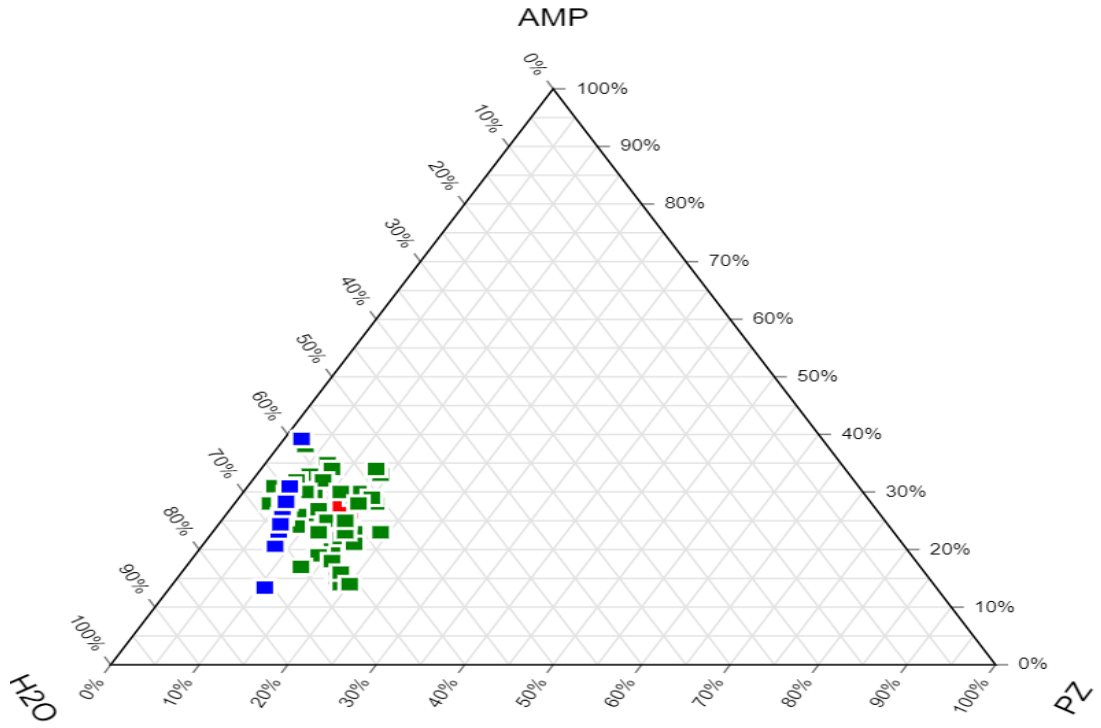

Figure 4.1: Ternary plot of loaded and unloaded samples in weight percentage (wt%) concentration.

4.4 Sample Preparation

In this section, sample preparations of loaded and unloaded CO_2 are discussed properly.

4.4.1 Unloaded CO_2 Samples

- Initially, 2 mol (172.60 g) of piperazine were mixed with 46.95 mol (845 g) of distilled water to prepare a PZ solution of approximately 2 mol/kg and mixing until dissolved. This solution was then used to prepare the sample by mixing it with AMP and distilled water.
- A total of around 3.56 mol (317.40 g) of AMP solution was used to prepare all unloaded samples. The AMP solution was always placed in the water bath to avoid precipitation and for easy handling with the PZ. The gravimetric system was utilized throughout the entirety of this thesis.
- In Appendix C the number of various concentrations of sample in grams used for a 30 mL bottle based on the weight measurement are presented. Proper labelling has been done to avoid mistakes with the recipes. It begins at AAS 1 and ends at AAS 41 for unloaded samples.

Figures 4.2 and 4.3 represent the unloaded sample preparation of CESAR1 solvent.

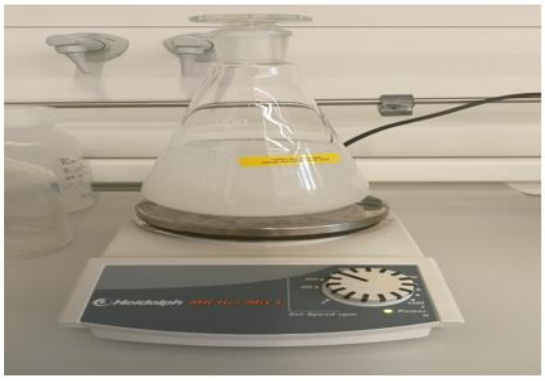

2 mol/kg PZ solution

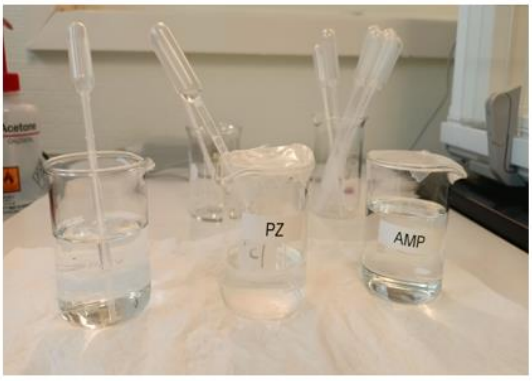

Sample making

Figure 4.2: Unloaded Sample preparation.

Figure 4.3: All 41 Unloaded prepared Sample (AMP+PZ+Water).

4.4.2 CO_2 Loaded Samples

CO_2 loaded samples were prepared from 6 mixtures design by utilizing the stock solution. It is described in the below section.

A. Stock Solution Preparation

- Approximately 2 mol/kg of PZ solution was prepared first by mixing around 0.861 mol (74.20 g) of PZ with 23.88 mol (430 g) of distilled water. Then, two stock solutions were made by following the weight ranges of AMP and PZ.
- Stock 1 was prepared using a combination of AMP (40 wt%), PZ (2 wt%), and H_2O (58 wt%). Approximately 12.65 mol of solution was made, consisting of 1.795 mol 8160.03 g) of AMP, 0.538 mol (46.40 g) of PZ from a 2 mol/kg PZ solution, and 10.313 mol (185.85 g) of distilled water.
- Stock 2 was prepared using a combination of AMP (15 wt%), PZ (12 wt%), and H_2O (73 wt%). A total of roughly 4.696 mol of solution were prepared, including 0.682 mol (60.84 g) of AMP, 3.259 mol (280.78 g) of PZ from a 2 mol/kg PZ solution, and 0.75 mol (13.60 g) of distilled water.

B. Mixtures Design

- Subsequently, six concentration design was prepared using the above two stock solution to prepare the sample recipes. The 1st, 3rd, and 5th mixtures were prepared from stock 1, using 130.07 g, 160.98 g, and 70 g, respectively. Subsequent mixtures were prepared as follows: the second, fourth, and sixth mixtures were made using 135.47 g, 130.83 g, and approximately 70 g from stock 2, respectively.
- The fifth and sixth mixtures were unloaded, while the first and third mixtures were loaded with a loading capacity of 0.4 (approximately 0.3245 mol (14.28 g) of CO_2 added for the first mixture and 0.3959 mol (17.47 g) of CO_2 for the third mixture). The 2nd and 4th mixtures, both had a loading capacity of 0.2 (about 0.2786 mol (12.26 g) of CO_2 for the 2nd mixture and around 0.2772 mol (12.20) of CO_2 for the 4th mixture).

After successful loading of CO_2, samples were prepared by mixing various combinations to see the effect of CO_2 as well as their precipitation behaviour. A total of 20 samples were prepared in 30 mL bottles using various mixes, including loading, and unloading. Figure 4.4 shows the schematic diagram of CO_2 loading apparatus using the online tool MS Visio.

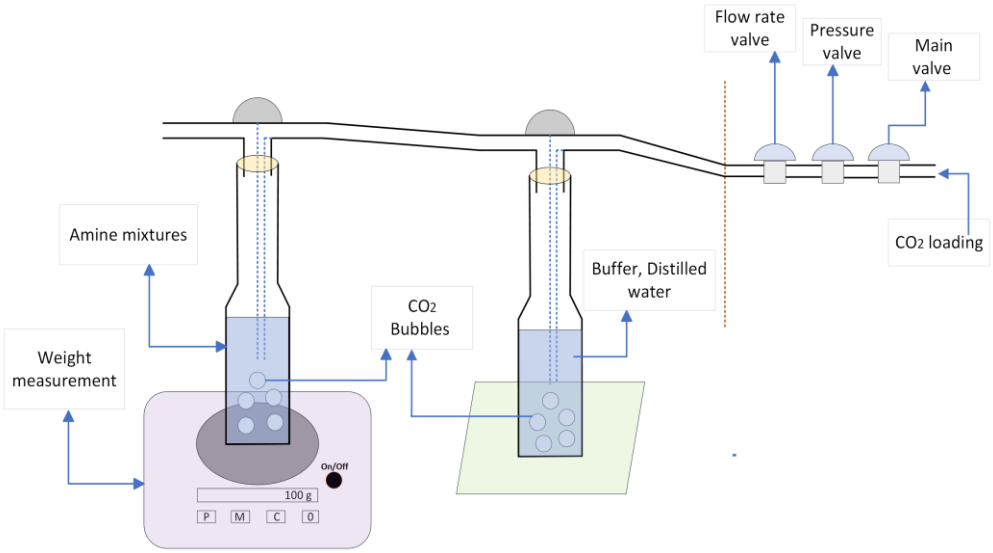

Figure 4.4: Schematic diagram of CO_2 loading apparatus.

Here, figure 4.5 represents all the prepared CO_2 loaded samples. Some samples got precipitation which will be discussed in the results section.

Figure 4.5: Prepared CO_2 loaded of 20 samples.

4.5 Instruments and Procedures

This section describes the measurement instruments used to measure density, pH, conductivity, and spectra. Figure 4.6 represents all the instruments used for this entire work.

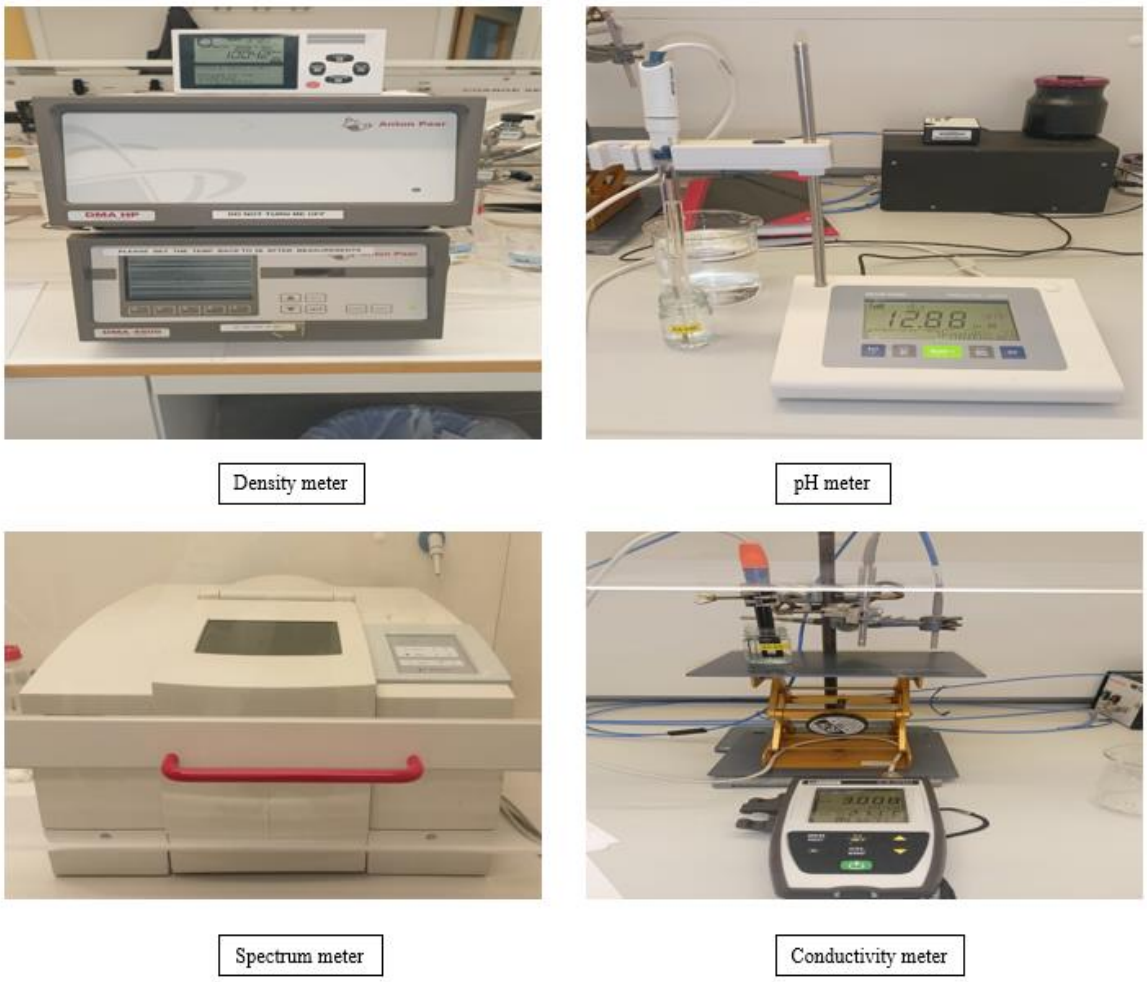

Figure 4.6: All the instruments used (Density meter, pH meter, Conductivity and Spectrum meter).

4.5.1 Density Measurement

Density, ρ is measured with an Anton Paar DMA 4500 with an intern measurement cell. The measurement range of DMA 4500 is from 273.15-363.15 K (0-90°C) which only works at normal atmosphere. Instrument accuracy for DMA 4500 is given as ± 0.00005 g/cm^3 by the manufacturer. Densities of unloaded and CO_2 loaded aqueous amine solutions was measured using DMA 4500. The procedure consisted of four main parts: density check, calibration, DMA 4500 operation, and cleaning and drying of measuring cells. Before conducting experiments, it was required to check the validity and precision of the DMA 4500. Since the density check was satisfactory, there was no need for calibration. If necessary, the CO_2 lab has a manual that outlines all the procedures and calibrations and cleaning as well. At first, the required ‘‘Density’’ method was activated. Then, the measurement cell was cleaned by injecting distilled water and ethanol, and then dried by injecting air into the measuring cell by turning

on the air pump. Next, a sample of approximately 5 ml of amine solution was injected into the measuring cell by a syringe without bubbles during every measurement. This process was observed through the viewing window, and the syringe was left in the injection position to prevent air from going on to the measuring cell. The reference temperature selected for this entire work was 23°C (296.15 K). The measurement will start when the temperature has reached its goal. The result will be displayed on the screen and make a little sound every time. Then, after measurements, it was required to cool down the instrument to 20 °C and cleaning and drying of the measuring cell.

4.5.2 pH Measurement

The pH of the CO_2 loaded and unloaded amine solutions were measured using the FiveEasy Plus FP20 pH meter from Mettler Toledo to understand the effect of the CO_2 loading and its characteristics. The InLab® Reach Pro-225 pH sensor was used for this entire experiment. Before operation, the pH sensor was calibrated against standard technical buffer solution of pH 7 and 10 and the result was satisfactory. It did not show any deviation from the reference value. The automatic correction for temperature compensates for temperature variations and deviation based on theoretical compensation. First, the electrode (sensor) was rinsed properly and placed in the sample to be measured. With auto endpoint, the instrument beeps when the signal is stable, and pH is displayed on the screen. During measurement the measurement mode icon, slope and offset was checked every time for better performance and to avoid the error. The electrode performance depends on the slope: 95-105% / Offset: ± 0-20 mV (good condition of electrode) which was maintained throughout all measurement. The same procedure was followed for the rest of the samples and after finishing all the amine samples the pH sensor was cleaned and rinsed properly and stored in the 3M KCl solution.

4.5.3 Conductivity Measurement

Conductivity here means the ability to conduct current in a medium and it has the SI unit Siemens per meter [S/m]. A conductivity measurement is therefore most often related to a standard temperature of 25°C (or 20°C) based on a temperature correction. The C.A 10141 conductivity meter cell has a built-in temperature sensor (PT1000) and can measure up to a range of 0 to 100°C. The temperature correction is used to correct and display the measured conductivity as of the chosen reference temperature. This is useful because the conductivity of a solution increases with increasing temperature. Equation 4.1 presents the temperature correction of the measured conductivity.

$$\sigma_{displayed} = \sigma_T/(1 - \alpha(T - T_{ref})/(100\%)) \quad (4.1)$$

Where, $\sigma_{displayed}$ = the conductivity displayed by the instrument, σ_T = the conductivity measured at temperature T, α = the linear temperature correction coefficient, T = the measured temperature (°C), T_{ref} = the reference temperature (20 or 25°C). The linear temperature correction coefficient α is used based on the solutions. The correction factor falls between 1.8 and 2.2%/°C for basic solution. Here the average factor is used 2.0%/°C. As amine blends are basic solution, in terms of this criteria, the correction factors from the manual conductivity measurement are utilized here.

Before starting measurement, the instrument was calibrated against standard solutions at 25°C and the measurement was satisfactory and between the range. At first, the device was turned on and then a short press on the SET button to select the conductivity measurement in mS/cm. After that, the measuring cell was placed in the amine solution. It is important that the solution covers the active part of the measuring cell. Then, reading was taken when the temperature and conductivity becomes stable. And after finishing the measurements, the cell was taken out of the solution, rinsed, and dried without touching the poles. Next, same procedure was followed for rest of the amine solutions and after finishing all the samples the measuring cell was cleaned and rinsed properly.

4.5.4 Spectrum One FTIR Spectrometer Measurement

A Spectrum One FTIR spectrometer from PerkinElmer was used for characterization of the chemical species. At first, a file was opened on the connected PC, where all the sample files would be saved. Then the FTIR spectrometer parameters were set and saved for this whole work. Next, the device configuration includes calibration of an empty cell at a scan step of 32 and a wavelength span between 400 and 4000 cm^{-1}. This is used as a reference spectrum in the database. An ATR-cell is used here for this FTIR measurements of spectra. After that, a drop of the amine sample was placed on the ATR crystal and covered by the lid. Following that, the scan option was clicked in the Spectrum One software. Before placing new samples, the crystal was rinsed and dried properly with distilled water and ethanol. Subsequently, all 41 unloaded and 20 loaded CO_2 samples were subjected to analysis using FTIR. The study focused on investigating the impact of the amount of loaded solution on the resulting plot After every 5 measurements, a background scan was performed to avoid any errors in the measurement. The experiment parameters used are presented in table 4.2.

Table 4.2: Experimental parameters for FTIR spectroscopy.

No.	Parameter	Value
1	Resolution	4 cm^{-1}
2	Data Interval	1 cm^{-1}
3	Scan	32
4	Scan type	Sample
5	Wavelength range	4000-400 cm^{-1}
6	Acquisition mode	Absorbance
7	Detector	MIR TGS (15000-370) cm^{-1}
8	Beamsplitter	OptKBr (7800-400) cm^{-1}
9	Source	MIR (8000-30) cm^{-1}

5 Results

In this section all the experimental results and summary of PLS-R model are reported in logical sequence. The PLS-R modelling with spectral peak identification has been carried out by my co-supervisor Peshalya Madhawi Kothalawala (PhD), which is presented in Appendix B.

5.1 Precipitation Behavior of Unloaded and Loaded Solution

The results from aqueous solutions of unloaded (0 mol CO_2/ mol amine) and the loaded AMP-PZ with different loading ratios at various blend ratios are shown in Tables 5.1 and 5.2, respectively. To see the proper visualization of the solubility of the prepared samples, cleared 30 mL sample-size bottles were used. Moreover, any uncertainty in the case of solvent precipitation, the solid sediments found shortly (within an hour) after preparing the solvent and loading of CO_2 were noted properly. The unloaded AMP-PZ solvent shows a high degree of stability for various concentrations, while precipitation occurred due to a higher total amine concentration. However, during the initial mixing, some samples with higher concentrations of AMP and PZ showed slight precipitation without CO_2. In particular, samples 28, 30, 31, and 34 had AMP to PZ molality (mol/kg) ratios of 3.32:1.8, 3.96:1.6, 3.43:1.7, and 4.07:1.5, respectively. This showed that higher total amine concentrations could cause the solvent system causing precipitation. These precipitated solutions dissolved within one and a half hours as the amines reacted and thoroughly mixed at room temperature. Although the AMP-PZ ratio is important, maintaining the total amine concentration for these solutions below this limit could enhance the solvent stability where a clear solution is necessary for practical applications.

Table 5.1 represents visual observation of the AMP-PZ unloaded solvent at various concentrations.

Table 5.1: Visual observation of the AMP-PZ unloaded solvent at various concentrations.

Samples No.	Amine (mol/kg)		Total Amine Concentration (mol/kg)	Visual Observation
	AMP	PZ		
1	3.21	1.5	4.71	C
2	4.5	0.3	4.8	C
3	4.18	0.8	4.98	C
4	4.07	0.9	4.97	C
5	3.96	0.7	4.66	C
6	3.32	1.7	5.02	C
7	3.43	1.5	4.93	C
8	2.78	1.8	4.58	C
9	3.1	1.1	4.2	C
10	2.68	2.2	4.88	C
11	2.36	1.7	4.06	C
12	2.25	1.6	3.85	C
13	3.21	1.1	4.31	C
14	2.03	1.5	3.53	C

Samples No.	Amine (mol/kg)		Total Amine Concentration (mol/kg)	Visual Observation
	AMP	PZ		
15	2.57	1.7	4.27	C
16	3.53	0.9	4.43	C
17	2.14	1.8	3.94	C
18	3.53	1.6	5.13	C
19	1.82	2.1	3.92	C
20	3.75	0.6	4.35	C
21	2.46	1.9	4.36	C
22	1.71	2.2	3.91	C
23	3	1.4	4.4	C
24	3.32	0.5	3.82	C
25	2.78	1.7	4.48	C
26	3.53	1.5	5.03	C
27	3.75	0.9	4.65	C
28	3.32	1.8	5.12	P
29	2.89	1.1	3.99	C
30	3.96	1.6	5.56	P
31	3.43	1.7	5.13	P
32	3.53	1.3	4.83	P
33	2.68	1.4	4.08	C
34	4.07	1.5	5.57	C
35	1.93	2.1	4.03	C
36	3.53	0.8	4.33	C
37	3.43	0.6	4.03	C
38	3	1.6	4.6	C
39	1.71	2.3	4.01	C
40	3.32	1.6	4.92	C
41	3.64	0.4	4.04	C

Here P is precipitation and C is a clear solution.

Table 5.2 presents a visual observation of the various CO_2 loadings at different amine concentrations from different mixtures design from stock solution. The sample has different loading capacities with a combination of high AMP and low PZ, and some solutions have balanced AMP and PZ ratios. A total of 20 solutions were utilized for CO_2 loading validation with varying amine concentrations. Samples 43, 44, 45, 46, 47, 54 and 55 showed precipitation with higher AMP concentrations and lower PZ amounts and comparatively high loading than other samples. This could be because the solvent was too saturated with CO_2 or maybe high AMP mixtures are not stable enough without enough PZ. As the CO_2 loading increases, more amine carbamates, bicarbonates and furthermore carbonates are formed. Regarding chemical structures and molecular weights of AMP and PZ, carbamates of AMP and PZ tend to precipitate. More often, clear solutions were found in samples with a more balanced AMP to PZ ratio with total lower amine concentrations. This suggests that the concentration and

percentage of the amines in the solution have a big effect on stability of the samples regrading precipitation.

Table 5.2: Visual observation of the AMP-PZ loaded solvent at various concentrations.

Samples No.	Amine (mol/kg)		Total Amine Concentration (mol/kg)	CO_2 Loading, α (mol_{CO2}/mol_{amine})	Visual Observation
	AMP	PZ			
42	2.82	1.07	3.89	0.28	C
43	3.36	0.83	4.19	0.32	P
44	4	0.63	4.63	0.35	P
45	4.81	0.23	5.04	0.40	P
46	4.92	0.24	5.16	0.40	P
47	3.8	0.65	4.45	0.35	P
48	3.66	0.71	4.37	0.34	C
49	2.81	1.08	3.89	0.28	C
50	3.47	0.85	4.32	0.32	C
51	4.05	0.59	4.64	0.36	C
52	1.81	1.41	3.22	0.20	C
53	1.84	1.43	3.27	0.20	C
54	5	0.24	5.24	0.27	P
55	4.87	0.24	5.11	0.12	P
56	3.01	0.93	3.94	0.10	C
57	3.16	0.88	4.04	0.09	C
58	3.95	0.59	4.54	0.31	C
59	3.69	0.72	4.41	0.28	C
60	1.82	1.41	3.23	0.10	C
61	1.82	1.41	3.23	0.08	C

The mixtures between AMP and PZ is for keeping the solvents physical stability. When there was a lot of AMP solvent compared to PZ, the solution becomes less stable, which causes the precipitation to form. High CO_2 loading shows how well the solvent is absorbing CO_2, but it also seems to raise the risk of precipitation. So, a balanced ratios of amine concentrations with CO_2 loading are essential to avoid the precipitation in the CESAR1 solvents for CO_2 capture process.

All the precipitated samples are shown in Appendix C in Figure 9.19.

5.2 Assessment of Density Measurements

In this section, the unloaded and loaded samples density measurement are reported with their possible discussion and interpretation.

A. Unloaded Samples Density

Figure 5.1 shows all density measurements of unloaded blend amine samples by the density meter at the laboratory, and the plotting was created with the help of Python code. The measurement of density was done to see the effect on the physical properties of different blended ratios of the amine concentration. Before measurement, the reference temperature was selected at 23°C for this entire work. The graph shows density measurements that generally range between around 0.99850 g/cm³ and 0.99970 g/cm³. However, in several samples, there are significant drops to lower values around 0.98750 g/cm^3. The sharp fluctuations are shown in samples number 17, 20, 30, 33, 34, 37, and 41, where the AMP-PZ ratios are 2.14:1.8, 3.75:0.6, 3.96:1.6, 4.07:1.5, 3.43:0.6, and 3.64:0.4 mol/kg, respectively. So, it can be said that those samples have significant lower concentration in PZ compared to AMP, they have a tendency to drop in density value. Those solution has a balanced amine ratios they did not show that much variations. As there are different blended amine ratios are used to see the variability of the density it cannot be directly said the reasons of fluctuating the value. It could be the effects of proper blending and also the random variations in the amine concentrations.

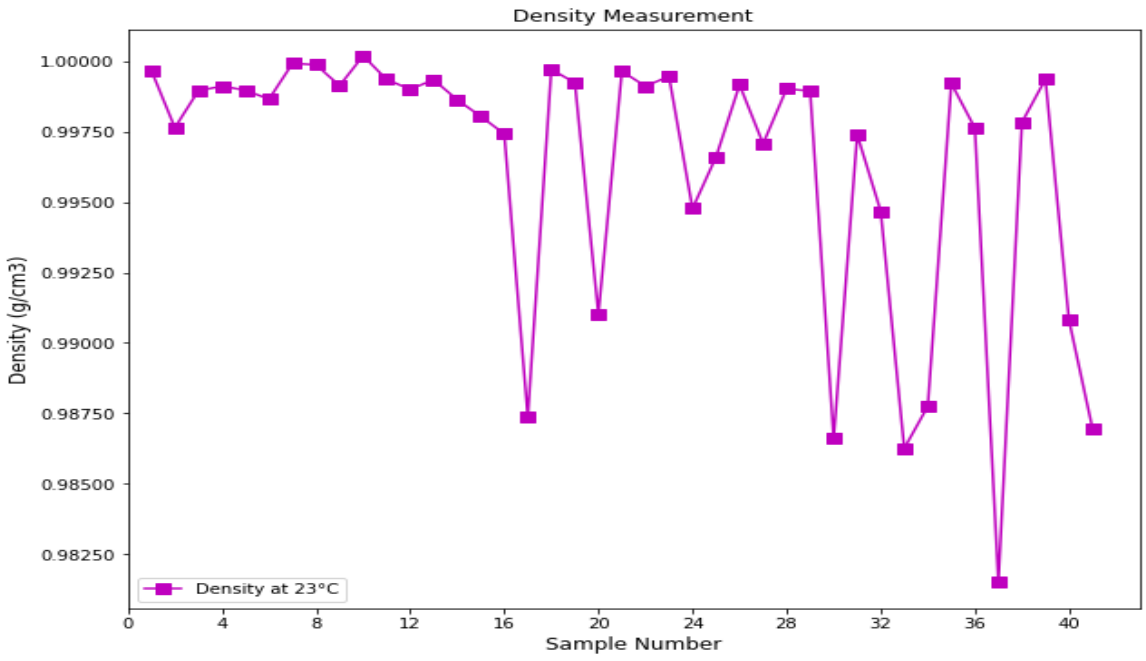

Figure 5.1: Density measurement of 41 unloaded samples at 23°C.

B. CO_2 Loaded Samples Density

The density plot of 20 CO_2-loaded samples at 23 °C is shown in Figure 5.2, along with their loading capacity (α) for different amine concentrations. Initially, between samples 42 and 53, the density stays consistently high and steady, with slight variations but near to 1.100 g/cm^3. Starting from sample 52, there was a significant decrease in density measurement until sample

54, at around 1.0585 g/cm^3. The density was then marginally stabilized for samples 55 and 56. Subsequently, there is a sharp decrease in the density of sample 58 to around 1.0209 g/cm^3, followed by an increase in sample numbers 59, 60, and 61. Therefore, it has been observed that CO_2 plays a substantial role in changing the density of the sample. However, the correlation between density and CO_2 loading indicates that when the sample absorbs a smaller amount of CO_2, its density accordingly declines. The connection between a high loading of CO_2 and an increased density suggests that the absorption of CO_2 is enhanced by its impact on the total measurement of densities. Furthermore, the variation in ratios of amines have a substantial influence on density. Samples 54 and 58 have a significantly lower PZ ratio in comparison to AMP.

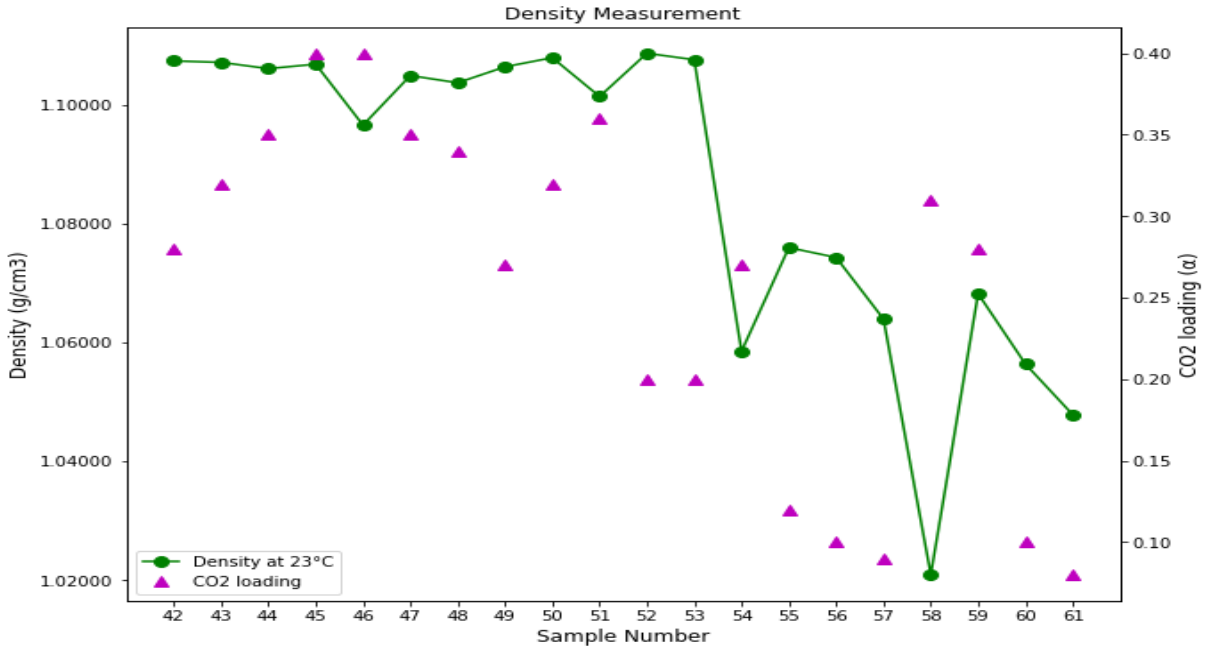

Figure 5.2: Density measurement of 20 CO_2 loaded samples at 23°C.

5.3 Analysis of pH Measurement

In this section, pH measurement of the CO_2 loaded and unloaded solution are visualized with their interpretation and discussion.

A. Unloaded Samples pH

Figure 5.3 represents the measurement of pH for all unloaded samples with different AMP-PZ ratios at 21°C. The measurement of pH for CESAR1 solvent is important to understand the reactivity in capturing CO_2. As amines are a basic solution, a clear view of the graph reveals that the pH ranges for all 41 unloaded samples ranges between 12.3 and 13.1, respectively. For various solutions, the pH has a very sharp oscillation, but the range is quite narrow and logical because there is no CO_2 loaded. Fluctuations are also caused due to different amine concentrations. For instance, from samples 7 to 15, the pH value has differed a little bit, ranging from approximately 12.44 to 12.64, where almost all concentrations have balanced AMP and PZ ratios. The samples with the most change, specifically 19 and 22, exhibit AMP:PZ ratios of 1.82:2.1 and 1.71:2.2 mol/kg, respectively. In both cases, the PZ ratio is greater than the AMP.

Upon examining various concentrations, it is observed that the samples with a lower PZ compared to AMP have a higher pH than those with a higher PZ concentration.

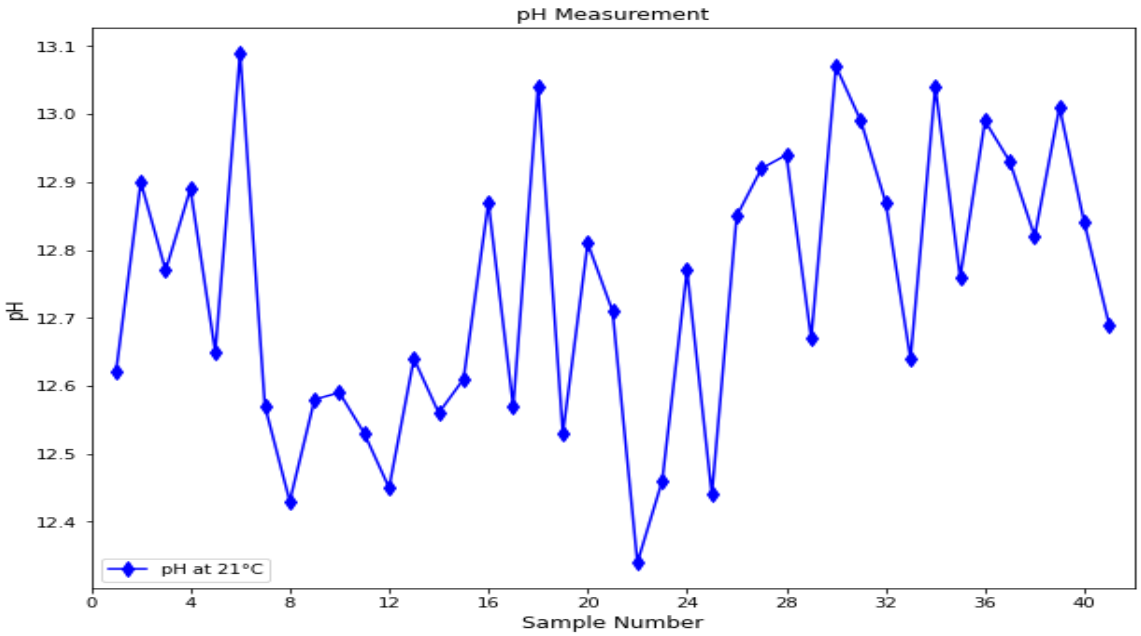

Figure 5.3: pH measurement of 41 unloaded samples at 21°C.

B. CO_2 Loaded Samples pH

Figure 5.4 shows all the pH measurements of loaded CO_2 samples at 21°C with respect to their loading ratio. This plot reveals that the pH values of CO_2-loaded samples range between 9.13 and 11.7. CO_2 reacts with water to form carbonic acid (H_2CO_3). Carbonic acid further breaks down into bicarbonates (HCO_3^-) and hydronium ions (H_3O^+), which lowers the solutions pH and makes it more acidic. Moreover, the amines AMP and PZ also react with CO_2 to form carbamates, which consume the H_3O^+ ions and balance the pH of the samples. Direct reaction with OH^- only at very high pH. CO_2 absorption results in formation of H_3O^+, that is, lowering of pH. Likewise, AMP and PZ are bases, so addition leads to increase of pH. As a result, CO_2 loading has a significant impact on changing the pH value for blended amines. From figures 4.9 and 4.10, it is clearly seen that the pH value declines after CO_2 being added with different amine mixtures. Also, the amount of amine concentration affects the pH. Samples 52 and 53 have the lowest pH, with amine ratios of 1.81:1.41 and 1.84:1.43 mol/kg of AMP-PZ, respectively. After that, for sample 54 and 55 the value pH increased like skyrocketing and reached around 11.7 for sample 55. This is because both samples have a very low CO_2 loading ratio compared to the other samples. Almost rest of the samples followed typical trend that high loading of CO_2 reduces the pH. Only the samples 58 and 59 showed different scenario which could be the reason of high AMP concentration compared to PZ, for both samples.

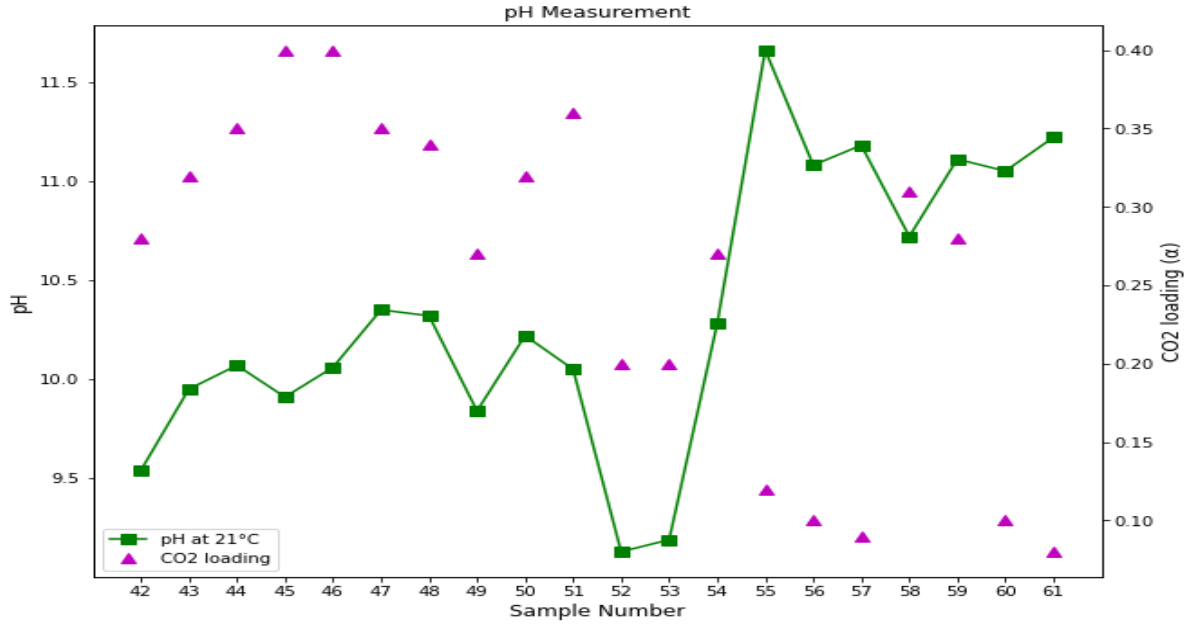

Figure 5.4: pH measurement of CO_2 loaded samples at 21°C.

5.4 Conductivity Measurement Analysis

This section provides the visualization of the conductivity measurements of CO_2 loaded and unloaded solution with proper explanation of their variation.

A. Unloaded Samples Conductivity

Figure 5.5 shows the conductivity measurement of unloaded samples at 21°C. As AMP and PZ dissolved in water and formed ionic species of their protonated form ($AMPH^+$, PZH^+ and OH); which increase their ionic strength in the samples and hence impacts on the conductivity. This plot reveals that the conductivity measurement ranges remain between approximately 1.2 and 4.5 mS/cm. The amine mixture concentrations show that samples 19 and 22 exhibit a higher PZ ratio than AMP, indicating high conductivity. Compared to samples with a lower PZ ratio than AMP, for instance, samples 2 to 7 show low conductivity. As there is no CO_2 loaded, the conductivity value ranges are quite narrow and low. From the conductivity plot those samples has high PZ ratio than AMP, they showed high conductivity than other samples. Likewise, 19 and 22, this trend is followed by samples 35 and 39. So, it can be said that PZ has a major impact on the conductivity of the amine samples. Moreover, from Table 5.1 it is clearly seen that those sample has a very balanced amine ratios for both AMP and PZ, they possess high conductivity. Additionally, Conductivity normally rises with temperature, since ions flow more readily in warmer solutions. Therefore, maintaining stable temperature is critical for reliable conductivity measurements.

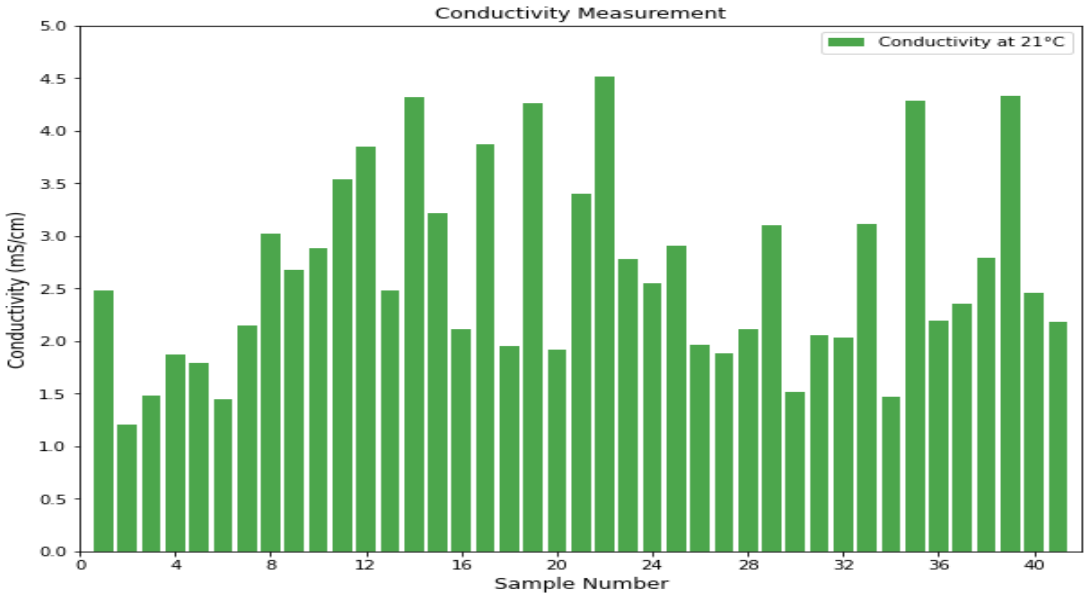

Figure 5.5: Conductivity measurement of unloaded samples at 21°C.

B. Loaded Samples Conductivity

Figure 5.6 presents the conductivity measurement of CO_2-loaded samples at 21°C. From both figures, it is clearly seen that CO_2 loading significantly affects the conductivity measurement of amine solution. Samples 52 and 53 have the highest conductivity, approximately 20 mS/cm. Although the CO_2 loading is not that high, but both samples have a very balanced AMP and PZ concentration. Overall, those samples have a high CO_2 loading, and their conductivity is also higher. Samples 55, 56 and 57 shows low conductivity because they have low CO_2 loading ratio as well as very little concentration of PZ compared to AMP by cross-checking Table 5.2. Samples with higher CO_2 loading will show increased conductivity due to the formation of bicarbonate and carbonate ions. So, combining AMP and PZ may result in higher conductivity due to increased CO_2 absorption and ion generation.

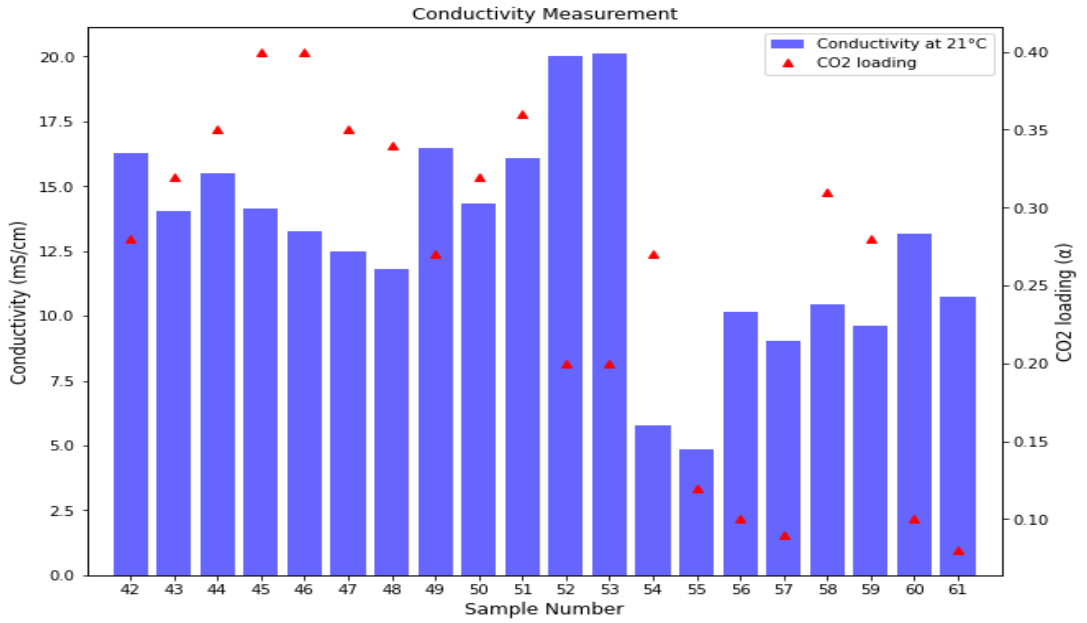

Figure 5.6: Conductivity measurement of CO_2 loaded samples at 21°C.

5.5 Summary of PLS-R Model for FTIR Spectra and Measured Physical Properties

All the prepared models are presented in Appendix section B and their possible interpretation and analysis are discussed under this section. This section provides a detailed discussion of the PLS-R models applied to the observed and pre-processed FTIR spectra for α-CO_2 loading, AMP, and PZ with their speciation of the species with band attribution and, variable ranges of the model for this study. It also includes the PLS-R models for the measured physical properties-density, pH, and conductivity.

5.5.1 Raw and Pre-processed FTIR Spectra for α - CO_2 Loading, AMP, and PZ Model

In Appendix B, Figure 9.1 represents the (a) raw spectra (full spectral range) and (b) pre-processed spectra (1800 - 700 cm^{-1}) for the speciation of 61 different concentration CESAR1 samples. IR band assignments are displayed next to the respective peaks, according to Table 9.1, respective to their CO_2 loading capacity. The variability range of the model as well as the identified IR bands for this study compared to literature findings are demonstrated in the individual model sections. Initially, all spectra were baseline corrected using the Whittaker filter with Lambda and Rho at 1000 and 0.001, respectively [42]. According to Figure and Table 9.1 and, the color code here is used for the following compounds: blue shade for CO_2 loading, yellow shade used in the PZ model, and green shade used in the AMP model. Some uncertainties are shown during the measurement of raw spectra for some of the samples, which is demonstrated in the discussion section.

5.5.2 Predicted PLS-R Model with Speciation for 'α – CO_2 Loading'

The predicted PLS-R model with speciation for 'α - CO_2 loading' with different loaded and unloaded samples is presented in Figure 9.2. The FTIR spectrum region for the CO_2 loading model is selected from 1575-1213 cm^{-1}. Five major FTIR peaks have evolved in Figure 9.2. No difference was noticed on the shape of the spectrum for the different loading ratios of CO_2, only the absorbance (a.u.) changed. PZ carbamate species $PZCOO^-$ and $^-OOCPZCOO^-$ (Piperazine mono-carbamates and dicarbamates) are formed when PZ reacts with CO_2. According to table 9.1, The PZ carbamate species for CO_2 loading model can be identified at the beginning of the peaks at 1260 cm^{-1} compared to the literatures at 1265 cm^{-1}, 1289 cm^{-1}, respectively [43, 44, 45], where the band attribution is in stretching vibration modes (νN-COO^-). After that the peaks drops and rise again and found a new peak for HCO_3^- species with symmetric stretching band (νsC-O) at 1349 cm^{-1}. Then, the peaks fall and rise again, and PZ carbamates species are ($PZCOO^-$ and $^-OOCPZCOO^-$) formed with the symmetrical (νsCOO^-) and asymmetrical (vasCOO^-) streching bands at 1416 cm^{-1} and 1533 cm^{-1}, respectively. Vibration band (δsNH_2^+) are identified as protonated species (PZH^+, H^+PZH^+) at 1470 cm^{-1} in literatures[43, 44, 45] and for this study. Moreover, Figure 9.3 represents the predicted vs. measured PLS-R model for CO_2 loading. The calibration data set has been fitted with the regression line with slope of 0.9757, using 3 Latent variables. The RMSEC of 0.0284 mol/mol, RMSEP of 0.0234 mol/mol with predicted R^2 value (0.972) which is close to 1 that indicates a high predictive accuracy and a good correlation between measured and predicted values. The

R^2 for calibration (0.956) and cross validation (0.930) also indicates the model has a good fit with predicted and measured values with maximum observations near the regression line. In addition, Figure 9.4 presents the (a) score plot LVs 1 vs. 2 with various CO_2 loading ratios and (b) T^2 vs. Q - residual plot for calibration and test samples and (c) regression coefficient corresponding to their wavenumber. In Figure 9.4 (a), latent variable 1 describes around 90% of the variation of the data, while latent variable 2 describes around 6.5% of the variation. The unloaded CO_2 samples 1 to 41 show clustering near the origin, close to zero on both axes. The sample with the highest CO_2 loading value (46) and that with the lowest CO_2 ratio (60, 61) appear isolated in the score plot, implying they have extreme loading ratios. Samples 43, 44, 47, and 48 have balanced loading ratios, comprising positive scores on LV 1 and LV 2. On the other hand, in Figure 9.4 (b), 97.72% indicates the proportion of the total variance in the data that is explained, and 2.28% is residual error that is not captured by principal components or latent variables. It helps to understand the model validation by ensuring that the model accurately captures the significant variations in the data. It uses specific thresholds to indicate the confidence level, helping to identify normal observations and potential anomalies or outliers. Here, samples 46, 52, and 53 have high T^2 and high Q value which could be outliers as they move far away from the normal observation. On the other hand, 9.4 (c), describes the most important wavenumbers regarding their regression vector.

5.5.3 Predicted PLS-R Model for 'AMP Concentration with Specition

Figure 9.5 demonstrates the PLS-R model of 'AMP concentration' with the selected wavelength region (1095 - 877cm^{-1}) for this study. AMP species can be identified at the initial peak in the wavelength region of 913 cm^{-1} where the band attribution is in the twisting band (τN-H). Although there is rise at 1000 cm^{-1}, the band related at this region for AMP species is not identified with cross reference. Then, the peak goes down and increases again at a region of 1046 cm^{-1} where the band is attributed by overlapping (*ν*C-O, *ν*C-N) stretching band. According to the Table 9.1, the $AMPH^+$ species got protonated through symmetrical (δsNH_3^+) and asymmetrical ($\delta asNH_3^+$) bending band at 1534 cm^{-1} and 1635 cm^{-1}, respectively, regrading literatures [44], [45] For simplicity, this wavelength region is not considered for the AMP model in our study. Also, Figure 9.6 represents (a) the predicted vs. measured PLS-R model and (b) the RMSEP model vs. LVs for AMP concentration after removing a possible outlier (sample 6). After removing the outliers, Figure 9.6 (a) shows that the RMSEP (0.1338 mol/kg) and RMSEC (0.1476 mol/kg) have a predicted R^2 value of 0.966 and a regression line slope of 0.9643, which is near to 1. The R^2 for calibration (0.965) and cross-validation (0.958) also increased after removing the outliers, indicating a good quality model with 2 LVs. Figure 9.6 (b) presents how RMSEP changes with a extend of latent variables. Here, 2 LVs are used for AMP model. Moreover, Figure 9.7 (a), LV 1 represents around 40% of the variations in the AMP concentration data, whereas LV 2 describes about 55% of the data. The highest and lowest AMP concentration samples are easy to identify from their score plots as well as their similarities. T^2 vs. Q-residues are displayed in Figure 9.7 (b), where nearly all samples indicate normal observation; only sample 46 exhibits some irregularities. Figure 9.7 (c) shows the regression coefficient for their wavelength with a positively correlated wavenumber, indicating that a rise in absorbance at that wavenumber relates to an increase in the response variable.

5.5.4 Predicted PLS-R Model for 'PZ Concentration' with Speciation

Figure 9.8 represents PLS-R model for PZ concentration corresponding to their wavelength. The wavelength that has been selected for the PZ model is from (1213 – 1096 cm^{-1}). There is no change in the spectrum for the PZ model but the absorbance (a.u.) changed. According to Table 9.1, cross referenced with the literature the PZ species can be identified at early peaks using the band attribution (νmC-N) at 1107 cm^{-1} of medium stretching band. There is a rise at 1179 cm^{-1} but no evidence found in the literature for related band in this region. It can be seen from Figure 9.9 (a) and (b) that after removing the outlier samples 45, 46, 60, and 61, the RMSEC (0.1829 mol/kg) and RMSEP (0.1611 mol/kg) with R^2 (predicted) are 0.907. The R^2_Y for calibration and cross-validation is 0.902 and 0.867, respectively. The slope of the regression line is 0.9108, which is a stable fit after removing the outlier samples. Figure 9.9 (b) shows how RMSEC, RMSEP and RMSECV are correlated with the latent variables. Here, 3 LVs use for this model to predict the response variable. In Figure 9.10 (a), LV 1 describes around 85% of the variation of the PZ data, while LV 2 comprises about 12% of the variation after removing outlier samples 45, 46, 60, and 61 from the regression model. There is some clustering shown in score plots with high PZ concentrations, which is essential to understanding the sample patterns and groupings. From Figure 9.10 (b), it is seen that the maximum data has normal observation, which explains that after removing the outliers, the model has good fit performance, whereas sample 54 shows high residue, which means this observation is not well explained by the model, but due to low leverage, it does not affect the model performance.

5.5.5 Raw and Pre-processed FTIR Spectra used in Density, pH, and Conductivity Model

Figure 9.11 shows the (a) raw spectra (full spectral range) and (b) pre-processed spectra (1920 - 500 cm^{-1}) for the PLS-R model of density, pH, and conductivity. The wavelength region selected for density, pH and conductivity models are (1080-502 cm^{-1}), (1835-502 cm^{-1}) and (1810-502 cm^{-1}), respectively. The color code here is used for the following compounds: purple for density model, dark yellow used in pH model, and turquoise used in the conductivity model.

5.5.6 Predicted PLS-R Model for Density Measurement

In this section the results for PLS-R model of density are discussed with possible demonstration in logical sequence. Figure 9.12 presents (a) predicted vs. measured PLS-R model and (b) T^2 vs. Q-residual plot for density. The RMSEP, RMSEC, and R^2 (Pred) are 0.0048 g/cm^3, 0.0123 g/cm3, and 0.995, respectively, with a regression slope of 0.9236. From the T^2 vs. Q residual plot, it is observed that samples 52 and 53 have extremely high T^2 and Q, which could be possible outliers or anomalies, but after a regression model, it is seen that they fit well with the line. So, removing this observation may reduce the quality of the model because it contains important information for the model. On the other hand, observations 58, 46, and 55 are far away from the fitted line after prediction, but they are not detected as outliers because they are in normal observation in the T^2 vs. Q-residual plot. So, to understand the model quality, it is essential to interpret the residual plot regarding T^2 carefully to find noise, measurement error, and outliers etc. In Figure 9.13 (a), the LV 1 describes almost 75% variation of the data while LV 2 describes around 11% of the data variation in density model. Clustering is shown for

unloaded samples around the origin of both axes, and it is easy to identify the different observations or samples by their score plots. The highest concentration samples here is 46 which have both positive scores on LV 1 and LV 2 components. The lowest concentration here is samples 60 and 61. In contrast, regression coefficient shows the most and least important variables between 600 and 1800 cm^{-1} wavenumbers.

5.5.7 Predicted PLS-R Model for pH Measurement

In this section the results for PLS-R model of pH are discussed with possible demonstration in logical sequence. Figure 9.14 shows (a) the predicted vs. measured PLS-R model and (b) the RMSEP model vs. LVs for pH. The pH model was calibrated with test set validation. In Figure 9.14 (a), the RMSEP is 0.1842, with predicted R^2 value 0.983 where the regression slope is 0.9840. The R^2 for calibration (0.963) and cross-validation (0.915) also indicating a good quality model with 3 LVs. Figure 9.14 (b) presents how RMSEP changes with a extend of latent variables. Here, 3 LVs are used for pH model. The unloaded sample shows clustering on both latent variables as their pH is comparatively higher than the CO_2 loaded samples in Figure 9.15 (a). The rest of the samples has scattering pattern with different CO_2 loadings. In figure 9.15 (b), Almost all calibration with validation dataset is in normal observation while samples 52, 53 are far away from the centre of the model in Figure 9.15 (b). It might be due to the low pH concentration with low CO_2 loading ratios. The plot of regression coefficients between 500 and 1835 cm^{-1} as given in Figure 9.15 (c) shows negatively and positively correlated wavenumbers to the model predictions.

5.5.8 PLS-R Model for Conductivity Measurement

The results from the PLS-R model of conductivity measurement are depicted below with reasonable demonstration. According to RMSEP variation with respect to number of latent variables, 4 LVs (Figure 9.16 (b)) were selected for the model. Figure 9.16 (a) shows how well model predicts for the test set samples with calibration where the RMSEP is 0.6321 mS/cm with R^2 of 0.990. That means the model has good fit with regression line slope 0.9871. In Figure 9.17 (a), LV 1 describes around 75% of the variation of the conductivity data, while LV 2 describes about 10% of variation. The unloaded sample shows clustering on both latent variables as their conductivity is comparatively lower than the CO_2 loaded samples in Figure 9.17 (a). The rest of the samples has scattering pattern with different CO_2 loadings. In figure 9.17 (b), Almost all calibration with validation samples is in normal observation of lower left quadrant. While samples 46, 52, 53 are in the lower right quadrant which could be the reason of measurement error or abnormalities. The plot of regression coefficients between 500 and 1810 cm^{-1} as given in Figure 9.17 (c) shows the most and least important correlated wavenumbers to predict the model performance.

5.5.9 Identified Outliers for AMP and PZ Model

By doing PLS modeling these 5 samples are identified as possible outliers where samples 6 is considered for AMP model and samples (45, 46, 60 and 61) considered for PZ model which is shown in Table 9.2 and figure 9.18 in Appendix B. The identified outliers have been removed from the original baseline dataset to do further PLS-R modelling.

6 Discussion

This part of the work presents the discussion of key findings of the experimental results followed by the PLS-R model, and uncertainties during tests and modeling.

The purpose of this study is to prepare different CESAR1 blend samples with unloading and loading of CO_2 concentrations for various range of AMP/PZ and to see the visual effects of their blend during preparation as well as during measurement of physical properties like density, pH, and conductivity. Furthermore, PLS-R modeling of identified spectral regions of interest from estimated FTIR spectroscopy and physical properties are conducted to evaluate the CESAR1 blend performance as the blend has a complex relationship of data variability with each other after loading of CO_2.

1. Summary of Findings

The summary of key findings during the experiments and PLS-R model are depicted below.

- **Experimental outputs**

Table 6.1 provides a summary of precipitation results with loaded and unloaded samples with different amine concentrations. For CO_2 loaded samples (43-47) has high CO_2 loading ratios (α) ranges from 0.32-0.40 with higher range of AMP concentration. And for the unloaded samples, the total amine concentrations reached a high level of approximately more than 5 mol/kg for these 4 precipitated samples. More details can be found in Table 5.1 and 5.2.

Table 6.1: Precipitation results for CO_2 loaded and unloaded blends.

Unloaded samples (1-41)	CO_2 loaded samples (42-61)
• Only 4 samples (28, 30, 31, 32) are **precipitated.** • Rest of the samples shown clear visualization.	• Samples 43 to 47 and 54, 55 are **precipitated.** • Rest of the samples shown clear visualization.

Table 6.2 presents the summary of measured physical properties data for density, pH Conductivity in a range. Density varies between 0.98 and 1.00 g/cm^3 for unloaded samples while for loaded samples it ranges from 1.02 to 1.11 g/cm^3. The pH ranges between (12.3-13.01), and (9.1-11.6) for unloaded and loaded samples, respectively. The conductivity ranges from (1.2-4.5) mS/cm for unloaded while for loading samples (5.8-21) mS/cm.

Table 6.2: Measured physical properties of prepared CESAR1 blends.

Measured Properties	**Unloaded (1-41), Ranges**	**Loaded (42-61), Ranges**
Density	0.98-1.00 g/cm3	1.02-1.11 g/cm3
pH	12.3-13.01	9.1-11.6
Conductivity	1.2-4.5 mS/cm	5.8-21 mS/cm

- **PLS-R Model Summary**

Table 6.3 provides the summary of the PLS-R model with wavenumber selected for preparing different model. Latent variables with the dataset of calibration and validation are decided corresponding to the RMSEP plot. The wavelength region selected for CO_2 loading, AMP, PZ, density, pH, and conductivity are (1575-1213) cm^{-1}, (1095-877) cm^{-1}, (1213-1096) cm^{-1}, (1080-502) cm^{-1}, (1835-502) cm^{-1}, (1810-502) cm^{-1}, (1810-502) cm^{-1}, (1810-502) cm^{-1}, respectively. The possible outliers are removed from the AMP and PZ model to increase the performance of the model. PLS-R modelling is crucial for CO_2 capture due to its capacity to handle complicated multicomponent systems with accurate quantitative analysis and provide real-time monitoring.

Table 6.3: Conducted PLS-R model summary.

Model	Wavenumber (cm^{-1})	Min–Max	No. of Samples		LV	RMSEP	R^2 (Pred)
			Calibration set	Validation set			
CO_2 Loading	1575-1213	0 - 0.4 CO_2 mol/ amine mol	41	20	3	0.0234 mol/mol	0.972
AMP	1095-877	1 - 4.5 mol/kg	40*	20	2	0.1338 mol/kg	0.966
PZ	1213-1096	0 - 2.5 mol/kg	37**	20	3	0.1611 mol/kg	0.907
Density	1080-502***	0.98 - 1.11 g/cm^3	41	20	3	0.0048 g/cm^3	0.995
pH	1835-502***	9.1 - 13.1	41	20	3	0.1842	0.983
Conductivity	1810-502***	1 - 22 mS/cm	41	20	4	0.6321 mS/cm	0.990

Here, * Sample 06 - outlier; removed; ** Samples 46, 61, 45, and 60 - outliers; removed in order; *** Decided based on preliminary PLS-R models.

2. Possible Uncertainties

The possible uncertainties faced during preparation of CESAR1 blend samples as well as experiment and the PLS-R model are listed below.

- Precipitation is a major concern during preparation of a wide range of AMP/ PZ blend samples with high CO_2 loading. Even without loading of CO_2, for high AMP and PZ concentrations, precipitation can occur. Here, to avoid the Precipitation AMP solution was always kept in the water bath during preparation of samples.

- Proper Concentration ratio also has a significant effect on the preparation of blend samples. Any error in the measurement and concentration can reduce the blend performance by giving wrong results. So, proper care should be taken to avoid any mistakes during preparation and experiments. Excel sheets with proper labelling of the samples can prevent this error.

- As the density meter screen is quite faulty, it may be possible to read any wrong results, but it was tried to avoid any error by proper visualization. So, instrumental faults also need to be noticed during experiments.

- The pH and conductivity were measured at room temperature. So, any increase or decrease in temperature could have a change in the measurement as they are correlated with temperature.

- During the measurement of FTIR spectra, for samples 29 to 41 as shown in figure 5.1 the baseline of raw spectra starts from different position which is quite unusual in spectroscopy. It may be the reason for the measurements on two different dates or any instrumental error.

- During the PLS-R model, it is important to identify the possible outliers to enhance the model quality. To avoid any error in the model scores plots, Q-residual plots as well as the regression coefficients need to be validated by proper identification.

3. Recommendations

- A wide range of amines with CO_2 loading could be used to monitor the effects of their blends. It may be possible to add other additives to the CESAR1 solvent to increase the absorption capacity, thermal stability and so on.
- Also, to mitigate the degradation and reclaiming of CESAR1 solvent, long-term evaluation of tests should be done to see the changes in solvent.
- Furthermore, NMR spectroscopy could be used to identify the mechanisms of CO_2 absorption at a molecular level.
- To find the best performance in the model, a large number of datasets should be used. Further development and validation of PLS-R model are still required for operation in a real CO_2 capture plant.
- It can be explored to see the effects of CESAR1 solvent in hybrid CO_2 capture systems that combine physical and chemical absorption in a small-scale operation.

7 Conclusion

To evaluate the effectiveness and technical advancements of new benchmark solvent CESAR1, implementation of PAT tools like FTIR spectroscopy in CO_2 capture process is essential to enhance laboratory analysis and plant operations. Various aqueous CESAR1 blend (AMP+PZ) samples are prepared with CO_2 loading to identify the effects of CO_2 at different amine concentration which can results in precipitation. Total 41 unloaded and 20 loaded samples are monitored to see the effect of their precipitation. Moreover, physical properties like density, pH and conductivity of these samples are measured to evaluate the aqueous CESAR1 blend stability, corrosivity, absorption capacity, solvent degradation and so on. Density and pH increase with the influence of CO_2, while conductivity decreases after adding CO_2 concentration. In the blend, AMP acts as a base that catalyzes the PZ reaction with CO_2. Quantification of AMP, PZ, CO_2 loading, $PZCOO^-$, $^-OOCPZCOO^-$ and HCO_3^- species enabling real-time monitoring of the absorption process of a CO_2 capture process, by using FTIR spectroscopy. Different species concerned with CESAR1 blend (AMP+PZ) are identified through speciation of pre-processed FTIR spectra including some stretching band which is tabulated in Table 9.1. Six PLS-R model were developed to predict the α-CO_2 loading, AMP, PZ, density, pH, and conductivity of the measured CESAR1 solvent, respectively. The models predictions are satisfactory where RMSEP are 0.0234 mol/mol, 0.1338 mol/kg, 0.1611 mol/kg, 0.0048 g/cm^3, 0.1842, 0.6321 mS/cm for α-CO_2 loading, AMP, PZ, density, pH, and conductivity, respectively. Overall, all the model has a good fit performance with the measured and predicted values. So, multivariate data analysis combined with spectroscopic analysis indicated that it could be utilized efficiently for online monitoring of the behaviour and quantification in an industrial CO_2 capture plant by developing several PLS-R models and evaluating their prediction.

8 References

[1] "Climate Change: Atmospheric Carbon Dioxide | NOAA Climate.gov." Accessed: Mar. 19, 2024. [Online]. Available: https://www.climate.gov/news-features/understanding-climate/climate-change-atmospheric-carbon-dioxide

[2] P. Friedlingstein *et al.*, "Global Carbon Budget 2022," *Earth Syst Sci Data*, vol. 14, no. 11, pp. 4811–4900, Nov. 2022, doi: 10.5194/ESSD-14-4811-2022.

[3] "Getting to know CCUS at PETRONAS | PETRONAS FLOW." Accessed: Mar. 20, 2024. [Online]. Available: https://www.petronas.com/flow/technology/getting-know-ccus-petronas

[4] "(PDF) IPCC Special Report on Carbon dioxide Capture and Storage." Accessed: Mar. 23, 2024. [Online]. Available: https://www.researchgate.net/publication/239877190_IPCC_Special_Report_on_Carbon_dioxide_Capture_and_Storage

[5] E. Blomen, C. Hendriks, and F. Neele, "Capture technologies: Improvements and promising developments," in *Energy Procedia*, Feb. 2009, pp. 1505–1512. doi: 10.1016/j.egypro.2009.01.197.

[6] D. Y. C. Leung, G. Caramanna, and M. M. Maroto-Valer, "An overview of current status of carbon dioxide capture and storage technologies," *Renewable and Sustainable Energy Reviews*, vol. 39. Elsevier Ltd, pp. 426–443, 2014. doi: 10.1016/j.rser.2014.07.093.

[7] "IEA GREENHOUSE GAS R&D PROGRAMME Further Assessment of Emerging CO 2 Capture Technologies for the Power Sector and their Potential to Reduce Costs IEAGHG Technical Report," 2019. [Online]. Available: www.ieaghg.org

[8] P. Madejski, K. Chmiel, N. Subramanian, and T. Kuś, "Methods and Techniques for CO2 Capture: Review of Potential Solutions and Applications in Modern Energy Technologies," *Energies*, vol. 15, no. 3. MDPI, Feb. 01, 2022. doi: 10.3390/en15030887.

[9] A. I. Osman, M. Hefny, M. I. A. Abdel Maksoud, A. M. Elgarahy, and D. W. Rooney, "Recent advances in carbon capture storage and utilisation technologies: a review," *Environmental Chemistry Letters*, vol. 19, no. 2. Springer Science and Business Media Deutschland GmbH, pp. 797–849, Apr. 01, 2021. doi: 10.1007/s10311-020-01133-3.

[10] C. Chao, Y. Deng, R. Dewil, J. Baeyens, and X. Fan, "Post-combustion carbon capture," *Renewable and Sustainable Energy Reviews*, vol. 138, Mar. 2021, doi: 10.1016/j.rser.2020.110490.

[11] "Oxy Fuel Combustion Technology Market - Industry Size, Trends,." Accessed: Mar. 25, 2024. [Online]. Available: https://www.openpr.com/news/3002662/oxy-fuel-combustion-technology-market-industry-size-trends

[12] T. N.Borhani and M. Wang, "Role of solvents in CO2 capture processes: The review of selection and design methods," *Renewable and Sustainable Energy Reviews*, vol. 114. Elsevier Ltd, Oct. 01, 2019. doi: 10.1016/j.rser.2019.109299.

[13] K. A. Hoff, E. F. Da Silva, I. Kim, A. Grimstvedt, and S. Ma'mun, "Solvent development in post combustion CO2 capture -Selection criteria and optimization of

solvent performance, cost and environmental impact," in *Energy Procedia*, Elsevier Ltd, 2013, pp. 292–299. doi: 10.1016/j.egypro.2013.05.114.

[14] S. Li, H. Li, Y. Yu, and J. Chen, "Simulation and performance comparison for CO2 capture by aqueous solvents of N-(2-hydroxyethyl) piperazine and another five single amines," *Processes*, vol. 9, no. 12, Dec. 2021, doi: 10.3390/pr9122184.

[15] Z. (Henry) Liang *et al.*, "Recent progress and new developments in post-combustion carbon-capture technology with amine based solvents," *International Journal of Greenhouse Gas Control*, vol. 40. Elsevier Ltd, pp. 26–54, Sep. 01, 2015. doi: 10.1016/j.ijggc.2015.06.017.

[16] K. A. Mumford, Y. Wu, K. H. Smith, and G. W. Stevens, "Review of solvent based carbon-dioxide capture technologies," *Frontiers of Chemical Science and Engineering*, vol. 9, no. 2. Higher Education Press, pp. 125–141, Jun. 24, 2015. doi: 10.1007/s11705-015-1514-6.

[17] P. Gunasekaran, A. Veawab, and A. Aroonwilas, "Corrosivity of single and blended amines in CO2 capture process," in *Energy Procedia*, Elsevier Ltd, 2013, pp. 2094–2099. doi: 10.1016/j.egypro.2013.06.088.

[18] B. Dutcher, M. Fan, and A. G. Russell, "Amine-based CO2 capture technology development from the beginning of 2013-A review," *ACS Appl Mater Interfaces*, vol. 7, no. 4, pp. 2137–2148, Feb. 2015, doi: 10.1021/am507465f.

[19] J. C. Morgan *et al.*, "Development of process model of CESAR1 solvent system and validation with large pilot data," 2022.

[20] J. Gomes, S. Santos, and J. Bordado, "Choosing amine-based absorbents for CO2 capture," *Environmental Technology (United Kingdom)*, vol. 36, no. 1, pp. 19–25, Jan. 2015, doi: 10.1080/09593330.2014.934742.

[21] R. Zhang, X. Zhang, Q. Yang, H. Yu, Z. Liang, and X. Luo, "Analysis of the reduction of energy cost by using MEA-MDEA-PZ solvent for post-combustion carbon dioxide capture (PCC)," *Appl Energy*, vol. 205, pp. 1002–1011, Nov. 2017, doi: 10.1016/j.apenergy.2017.08.130.

[22] C. Nwaoha *et al.*, "Advancement and new perspectives of using formulated reactive amine blends for post-combustion carbon dioxide (CO2) capture technologies," *Petroleum*, vol. 3, no. 1. KeAi Communications Co., pp. 10–36, Mar. 01, 2017. doi: 10.1016/j.petlm.2016.11.002.

[23] X. Li, S. Wang, and C. Chen, "Experimental study of energy requirement of CO2 desorption from rich solvent," in *Energy Procedia*, Elsevier Ltd, 2013, pp. 1836–1843. doi: 10.1016/j.egypro.2013.06.063.

[24] P. Brúder, A. Grimstvedt, T. Mejdell, and H. F. Svendsen, "CO2 capture into aqueous solutions of piperazine activated 2-amino-2-methyl-1-propanol," *Chem Eng Sci*, vol. 66, no. 23, pp. 6193–6198, Dec. 2011, doi: 10.1016/j.ces.2011.08.051.

[25] E. Sanchez Fernandez, E. L. V. Goetheer, G. Manzolini, E. Macchi, S. Rezvani, and T. J. H. Vlugt, "Thermodynamic assessment of amine based CO2 capture technologies in power plants based on European Benchmarking Task Force methodology," *Fuel*, vol. 129, pp. 318–329, Aug. 2014, doi: 10.1016/j.fuel.2014.03.042.

[26] M. van der Spek, R. Arendsen, A. Ramirez, and A. Faaij, "Model development and process simulation of postcombustion carbon capture technology with aqueous

AMP/PZ solvent," *International Journal of Greenhouse Gas Control*, vol. 47, pp. 176–199, Apr. 2016, doi: 10.1016/j.ijggc.2016.01.021.

[27] P. Moser *et al.*, "ALIGN-CCUS: Results of the 18-month test with aqueous AMP/PZ solvent at the pilot plant at Niederaussem – solvent management, emissions and dynamic behavior," *International Journal of Greenhouse Gas Control*, vol. 109, Jul. 2021, doi: 10.1016/j.ijggc.2021.103381.

[28] M. Rabensteiner, G. Kinger, M. Koller, and C. Hochenauer, "Pilot plant study of aqueous solution of piperazine activated 2-amino-2-methyl-1-propanol for post combustion carbon dioxide capture," *International Journal of Greenhouse Gas Control*, vol. 51, pp. 106–117, Aug. 2016, doi: 10.1016/j.ijggc.2016.04.035.

[29] "Henderson–Hasselbalch equation - Wikipedia." Accessed: May 24, 2024. [Online]. Available: https://en.wikipedia.org/wiki/Henderson%E2%80%93Hasselbalch_equation

[30] J. G. Webster, *The measurement, instrumentation, and sensors handbook*. CRC Press, 1999.

[31] "Beer Lambert Law | Transmittance & Absorbance | Edinburgh Instruments." Accessed: May 25, 2024. [Online]. Available: https://www.edinst.com/blog/the-beer-lambertlaw/#:~:text=The%20Beer%2DLambert%20law%20states,calculated%20by%20measuring%20its%20absorbance.

[32] "electromagnetic-waves.png." Accessed: Apr. 17, 2024. [Online]. Available: https://cdn1.byjus.com/wp-content/uploads/2020/11/electromagnetic-waves.png

[33] Sun, D. Fourier Transform Infrared (FTIR) Spectroscopy. In Infrared spectroscopy for food quality analysis and control, 2009. Amsterdam: Academic Press/Elsevier

[34] J. J. Ojeda and M. Dittrich, "Fourier transform infrared spectroscopy for molecular analysis of microbial cells," *Methods in Molecular Biology*, vol. 881, pp. 187–211, 2012, doi: 10.1007/978-1-61779-827-6_8.

[35] M. Koç and E. Karabudak, "History of spectroscopy and modern micromachined disposable Si ATR-IR spectroscopy," *Applied Spectroscopy Reviews*, vol. 53, no. 5. Taylor and Francis Inc., pp. 420–438, May 28, 2018. doi: 10.1080/05704928.2017.1366341.

[36] P. R. Griffiths and J. A. De Haseth, "Fourier Transform Infrared Spectrometry: Second Edition," *Fourier Transform Infrared Spectrometry: Second Edition*, pp. 1–529, Jun. 2006, doi: 10.1002/047010631X.

[37] "Silverstein, R. M., Webster, F. X. & Kiemle, D. J. Infrared spectrometry. In Spectrometric identification of organic compounds (7th ed.), 2005. Hoboken, NJ: John Wiley & Son.

[38] B. H. Stuart, "Infrared Spectroscopy: Fundamentals and Applications," *Infrared Spectroscopy: Fundamentals and Applications*, pp. 1–224, Jul. 2005, doi: 10.1002/0470011149.

[39] "What is Multivariate Data Analysis? | Analytics Steps." Accessed: May 11, 2024. [Online]. Available: https://www.analyticssteps.com/blogs/what-multivariate-data-analysis

[40] "Multivariate Data Analysis: In Practice : an Introduction to Multivariate ... - Kim H. Esbensen, Dominique Guyot, Frank Westad, Lars P. Houmoller - Google Bøker."

Accessed: May 11, 2024. [Online]. Available: https://books.google.no/books?id=Qsn6yjRXOaMC&printsec=frontcover&source=gbs_atb#v=onepage&q&f=false

[41] M. H. W. N. Jinadasa, K.-J. Jens, and M. Halstensen, "Process Analytical Technology for CO2 Capture," in *Carbon Dioxide Chemistry, Capture and Oil Recovery*, InTech, 2018. doi: 10.5772/intechopen.76176.

[42] P. H. C. Eilers, "A perfect smoother," *Analytical Chemistry*, vol. 75, no. 14. pp. 3631–3636, Jul. 15, 2003. doi: 10.1021/ac034173t.

[43] K. Robinson, A. McCluskey, and M. I. Attalla, "An ATR-FTIR study on the effect of molecular structural variations on the CO2 absorption characteristics of heterocyclic amines, part II," *ChemPhysChem*, vol. 13, no. 9, pp. 2331–2341, Jun. 2012, doi: 10.1002/cphc.201200066.

[44] A. Zanone, D. T. Tavares, and J. L. de Paiva, "An FTIR spectroscopic study and quantification of 2-amino-2-methyl-1-propanol, piperazine and absorbed carbon dioxide in concentrated aqueous solutions," *Vib Spectrosc*, vol. 99, pp. 156–161, Nov. 2018, doi: 10.1016/j.vibspec.2018.03.007.

[45] A. Zanone, D. T. Tavares, and J. L. de Paiva, "QUANTITATIVE SPECIATION OF THE LIQUID PHASE BY FTIR SPECTROSCOPY IN THE SYSTEM AMP-PZ-CO2-H2O," *Quim Nova*, vol. 45, no. 6, pp. 674–679, 2022, doi: 10.21577/0100-4042.20170883.

9 Appendices

Appendix A – Signed final project topic description.

Appendix B – Prepared PLS-R model for measured FTIR spectra and physical properties (Density, pH, and Conductivity).

Appendix C – Observation of precipitated samples.

Appendix D – Excel sheet record for the preparation of samples and estimated data of density, pH, and conductivity.

Appendix A – Signed final project topic description.

University of South Eastern Norway

Faculty of Technology, Natural Sciences and Maritime Sciences, Campus Porsgrunn

FMH606 Master's Thesis

Title: Monitoring a New Benchmark Solvent for CO_2 Capture: Pushing Technical Boundaries

USN supervisor: Maths Halstensen, Kjell-Arne Solli, Peshalya Kothalawala

External partner: TCM

Task background:

Speciation of CO_2 with monoethanolamine (MEA), the most widely used solvent in post combustion capture (PCC) of CO_2, has been well documented in literature. Presently, CESAR1 is proposed as the new benchmark solvent. CESAR1 is a blend made of aqueous 2-amino-2-methylpropan-1-ol (AMP) and piperazine (PZ). Compared to MEA, CESAR1 shows significantly lower specific energy demand for regeneration, lower degradation rates, larger capture capacity, and is less corrosive. Several studies have been conducted to test the effect of the AMP/PZ ratio. However, all these studies are based on off-line laboratory analytical techniques. Inline monitoring of species ratios is crucial for the predictive modelling of PCC systems. Moreover, spectroscopy is recognized as an efficient approach for monitoring mixed amine systems, given the high complexity of the solvent blend.

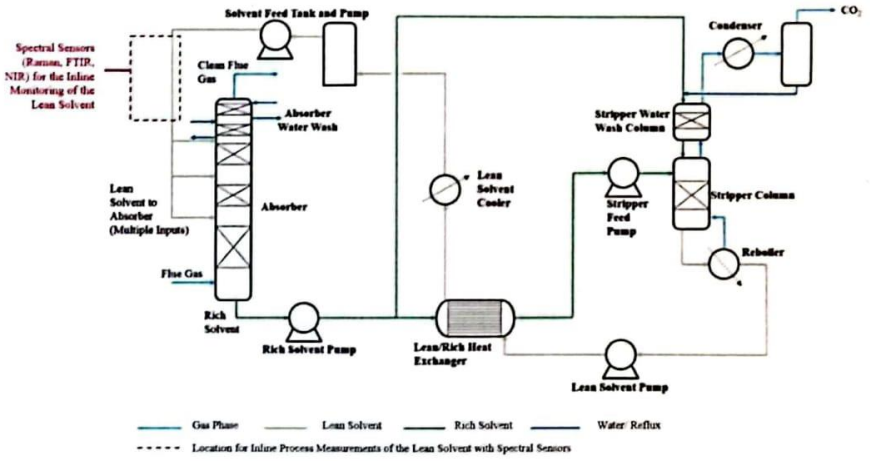

Figure 1: Schematic of TCM Amine Plant (Morgan et al., 2022)

Task description:

The primary objective of this project is to conduct experimental work to identify spectral regions of interest for the speciation of CESAR1. With the guidance from supervisors, multivariate regression modelling for the speciation of CESAR1 will be conducted. This work will be an integral component of a forthcoming scientific journal paper. Furthermore, there is the potential for a summer job opportunity linked to this project. This project will be carried out in collaboration with URGENT and TCM.

Student category: EET and PT

Is the task suitable for online students (not present at the campus)? No

Practical arrangements: Analytical instruments and chemicals required are available in the laboratory.

Supervision:

As a general rule, the student is entitled to 15-20 hours of supervision. This includes necessary time for the supervisor to prepare for supervision meetings (reading material to be discussed, etc).

Signatures:

Supervisor (date and signature): 3/1-2024

Student (write clearly in all capitalized letters): ALAMGIR ALAM

Student (date and signature): 30/01/2024 Alamgir Alam

Appendix B – Prepared PLS-R model for measured FTIR spectra and physical properties (Density, pH, and Conductivity).

1. Raw and Pre-processed FTIR Spectra used in CO_2 Loading, AMP, and PZ Model

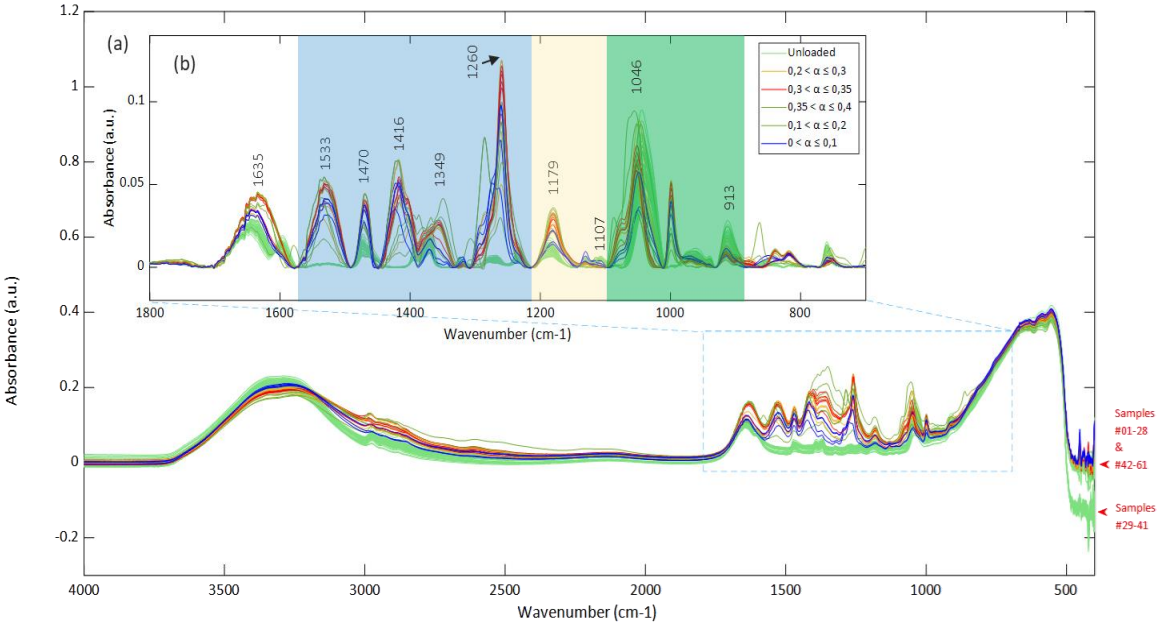

Figure 9.1: FTIR spectra (a) raw spectra (full spectral range), (b) preprocessed spectra (1800 - 700 cm^{-1}), IR band assignments (according to Table 9.1) are displayed next to the respective peaks, Color Code: Blue - for CO_2 loading; Yellow - used in PZ model; Green - used in AMP model.

2. PLS-R Models, Identified and Corresponding Literature IR Bands, Variable Ranges of the Models

Table 9.1: PLS-R models, identified and corresponding literature IR bands, variable ranges of the model.

Compound	Specie Concerned	Band Attribution	Wavenumber (cm^{-1})		
			IR Bands Reported in Literature	Identified IR Bands in the Study	Variable Range of Models (cm^{-1})
α (CO_2 Loading)	$PZCOO^-$, ^-OOC-PZ-COO^-	νasCOO$^-$ (asymmetric stretching band)	1524 [43, 44, 45], 1546 [43, 44, 45]	1533	1575-1213
		νsCOO$^-$ (Symmetric stretching band)	1425*[43], 1432 [43]	1416	
		νN–COO$^-$ (Stretching vibration)	1265*[43, 44, 45], 1276 [43], 1289 [43, 44, 45], 1294 [43]	1260	
	HCO_3^-	νsC–O (Symmetric stretching band)	(1360-1354) [43], 1355 [44, 45]	1349	
		νasC–O (Asymmetric stretching band)	1382 [44, 45]	-	
PZ	PZH^+ and $^+HPZH^+$	δsNH_2^+ (Vibration band)	1470 [43, 44, 45]	1470	1213-1096
	PZ	νmC–N (Medium stretching band)	1130 [45], 1100 [45], 1087 [45]	1107	
AMP	$AMPH^+$	$\delta asNH_3^+$ (Asymmetric bending band) δsNH_3^+ (Symmetric bending band)	1636 [44, 45] 1534 [44, 45]	1635 1533	1095-877
	AMP	νC–N and νC–O overlap (Stretching band) τN-H (Twisting band)	1044 [44, 45] 915 [44, 45]	1046 913	

3. Predicted PLS-R Model with speciation for 'α – CO_2 Loading'

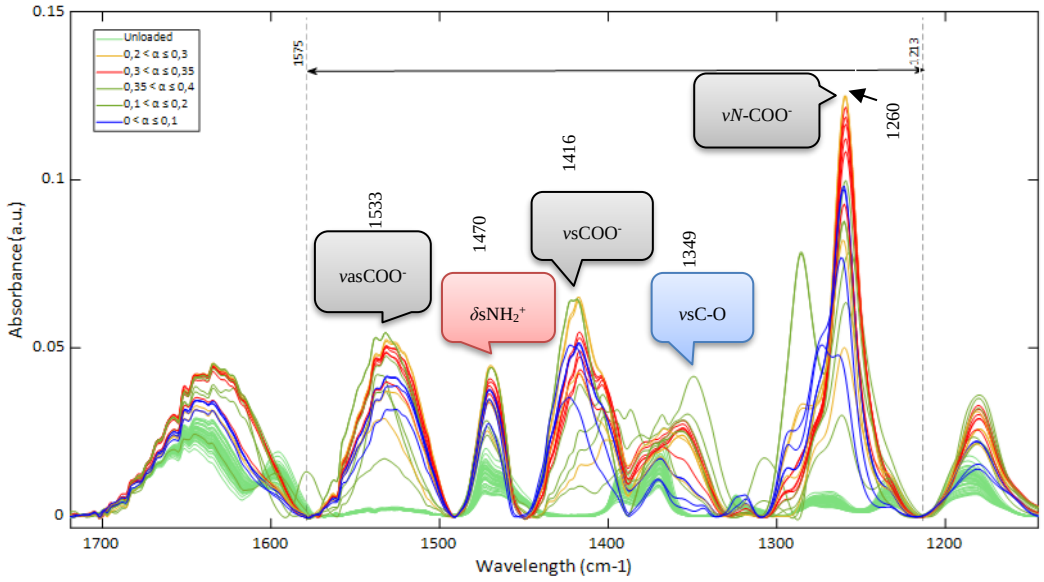

Figure 9.2: Predicted PLS-R Model with speciation for 'α - CO_2 Loading' with wavelength region (1575 - 1213 cm^{-1}).

3(a). Predicted vs. Measured PLS Model for 'α – CO_2 Loading' (1575-1213 cm^{-1}, Cal/Val, 3-LV)

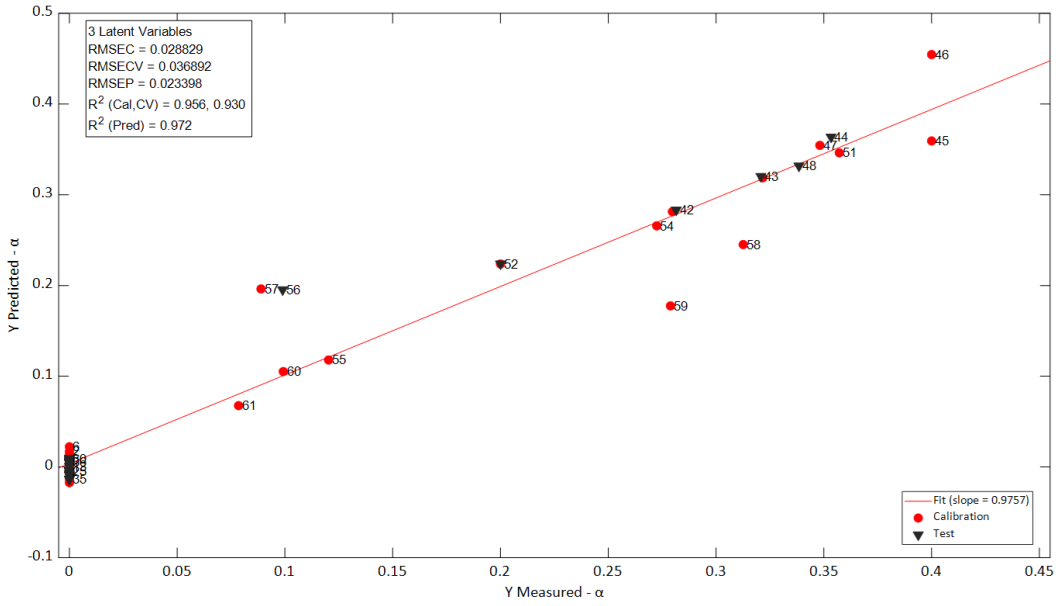

Figure 9.3: Predicted vs. measured PLS-R model for 'α – CO_2 loading' with wavelength region (1575 - 1213 cm^{-1}).

3(b). Score plots, T^2 vs. Q-Residual Plots and Regression Vector for 'α – CO_2 Loading' Model (1575-1213 cm^{-1}, Cal/Val, 3-LV)

(a)

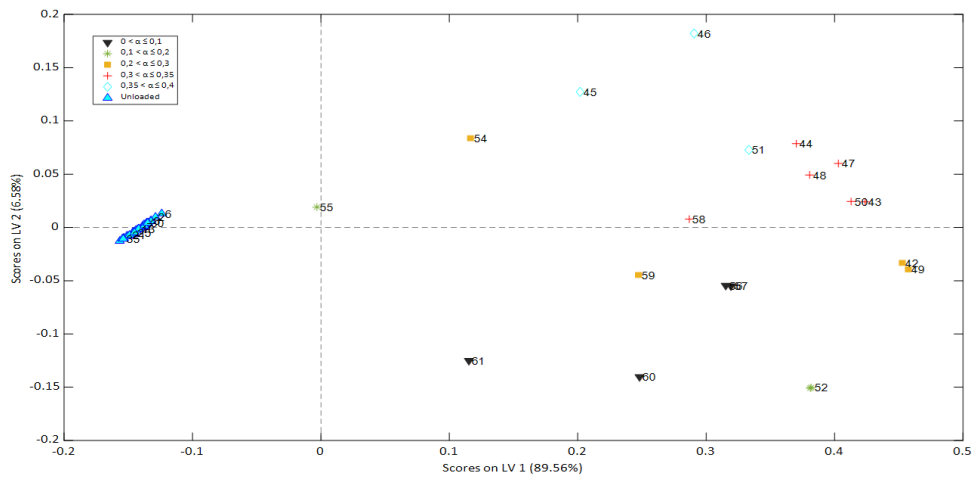

(b)

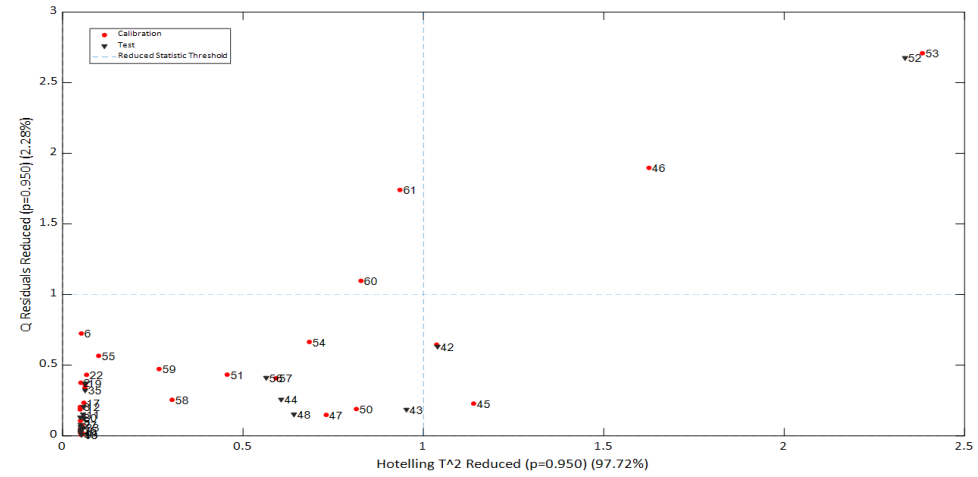

(c)

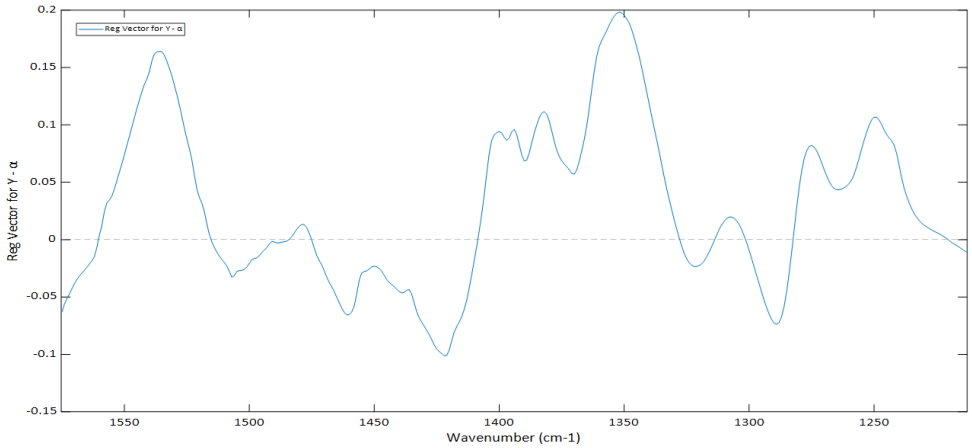

Figure 9.4: Results from PLS-R model for CO_2 loading; (a) score plot of LV 1 vs. 2 showing different loading ratios and (b) T^2 vs. Q plot for calibration and test samples (c) regression coefficient corresponding to their wavenumber.

4. Predicted PLS-R Mode with speciation for ‘AMP Concentration

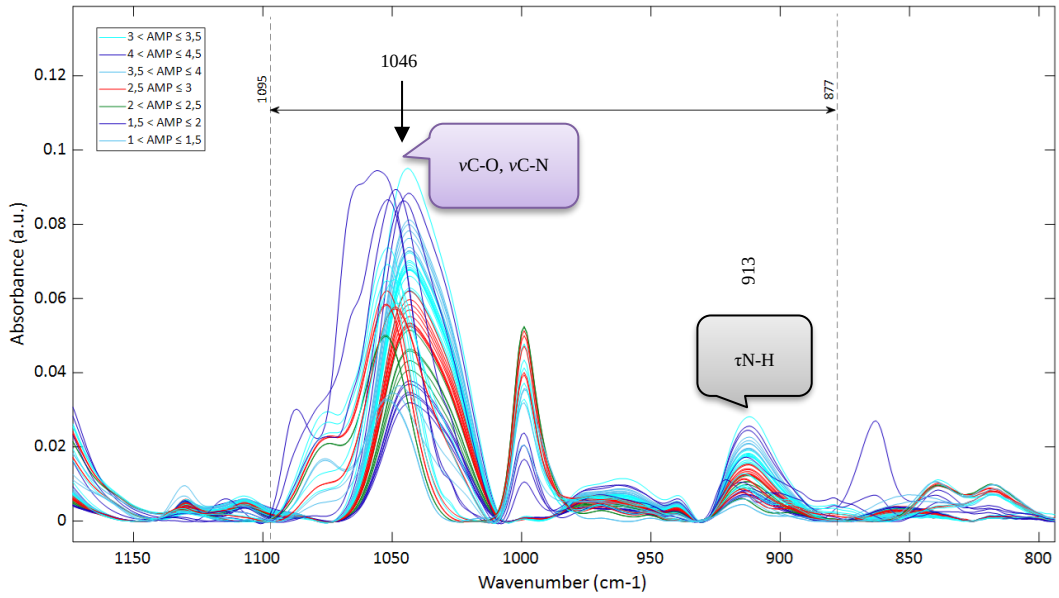

Figure 9.5: Predicted PLS-R model for ‘AMP concentration’ with wavelength region (1095 - 877 cm^{-1}).

4(a). Predicted vs. Measured PLS-R Model for ‘AMP Concentration’ with RMSEP, PLS (1095-877 cm^{-1}, Cal/Val, 2-LV) without Outliers

(a)

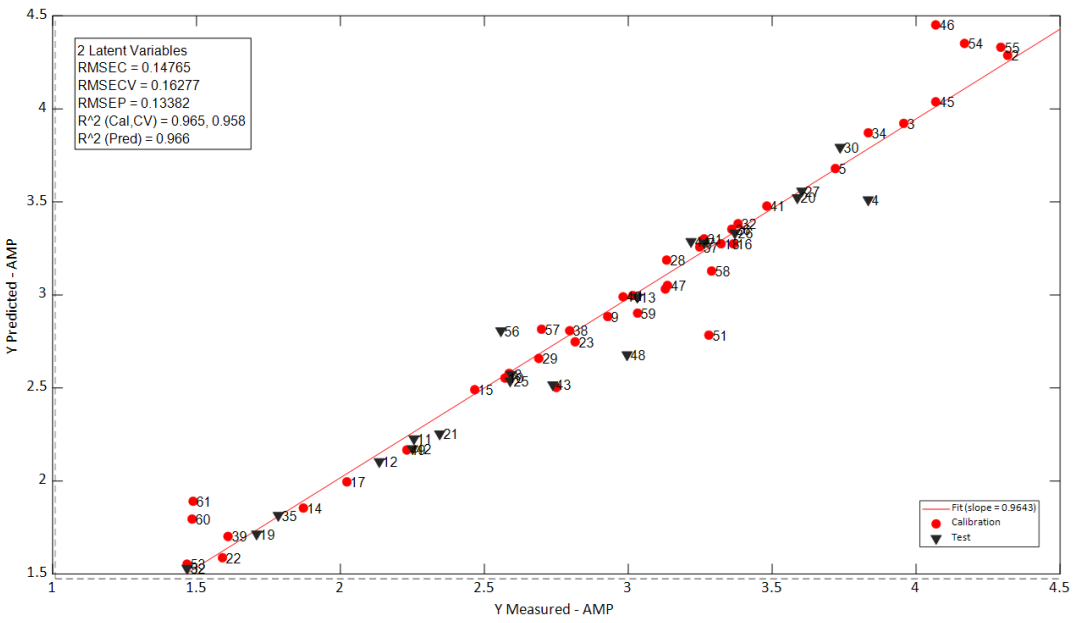

(b)

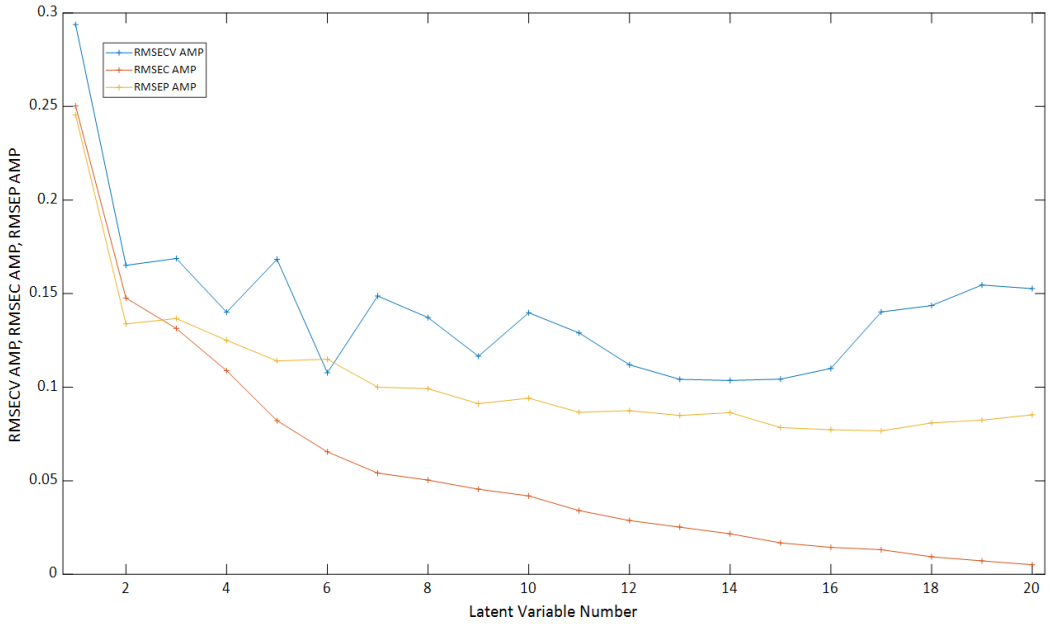

Figure 9.6: Results from PLS-R model (a) Predicted vs. measured PLS-R model for 'AMP concentration' and (b) RMSEP, RMSEC model vs. LVs for 'AMP Concentration' with wavelength region (1095 - 877 cm^{-1}).

4(b). Score, T^2 vs. Q-Residual, Regression coefficients for 'AMP' Model (1095-877 cm^{-1}, Cal/Val, 2-LV) without Outliers

(a)

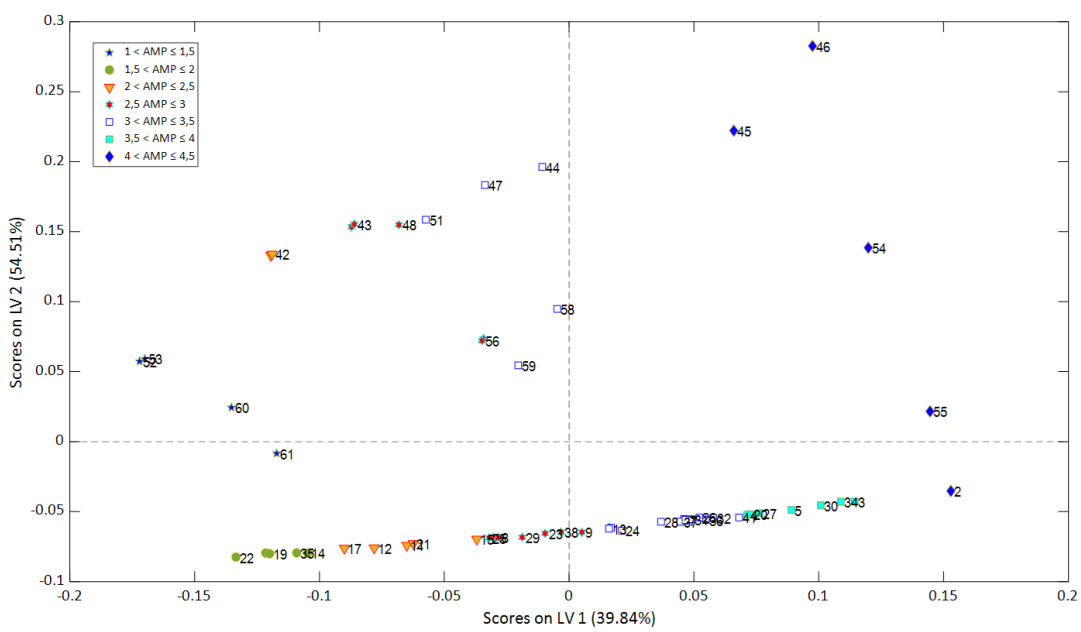

(b)

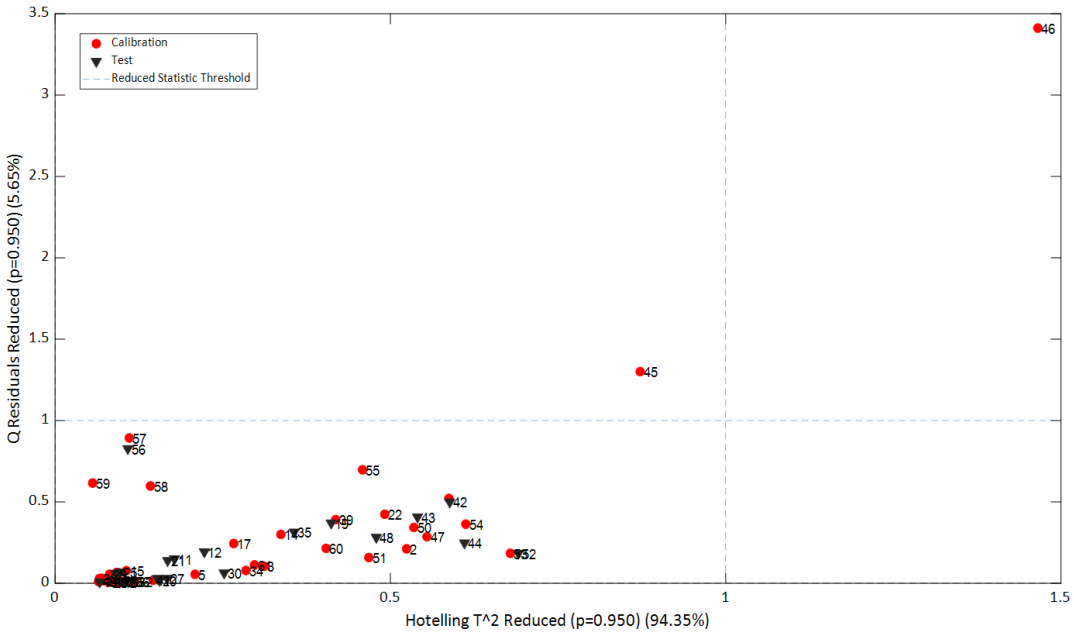

(c)

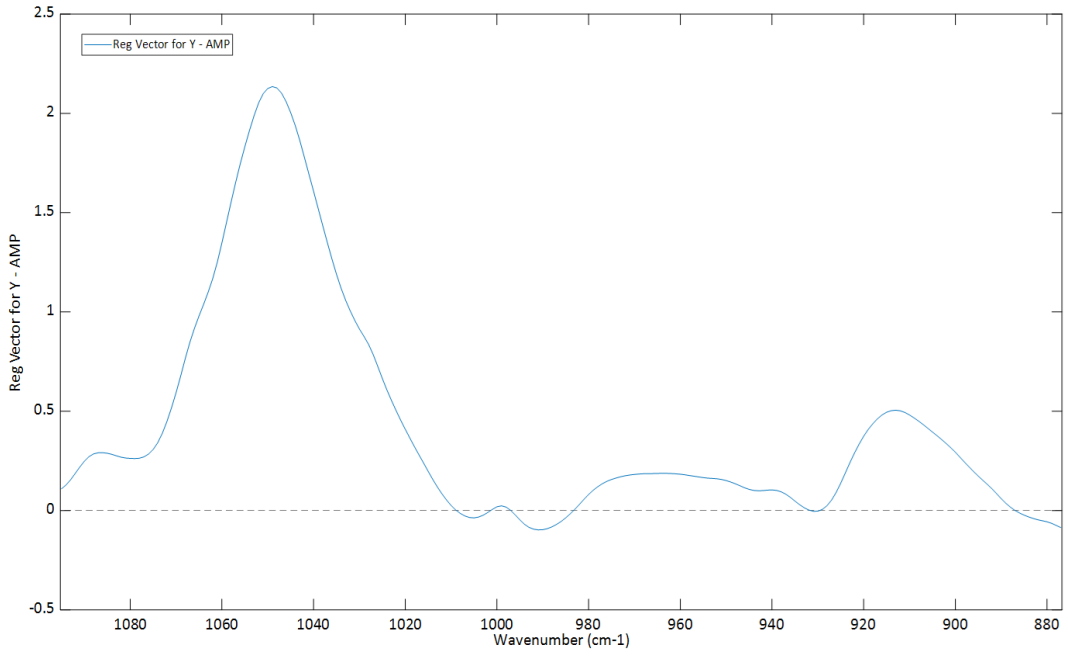

Figure 9.7: Results from PLS-R model for AMP; (a) score plot of LV 1 vs. 2 with different AMP concentrations, (b) T^2 vs. Q - residual plot and (c) regression coefficient with wavenumber without outliers.

5. Predicted PLS-R Model for 'PZ Concentration'

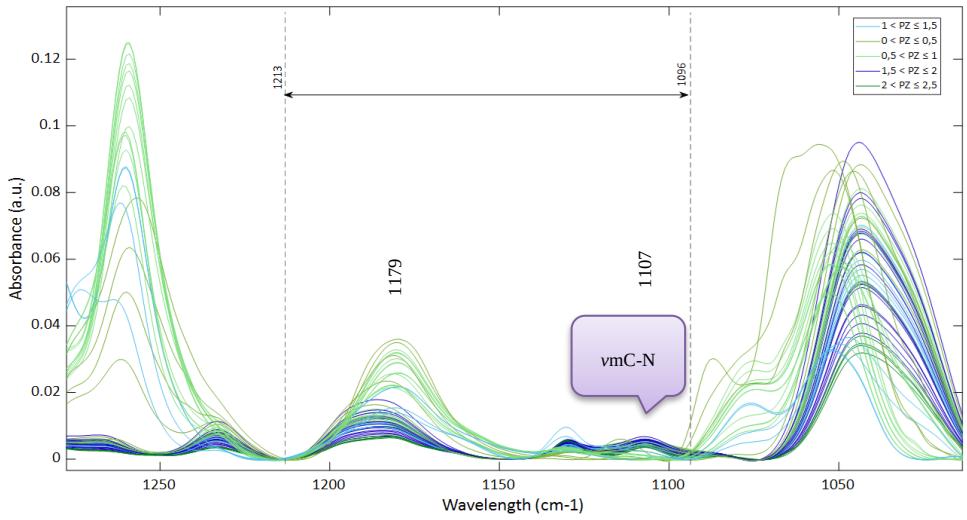

Figure 9.8: Predicted PLS-R model for 'PZ concentration' with wavelength region (1213 - 1096 cm^{-1}).

5(a). Predicted vs. Measured PLS-R Model for 'PZ Concentration' with RMSEP, (1213-1096 cm^{-1}, Cal/Val, 3-LV) without Outliers

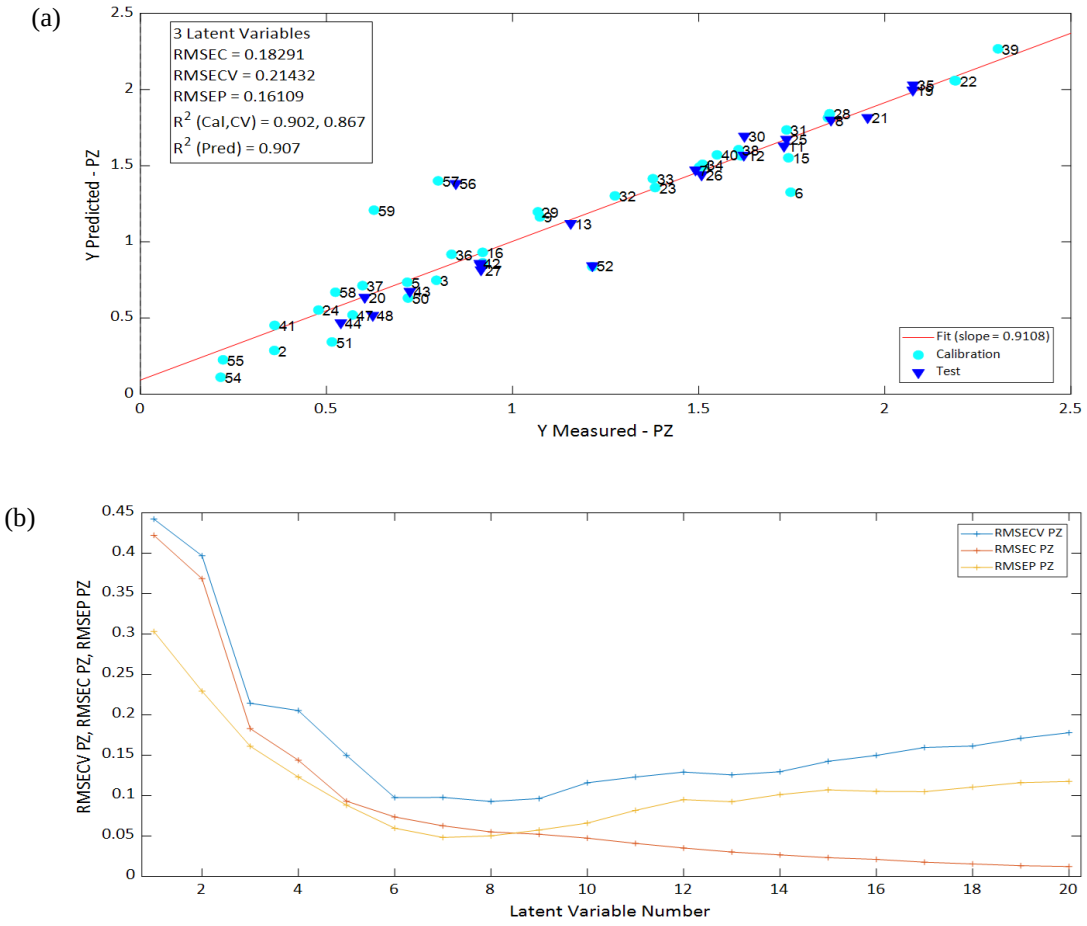

Figure 9.9: Results from PLS-R model (a) Predicted vs. measured PLS-R model for 'PZ concentration' and (b) RMSEP, RMSEC model vs. LVs for 'PZ Concentration' with wavelength region (1213 - 1096 cm^{-1}) after removing outlier (samples 45, 46, 60 and 61).

5(b). Score and T^2 vs. Q-Residual Plots for 'PZ' Model (1213-1096 cm^{-1}, Cal/Val, 3-LV)

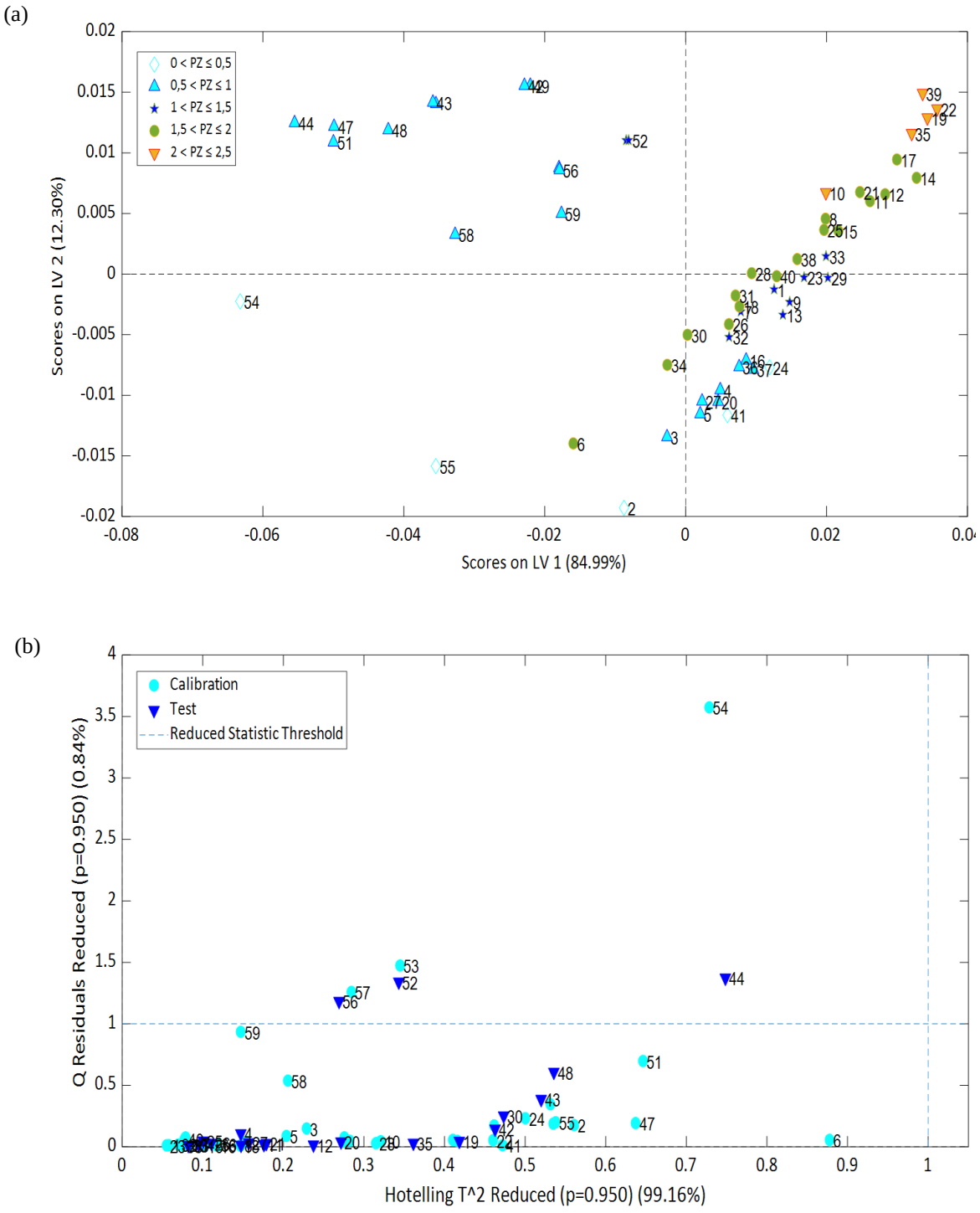

Figure 9.10: Results from PLS-R model for PZ; (a) score plot of LV 1 vs. 2 with different PZ concentrations, (b) T^2 vs. Q – residual plot after removing outlier samples (45, 46, 60 and 61).

6. Raw and Pre-processed FTIR Spectra used in Density, pH, and Conductivity Model

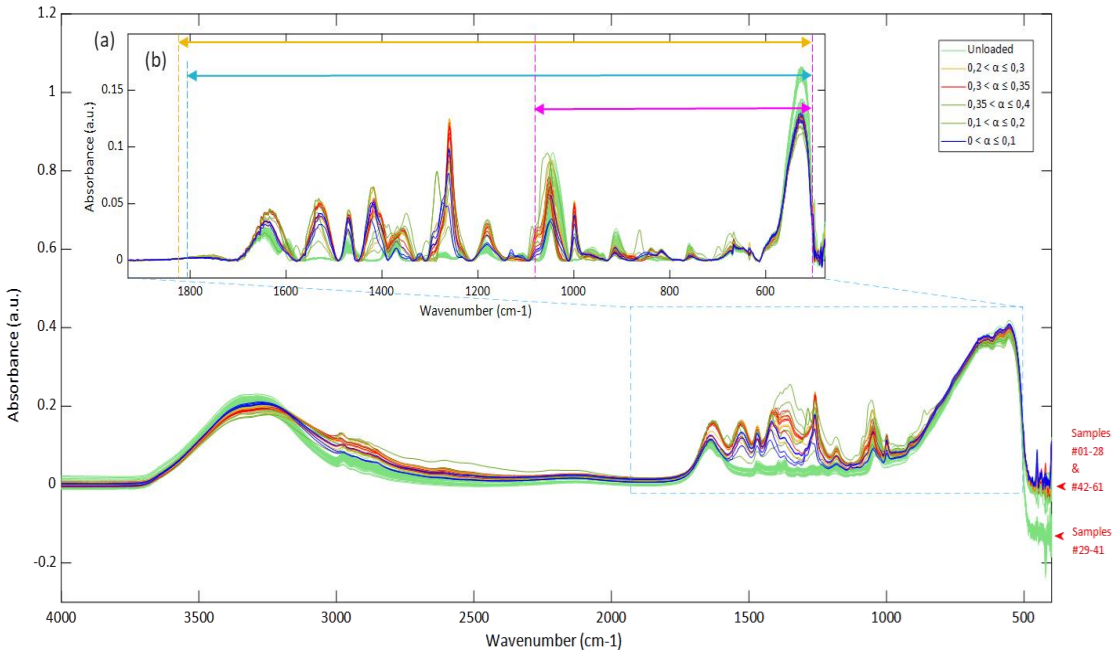

Figure 9.11: FTIR spectra (a) raw spectra (full spectral range), (b) preprocessed spectra wavelength region (1920 - 500 cm^{-1}), Color Code: Purple - used in density model; Dark Yellow - used in pH model; Turquoise - used in conductivity model.

7. Predicted vs. Measured PLS-R Model for 'Density' with T^2 vs. Q-Residual plot (1080-502 cm^{-1}, Cal/Val, 3-LV)

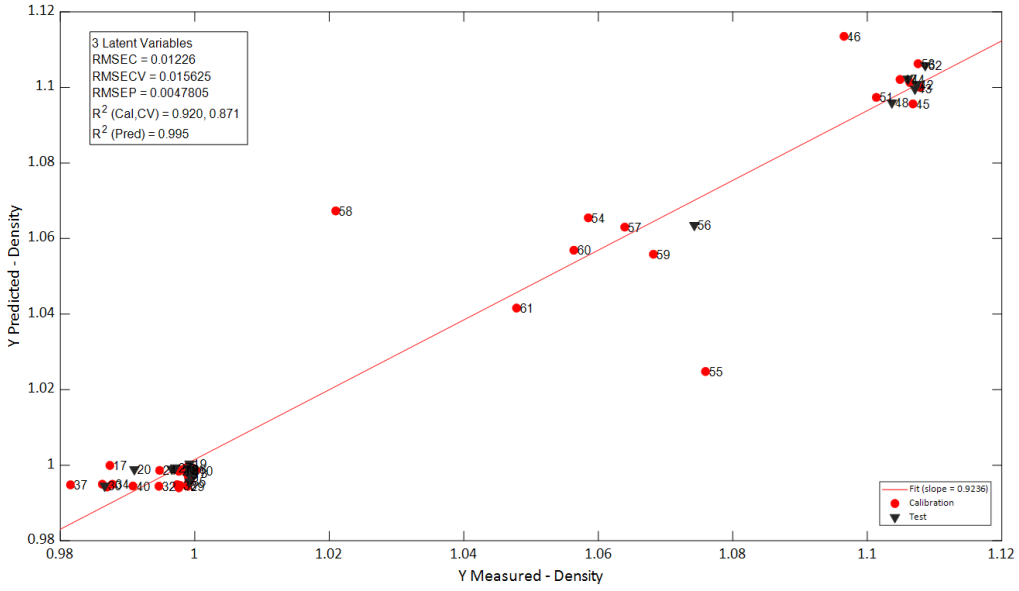

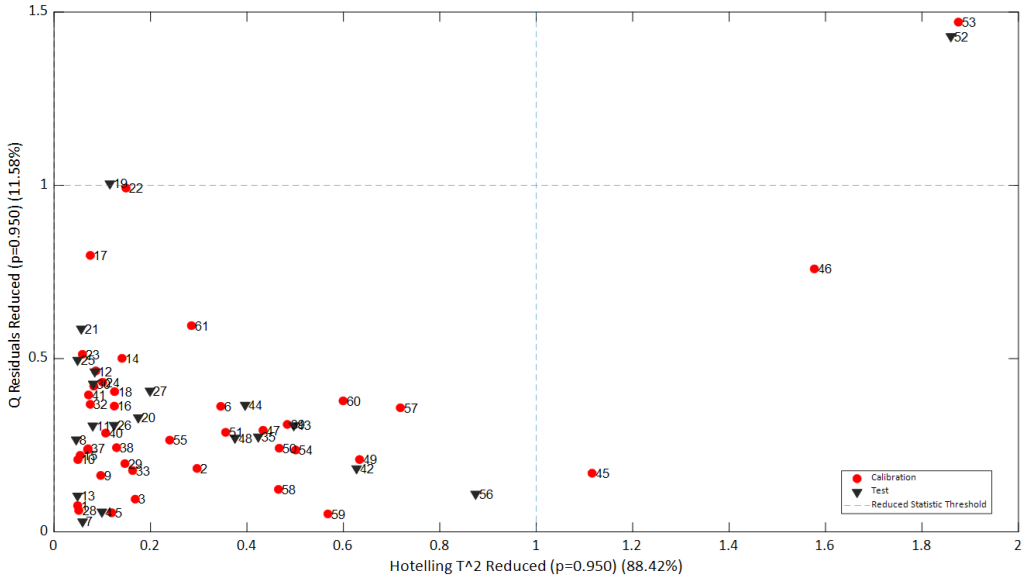

Figure 9.12: Results from PLS-R model (a) Predicted vs. measured PLS-R model for 'Density' and, (b) Hotelling T^2 vs. Q-residual plot.

7(a). Score and Regression vector for 'Density' Model (1080-502 cm^{-1}, Cal/Val, 3-LV)

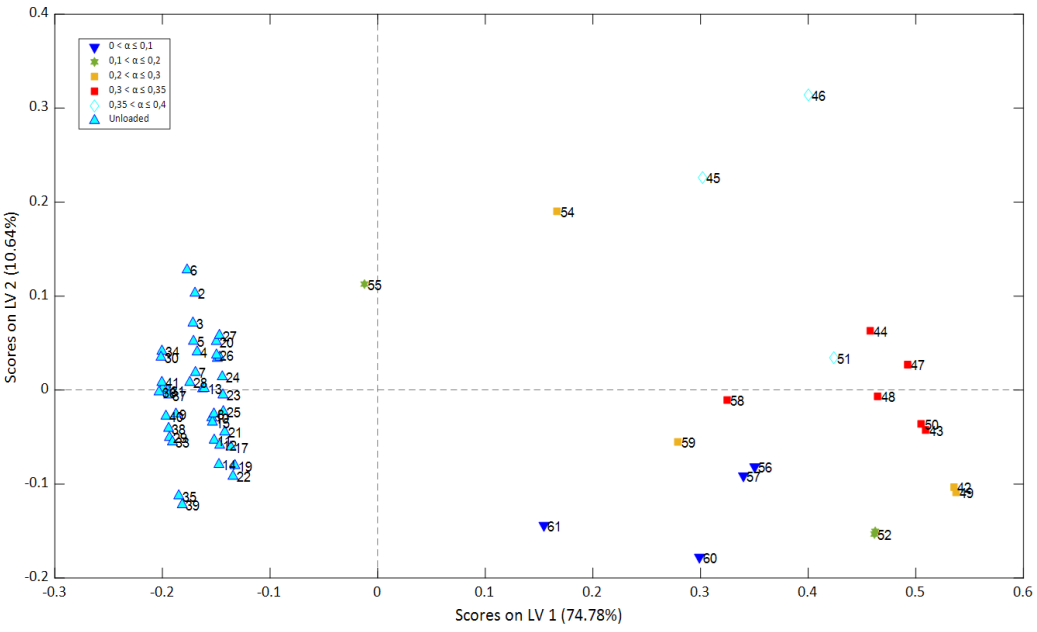

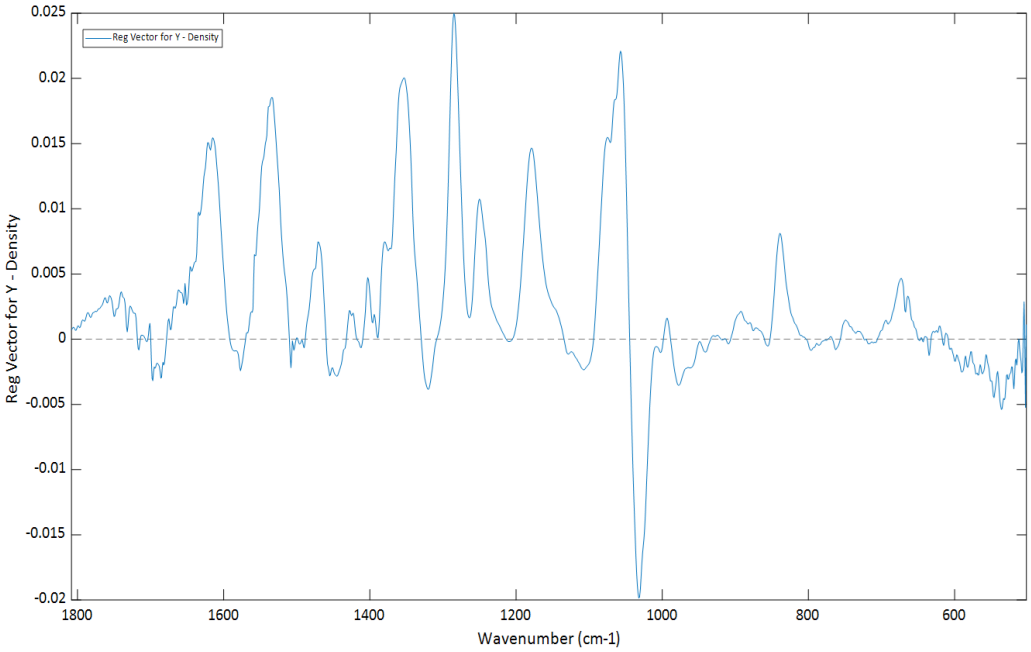

Figure 9.13: Results from PLS-R model for Density; (a) score plot of LV 1 vs. 2 with different loading ratio, (b) regression vector (1080-502 cm^{-1}, cal/val, 3-LV) for Density.

8. Predicted vs. Measured PLS-R Model for 'pH' with RMSEP plot, (1835-502 cm^{-1}, Cal/Val, 3-LV)

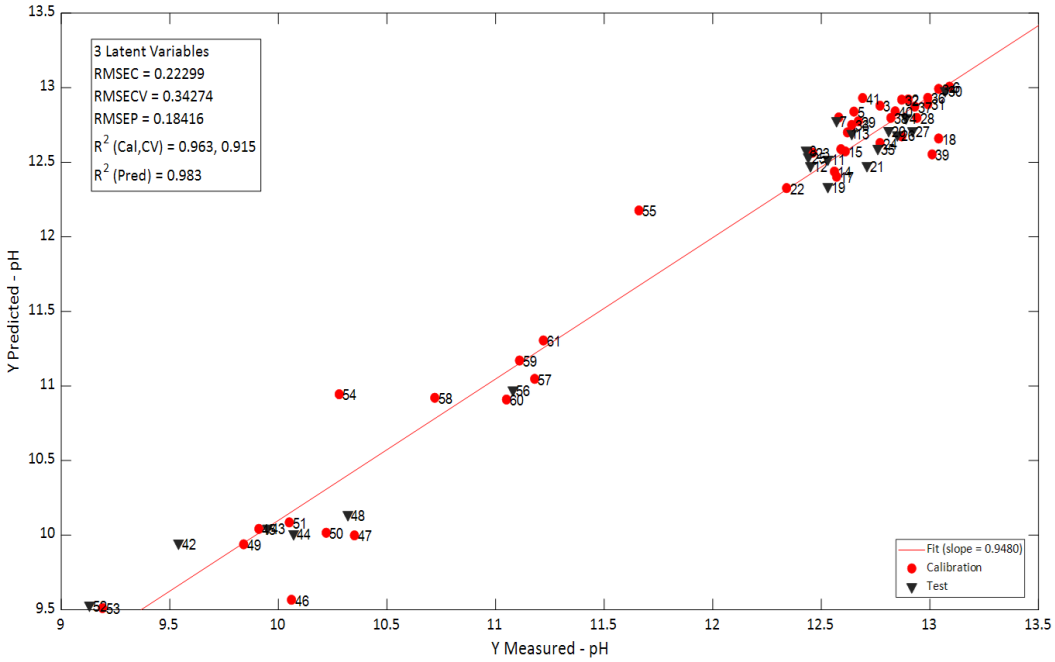

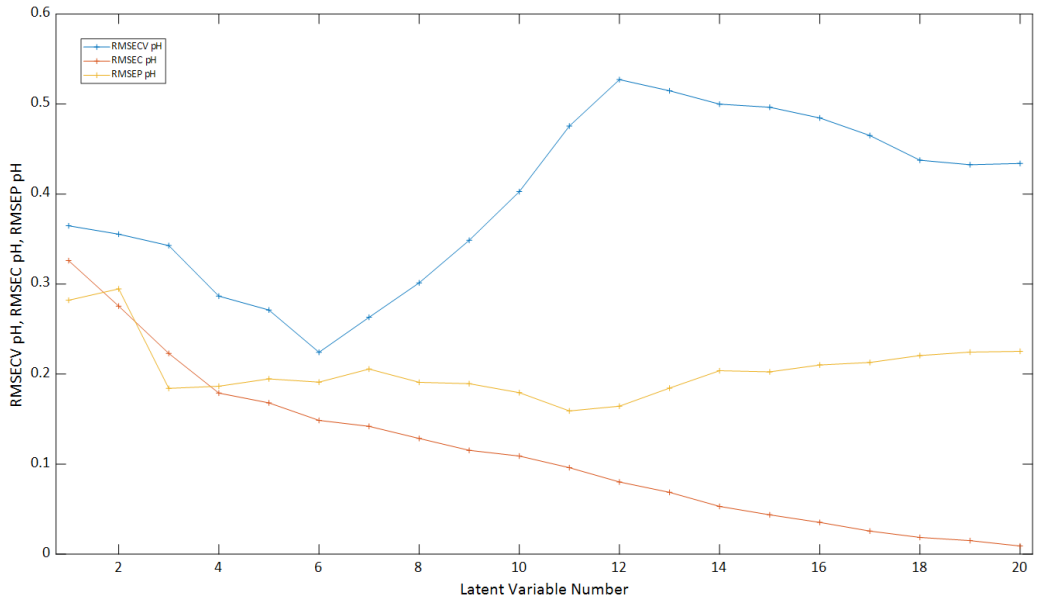

Figure 9.14: Results from PLS-R model (a) Predicted vs. measured PLS-R model for 'pH' and (b) RMSEP with respect to number of latent variables.

8(a). Score, T^2 vs. Q-Residual and Regression coefficients for 'pH' Model (1835-502 cm^{-1}, Cal/Val, 3-LV)

(a)

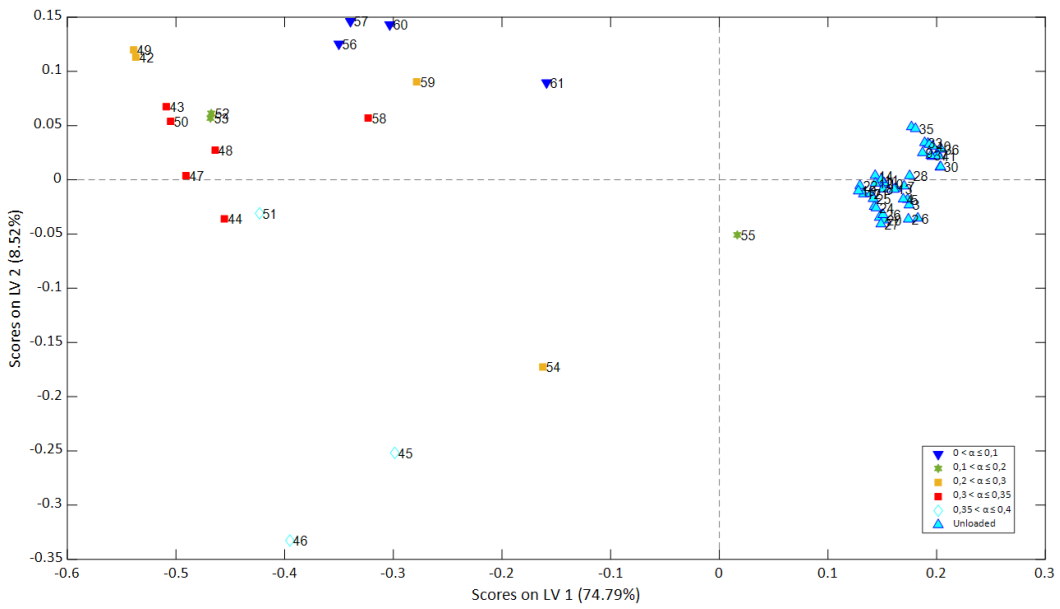

(b)

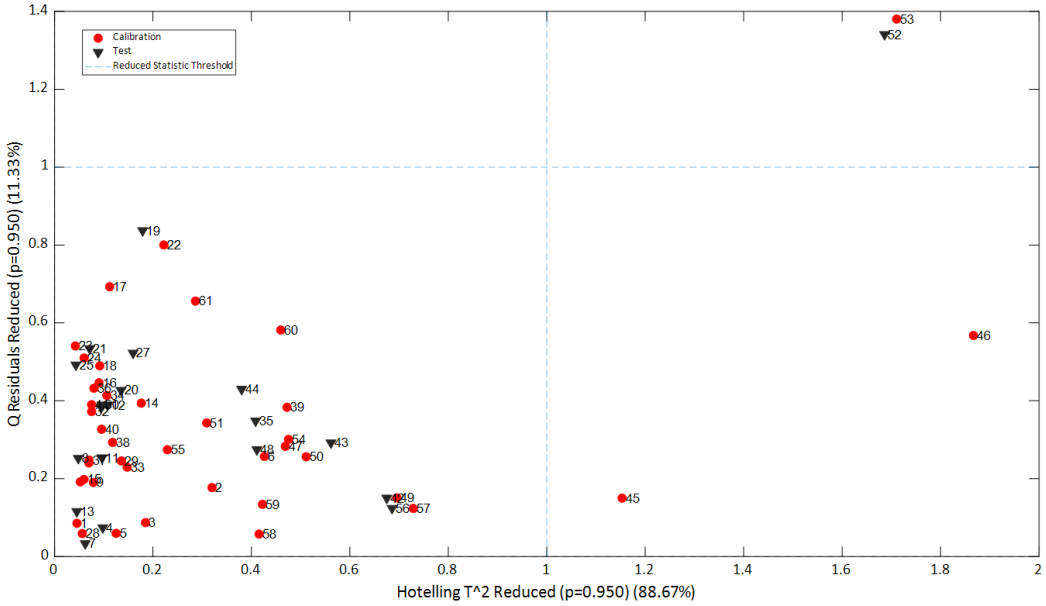

(c)

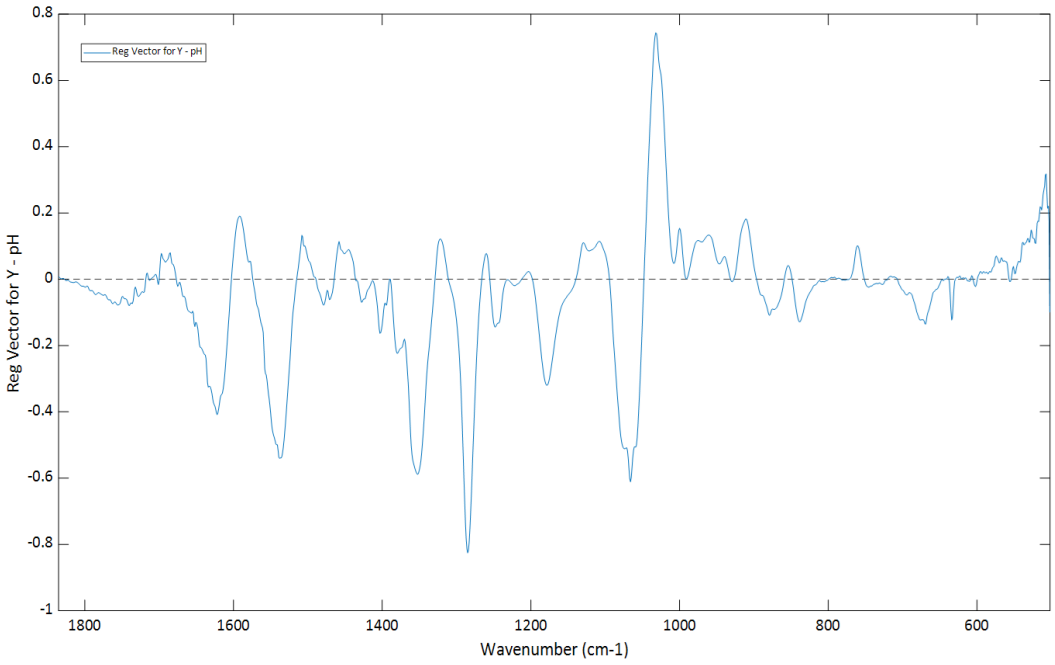

Figure 9.15: Results from PLS-R model for pH; (a) score plot of LV 1 vs. 2, (b) T^2 vs. Q - residual plot and (c) regression coefficient with respect to wavenumber.

9. Predicted vs. Measured PLS-R Model for 'Conductivity' with RMSEP plot, (1810-502 cm^{-1}, Cal/Val, 4-LV)

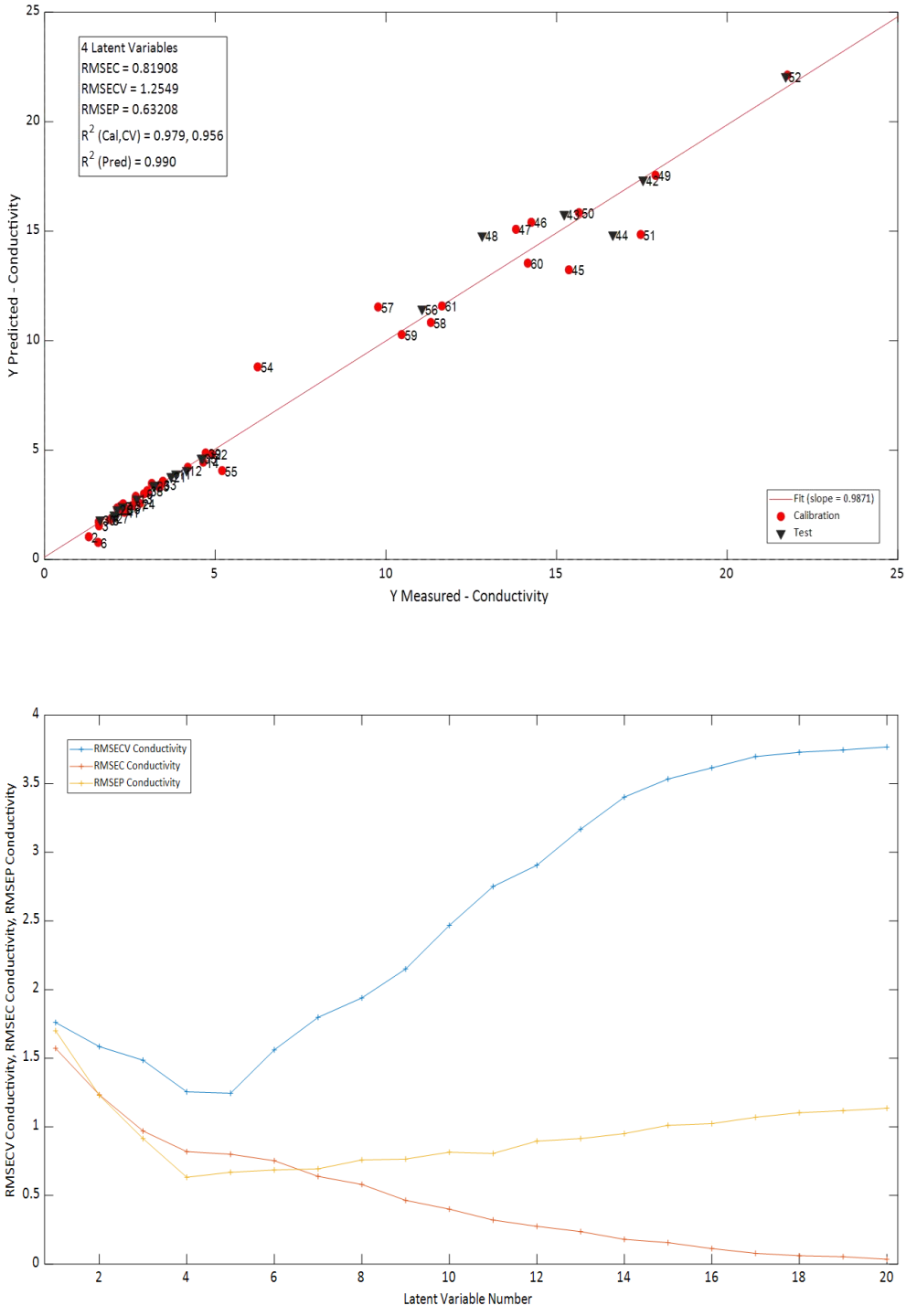

Figure 9.16: Results from PLS-R model (a) Predicted vs. measured PLS-R model for 'Conductivity' and (b) RMSEP with respect to number of latent variables.

9(a). Score, T^2 vs. Q-Residual and Regression coefficients for 'Conductivity' Model (1810-502 cm^{-1}, Cal/Val, 4-LV)

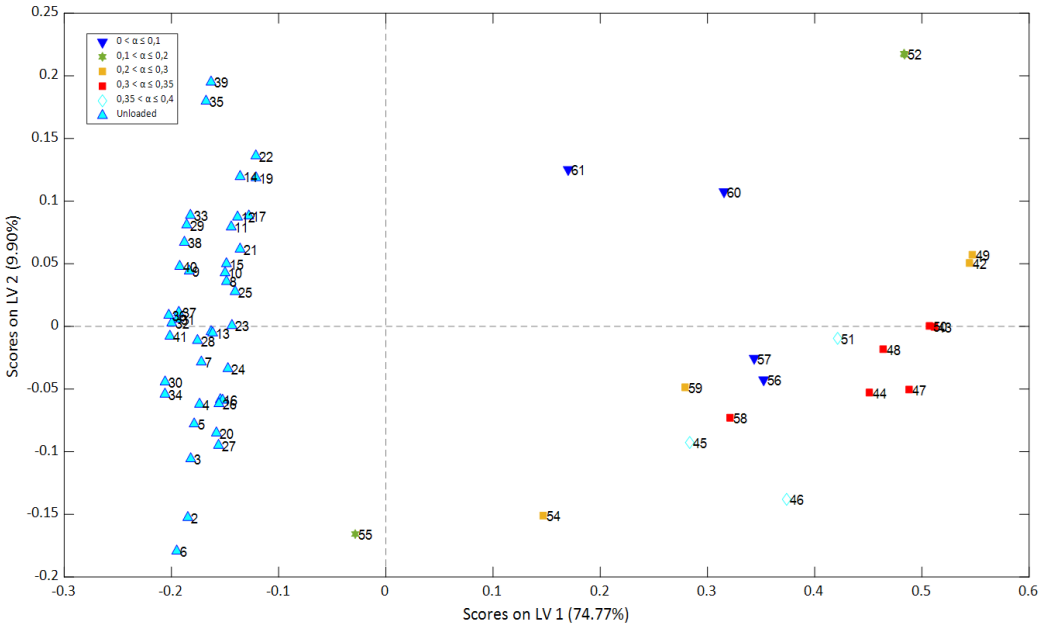

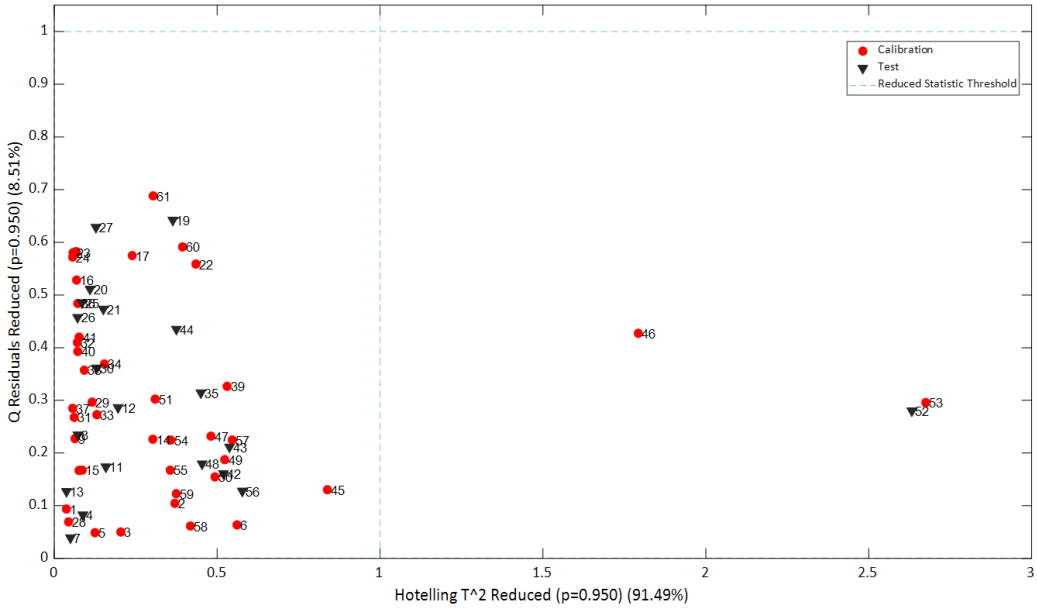

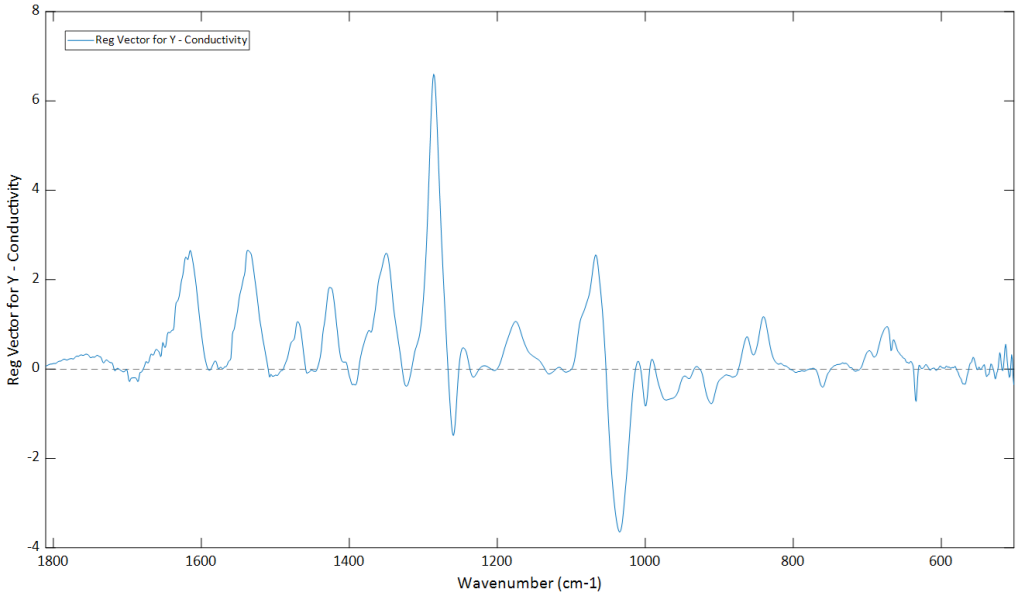

Figure 9.17: Results from PLS-R model for conductivity; (a) score plot of LV 1 vs. 2, (b) T^2 vs. Q - residual plot and (c) regression coefficient with respect to wavenumber.

10. Identified Outliers for AMP and PZ Model

Table 9.2: Identified outliers by using the PLS model.

Outliers for AMP model	Outliers for PZ model
6	45, 46, 60 and 61

(a)

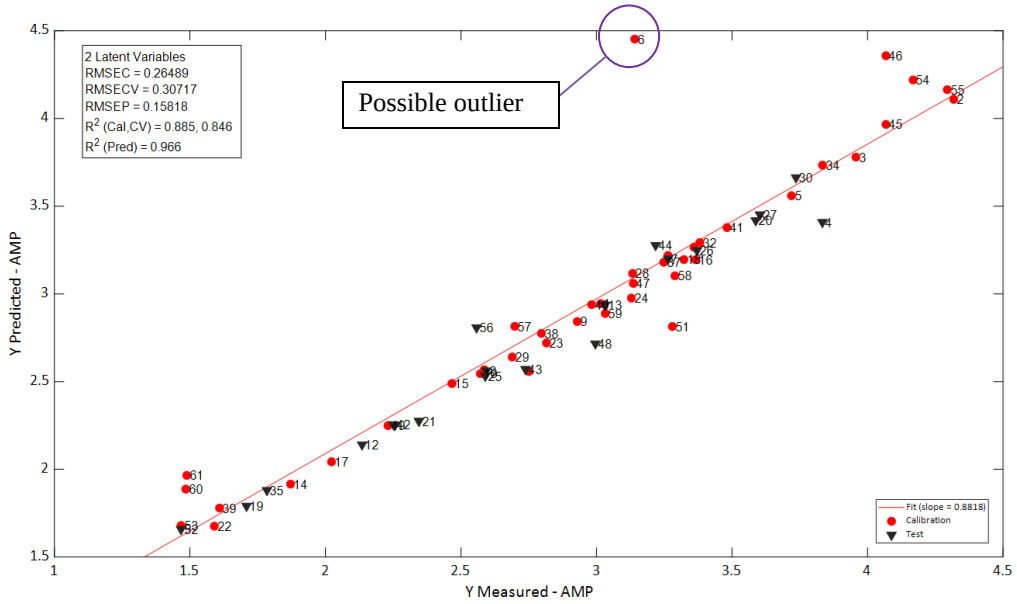

(b)

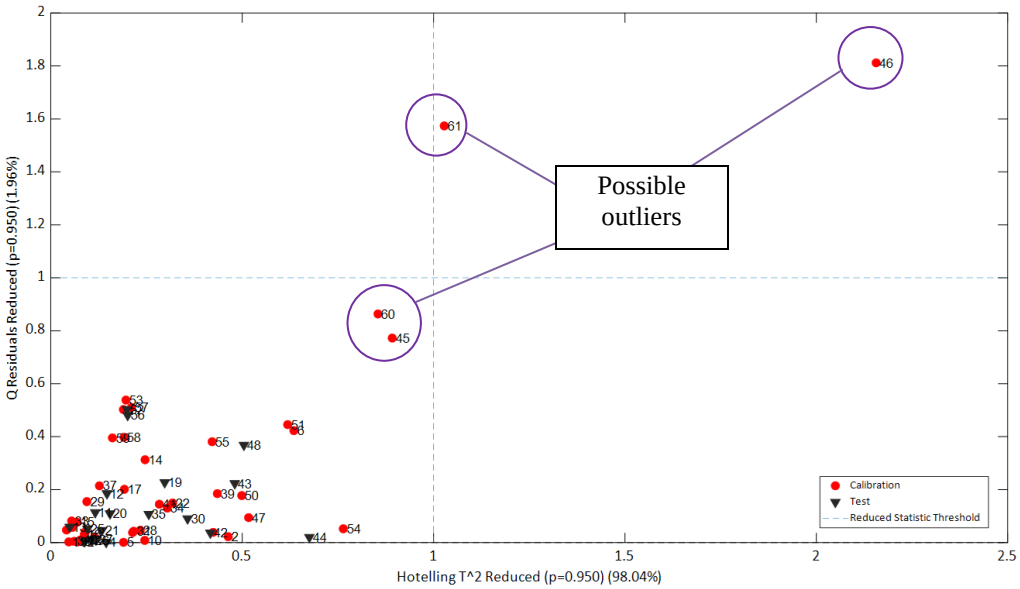

Figure 9.18: Possible identified outliers for (a) AMP model and (b) PZ model.

Appendix C – Observation of precipitated samples.

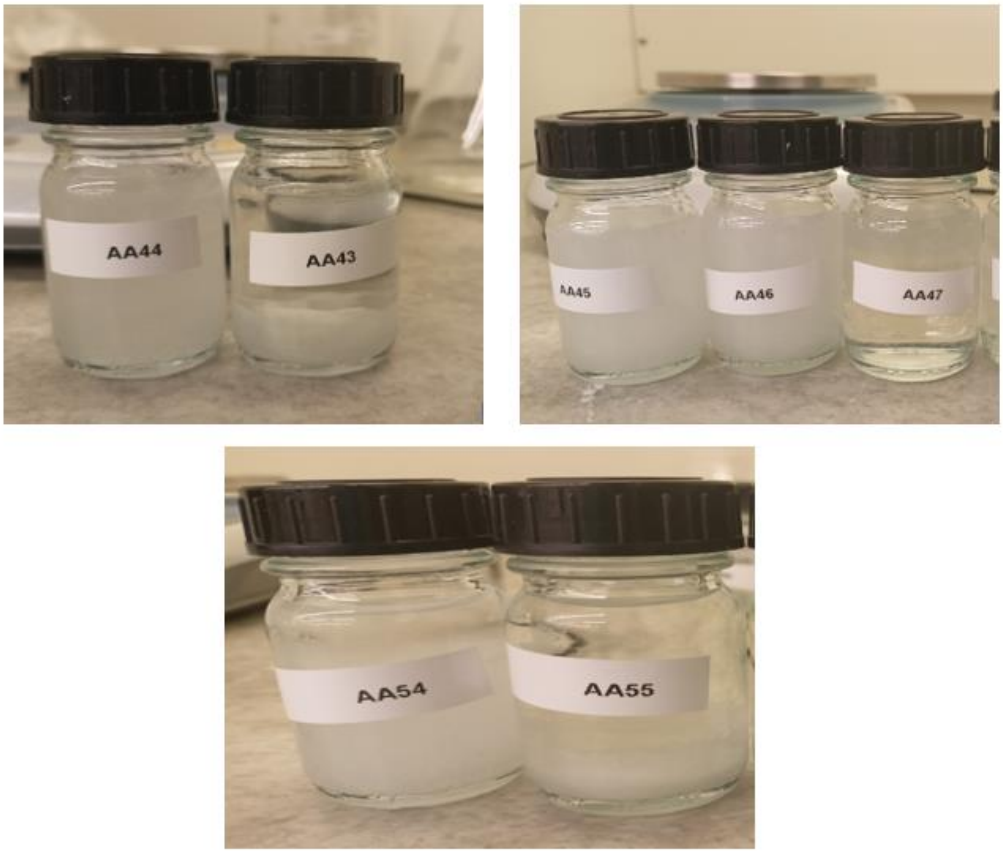

Figure 9.19: Precipitated samples.

Appendix D – Excel sheet record for the preparation of samples and estimated data of density, pH, and conductivity.

Label	Sample NO	AMP: wt%	Vol. AMP (mL)	PZ : wt%	Vol. PZ (mL)	H2O: wt%	Vol. H2O (mL)	T.vol (L)	Initial Amp (mol/L)	Initial Pz (mol/L)	Initial H2O (mol/L)	Initilal AMP (g in 30 ml*)	Initial PZ (g in 30 ml*)	H2O (g in 30 mL*)	Actual AMP (g in 30 ml*)	Actual PZ (g in 30 mL*)	Actual H2O (g in 30 ml*	Total (g)
AAS1	1	27	28.90792291	13	13.0260521	60	60	0.101933975	3	1.5	32.7	7.9	3.8	17.7	7.9192	3.8107	17.7305	29.4604
AAS2	2	38	40.68522484	3	3.006012024	59	59	0.102691237	4.2	0.3	31.9	11.1	0.9	17.2	11.2213	0.9041	17.0277	29.1531
AAS3	3	35	37.4732334	7	7.014028056	58	58	0.102487261	3.8	0.8	31.4	10.2	2	17	10.38	2.0163	17.0311	29.4274
AAS4	4	34	36.40256959	8	8.016032064	58	58	0.102418602	3.7	0.9	31.4	10	2.3	17	10.0481	2.3138	17.0422	29.4041
AAS5	5	33	35.33190578	6	6.012024048	61	61	0.10234393	3.6	0.7	33.1	9.7	1.8	17.9	9.7864	1.823	17.9071	29.5165
AAS6	6	28	29.97858672	15	15.03006012	57	57	0.102008647	3.1	1.7	31	8.2	4.4	16.8	8.2613	4.4405	16.8025	29.5043
AAS7	7	29	31.04925054	13	13.0260521	58	58	0.102075303	3.2	1.5	31.5	8.5	3.8	17	8.627	3.8091	17.2127	29.6488
AAS8	8	23	24.62526767	16	16.03206413	61	61	0.101657332	2.5	1.8	33.3	6.8	4.7	18	6.8407	4.7297	18.0214	29.5918
AAS9	9	26	27.8372591	9	9.018036072	65	65	0.101855295	2.9	1	35.4	7.7	2.7	19.1	7.714	2.7328	19.1006	29.5474
AAS10	10	23	24.62526767	19	19.03807615	58	58	0.101663344	2.5	2.2	31.7	6.8	5.6	17.1	6.8185	5.606	17.3217	29.7462
AAS11	11	20	21.41327623	15	15.03006012	65	65	0.101443336	2.2	1.7	35.6	5.9	4.4	19.2	5.9454	4.405	19.2225	29.5729
AAS12	12	19	20.34261242	14	14.02805611	67	67	0.101370669	2.1	1.6	36.7	5.6	4.1	19.8	5.6281	4.1301	19.8139	29.5721
AAS13	13	27	28.90792291	10	10.02004008	63	63	0.101927963	3	1.1	34.3	7.9	2.9	18.5	7.9345	2.9246	18.5048	29.3639
AAS14	14	17	18.2012848	13	13.0260521	70	70	0.101227337	1.9	1.5	38.4	5	3.9	20.7	5.0226	3.9191	21.1695	30.1112
AAS15	15	22	23.55460385	15	15.03006012	63	63	0.101584664	2.4	1.7	34.4	6.5	4.4	18.6	6.503	4.4357	18.6365	29.5752
AAS16	16	30	32.11991435	8	8.016032064	62	62	0.102135946	3.3	0.9	33.7	8.8	2.3	18.2	8.8301	2.3315	18.273	29.4346
AAS17	17	18	19.27194861	16	16.03206413	66	66	0.101304013	2	1.8	36.2	5.3	4.7	19.5	5.3769	4.7471	19.7027	29.8267
AAS18	18	29	31.04925054	14	14.02805611	57	57	0.102077307	3.2	1.6	31	8.5	4.1	16.8	8.8135	4.1362	16.8095	29.7592
AAS19	19	15	16.05995717	18	18.03607214	67	67	0.10109602 9	1.7	2.1	36.8	4.5	5.3	19.9	4.5472	5.3371	19.9694	29.8537
AAS20	20	32	34.26124197	5	5.01002004	63	63	0.102271262	3.5	0.6	34.2	9.4	1.5	18.5	9.4393	1.5328	18.5461	29.5182
AAS21	21	21	22.48394004	17	17.03406814	62	62	0.101518008	2.3	1.9	33.9	6.2	5	18.3	6.2124	5.0028	18.5078	29.723
AAS22	22	14	14.98929336	19	19.03807615	67	67	0.10102737	1.6	2.2	36.8	4.2	5.6	19.9	4.2159	5.612	19.914	29.7419
AAS23	23	25	26.76659529	12	12.0240481	63	63	0.101790643	2.8	1.4	34.4	7.4	3.5	18.6	7.4184	3.5216	18.6198	29.5598
AAS24	24	28	29.97858672	4	4.008016032	68	68	0.101986603	3.1	0.5	37	8.2	1.2	20	8.2095	1.2132	20.0134	29.4361
AAS25	25	23	24.62526767	15	15.03006012	62	62	0.101655328	2.5	1.7	33.9	6.8	4.4	18.3	6.8267	4.4225	18.3255	29.5747
AAS26	26	30	32.11991435	13	13.0260521	57	57	0.102145966	3.3	1.5	31	8.8	3.8	16.7	8.8167	3.8114	16.7182	29.3463
AAS27	27	32	34.26124197	8	8.016032064	60	60	0.102277274	3.5	0.9	32.6	9.4	2.3	17.6	9.4306	2.3151	17.6177	29.3634
AAS28	28	28	29.97858672	16	16.03206413	56	56	0.102010651	3.1	1.8	30.5	8.2	4.7	16.5	8.248	4.7106	16.572	29.5306
AAS29	29	24	25.69593148	9	9.018036072	67	67	0.101713968	2.6	1	36.6	7.1	2.7	19.8	7.1073	2.7281	19.814	29.6494
AAS30	30	33	35.33190578	14	14.02805611	53	53	0.102359962	3.6	1.6	28.7	9.7	4.1	15.5	9.8002	4.1136	15.5128	29.4266
AAS31	31	29	31.04925054	15	15.03006012	56	56	0.102079311	3.2	1.7	30.5	8.5	4.4	16.5	8.5905	4.4162	16.522	29.5287
AAS32	32	30	32.11991435	11	11.02204409	59	59	0.102141958	3.3	1.3	32.1	8.8	3.2	17.3	8.8768	3.2347	17.3387	29.4502
AAS33	33	23	24.62526767	12	12.0240481	65	65	0.101649316	2.5	1.4	35.5	6.8	3.5	19.2	6.813	3.506	19.2371	29.5561
AAS34	34	34	36.40256959	13	13.0260521	53	53	0.102428622	3.7	1.5	28.7	10	3.8	15.5	10.0435	3.8233	15.5216	29.3884
AAS35	35	16	17.13062099	18	18.03607214	66	66	0.101166693	1.8	2.1	36.2	4.7	5.3	19.6	4.722	5.3109	19.6599	29.6928
AAS36	36	30	32.11991435	7	7.014028056	63	63	0.102133942	3.3	0.8	34.2	8.8	2.1	18.5	8.824	2.1218	18.519	29.4648
AAS37	37	29	31.04925054	5	5.01002004	66	66	0.102059271	3.2	0.6	35.9	8.5	1.5	19.4	8.5226	1.5135	19.4008	29.4369
AAS38	38	25	26.76659529	14	14.02805611	61	61	0.101794651	2.8	1.6	33.3	7.4	4.1	18	7.408	4.1141	18.1937	29.7158
AAS39	39	14	14.98929336	20	20.04008016	66	66	0.101029374	1.6	2.3	36.3	4.2	5.9	19.6	4.276	5.916	19.6141	29.8061
AAS40	40	28	29.97858672	14	14.02805611	58	58	0.102006643	3.1	1.6	31.6	8.2	4.1	17.1	8.224	4.1284	18.5848	30.9372
AAS41	41	31	33.19057816	3	3.006012024	66	66	0.10219659	3.4	0.3	35.8	9.1	0.9	19.4	9.1486	0.9162	19.4141	29.4789
											Total	315.3	145.7	745.8	317.3918	146.5372	749.4664	

*Actual Amp mol/L	*Actual PZ mol/L	*Actual H2O mol/L	Actual AMP: wt%	Actual PZ: wt%	Actual H2O: wt%	AMP, mol/kg	PZ,mol/kg	Water, mol/kg	Density (g/cm³)	D. Temperature (°C)	pH	pH Temperature (°C)	Conductivity (mS/cm)	C. Temperature (°C)	Corrected Conductivity (mS/cm)*
3	1.5	32.8	26.9	12.9	60.2	3.21	1.5	32.8	0.99967	23	12.62	21.1	2.659	21.5	2.485
4.2	0.3	31.5	38.5	3.1	58.4	4.5	0.3	31.5	0.99764	23.01	12.9	21.4	1.293	21.3	1.204
3.9	0.8	31.5	35.3	6.9	57.9	4.18	0.8	31.5	0.99895	23.01	12.77	21.2	1.592	21.2	1.48
3.8	0.9	31.5	34.2	7.9	58	4.07	0.9	31.5	0.99911	23.01	12.89	21.45	2.039	20.6	1.874
3.7	0.7	33.1	33.2	6.2	60.7	3.96	0.7	33.1	0.99897	23.01	12.65	21.3	1.917	21.4	1.788
3.1	1.7	31.1	28	15.1	56.9	3.32	1.7	31.1	0.99865	23.01	13.09	21.45	1.568	20.6	1.441
3.2	1.5	31.8	29.1	12.8	58.1	3.43	1.5	31.8	0.99992	23.01	12.57	21.6	2.283	21.8	2.146
2.6	1.8	33.3	23.1	16	60.9	2.78	1.8	33.3	0.99987	23.02	12.43	21.55	3.234	21.4	3.017
2.9	1.1	35.3	26.1	9.2	64.6	3.1	1.1	35.3	0.99913	23.01	12.58	21.25	2.907	20.7	2.677
2.5	2.2	32.1	22.9	18.8	58.2	2.68	2.2	32.1	1.00019	23.01	12.59	21.5	3.139	20.65	2.888
2.2	1.7	35.6	20.1	14.9	65	2.36	1.7	35.6	0.99935	23.01	12.53	21.4	3.848	20.7	3.543
2.1	1.6	36.7	19	14	67	2.25	1.6	36.7	0.999	23	12.45	21.3	4.162	21	3.854
3	1.1	34.2	27	10	63	3.21	1.1	34.2	0.99934	23.01	12.64	21.55	2.702	20.65	2.486
1.9	1.5	39.2	16.7	13	70.3	2.03	1.5	39.2	0.99863	23	12.56	21.3	4.647	21.2	4.319
2.4	1.7	34.5	22	15	63	2.57	1.7	34.5	0.99804	23	12.61	21.35	3.464	21.15	3.216
3.3	0.9	33.8	30	7.9	62.1	3.53	0.9	33.8	0.99742	23	12.87	21.4	2.294	20.8	2.116
2	1.8	36.5	18	15.9	66.1	2.14	1.8	36.5	0.98738	23	12.57	21.5	4.194	20.8	3.869
3.3	1.6	31.1	29.6	13.9	56.5	3.53	1.6	31.1	0.99971	23	13.04	21.3	2.128	20.65	1.958
1.7	2.1	36.9	15.2	17.9	66.9	1.82	2.1	36.9	0.99923	23	12.53	21.25	4.631	20.7	4.264
3.5	0.6	34.3	32	5.2	62.8	3.75	0.6	34.3	0.99102	23	12.81	21.6	2.092	20.6	1.923
2.3	1.9	34.2	20.9	16.8	62.3	2.46	1.9	34.2	0.99964	22.99	12.71	21.55	3.707	20.5	3.401
1.6	2.2	36.8	14.2	18.9	67	1.71	2.2	36.8	0.99911	23.02	12.34	21.3	4.908	20.65	4.515
2.8	1.4	34.5	25.1	11.9	63	3	1.4	34.5	0.99946	23.01	12.46	21.25	3.008	20.9	2.78
3.1	0.5	37	27.9	4.1	68	3.32	0.5	37	0.99477	23.02	12.77	21.75	2.793	20.15	2.546
2.6	1.7	33.9	23.1	15	62	2.78	1.7	33.9	0.9966	23.02	12.44	21.35	3.2	20	2.909
3.3	1.5	30.9	30	13	57	3.53	1.5	30.9	0.99916	23.02	12.85	21.2	2.129	20.8	1.964
3.5	0.9	32.6	32.1	7.9	60	3.75	0.9	32.6	0.99707	23.02	12.92	21.2	2.026	21.2	1.883
3.1	1.8	30.7	27.9	16	56.1	3.32	1.8	30.7	0.99902	23.02	12.94	21.15	2.298	20.7	2.116
2.7	1.1	36.7	24	9.2	66.8	2.89	1.1	36.7	0.99894	23.02	12.67	21.35	3.365	20.8	3.104
3.7	1.6	28.7	33.3	14	52.7	3.96	1.6	28.7	0.9866	23.02	13.07	21.35	1.629	21.4	1.52
3.2	1.7	30.6	29.1	15	56	3.43	1.7	30.6	0.99739	23.02	12.99	21.25	2.225	20.8	2.053
3.3	1.3	32.1	30.1	11	58.9	3.53	1.3	32.1	0.99467	23.02	12.87	21.35	2.212	20.7	2.037
2.5	1.4	35.6	23.1	11.9	65.1	2.68	1.4	35.6	0.98626	23.02	12.64	21.3	3.402	20.4	3.115
3.8	1.5	28.7	34.2	13	52.8	4.07	1.5	28.7	0.98775	23.02	13.04	21.6	1.582	21.2	1.47
1.8	2.1	36.4	15.9	17.9	66.2	1.93	2.1	36.4	0.99921	23.02	12.76	21.22	4.597	21.44	4.291
3.3	0.8	34.3	29.9	7.2	62.9	3.53	0.8	34.3	0.99763	23.02	12.99	21.28	2.356	21.4	2.198
3.2	0.6	35.9	29	5.1	65.9	3.43	0.6	35.9	0.98152	23.01	12.93	21.4	2.566	20.52	2.355
2.8	1.6	33.7	24.9	13.8	61.2	3	1.6	33.7	0.99783	23	12.82	21.32	3.007	21.24	2.797
1.6	2.3	36.3	14.3	19.8	65.8	1.71	2.3	36.3	0.99936	23	13.01	21.28	4.717	20.54	4.331
3.1	1.6	34.4	26.6	13.3	60.1	3.32	1.6	34.4	0.99081	23	12.84	21.24	2.669	20.62	2.454
3.4	0.4	35.9	31	3.1	65.9	3.64	0.4	35.9	0.98696	23	12.69	21.36	2.336	21.5	2.183

CO2 Loading

	MW (g/mol)	Density (g/mL)
AMP	89.14	0.934
PZ	86.14	0.998

	MW (g/mol)	Density (g/mL)
H2O	18	0.934
AMP	89.14	0.998
PZ	86.14	1

							L. ratio	0.4	0.2	0.4	0.2	Unload	Unload							
Conc.	AMP	40.00%	15.00%	40.00%	15.00%	40.00%	15.00%	40.00%	15.00%	40.00%	15.00%	40.00%	15.00%							
	PZ	2.00%	12.00%	2.00%	12.00%	2.00%	12.00%	2.00%	12.00%	2.00%	12.00%	2.00%	12.00%							
Label	Sample No.	C1	C2	C3	C4	C5	C6	Actual C1 (g)	Actual C2 (g)	Actual C3 (g)	Actual C4 (g)	Actual C5 (g)	Actual C6 (g)	AMP, mol	PZ, mol	CO2, mol	AMP, mol/L	PZ, mol/L	CO2, mol/L	
AA 42	42	9	21	-	-	-	-	9.6	21.4					0.079	0.032	0.031	2.636	1.068	1.043	
AA 43	43	15	15	-	-	-	-	15.21	15.31					0.094	0.025	0.038	3.134	0.829	1.271	
AA 44	44	21	9	-	-	-	-	21.27	9.93					0.112	0.019	0.046	3.739	0.626	1.542	
AA 45	45	12	-	18	-	-	-	12.01		18.02				0.135	0.007	0.057	4.492	0.232	1.890	
AA 46	46	18	-	12	-	-	-	18.15		12.6				0.138	0.007	0.058	4.600	0.238	1.935	
AA 47	47	19.5	-	-	10.5	-	-	19.74			10.6			0.106	0.019	0.044	3.547	0.645	1.460	
AA 48	48	18	-	-	12	-	-	18.23			12.3			0.103	0.021	0.042	3.417	0.712	1.397	
AA 49	49	-	21	9	-	-	-		21.75	9.4				0.079	0.032	0.031	2.626	1.083	1.038	
AA 50	50	-	15	15	-	-	-		15.6	15.8				0.097	0.025	0.039	3.238	0.847	1.314	
AA 51	51	-	9	21	-	-	-		9.13	21.84				0.113	0.018	0.047	3.779	0.593	1.562	
AA 52	52	-	16.5	-	13.5	-	-		16.64		13.58			0.051	0.042	0.019	1.695	1.403	0.620	
AA 53	53	-	13.5	-	16.5	-	-		13.57		17.07			0.052	0.043	0.019	1.719	1.423	0.628	
AA 54	54	-	-	21	-	9	-			21.26		9.95		0.140	0.007	0.040	4.668	0.242	1.338	
AA 55	55	-	-	9	-	21	-			9.15		21.29		0.137	0.007	0.017	4.553	0.236	0.576	
AA 56	56	-	-	-	18	12	-				18.04	12.01		0.084	0.028	0.011	2.808	0.931	0.370	
AA 57	57	-	-	-	16.5	13.5	-				16.6	13.52		0.089	0.026	0.010	2.953	0.875	0.340	
AA 58	58	-	-	21	-	-	9			21.23			9.11	0.111	0.018	0.040	3.687	0.587	1.336	
AA 59	59	-	-	18	-	-	12			18.45			12.3	0.103	0.021	0.035	3.450	0.714	1.161	
AA 60	60	-	-	-	15	-	15				15.03		15.26	0.051	0.042	0.009	1.699	1.407	0.308	
AA 61	61	-	-	-	12	-	18				11.87		18.38	0.051	0.042	0.007	1.697	1.405	0.243	
	Total	112.5	120	144	114	55.5	54	114.21	123.33	147.75	115.09	56.77	55.05							
	Appr. total	130	135	160	130	70	70													

H2O	H2O	AMP	PZ	CO2	AMP	PZ	H2O	CO2	α	AMP	PZ	Water						
mol	g	w g	w g	w g	% w/w	% w/w	% w/w	% w/w	CO2 mol/(AMP+ PZ mol)	mol/kg	mol/kg	mol/kg	Density, g/cm3	D. temp (°C)	pH	pH temp.	Conductivity	Conductivity. temp	Corrected . Conductivity
1.331	23.95	7.05	2.76	1.376647101	20.06%	7.86%	68.16%	3.92%	0.28	2.82	1.07	44.35	1.10733	23.02	9.54	21.5	17.535	21.2	16.296
1.230	22.14	8.3805	2.1414	1.677792261	24.41%	6.24%	64.47%	4.89%	0.32	3.36	0.83	41	1.10708	23.02	9.95	21.45	15.225	20.8	14.045
1.178	21.20	9.9975	1.617	2.035533658	28.69%	4.64%	60.83%	5.84%	0.35	4	0.63	39.26	1.10603	23.01	10.07	21.6	16.65	21.25	15.488
1.001	18.02	12.012	0.6006	2.494389737	36.26%	1.81%	54.39%	7.53%	0.40	4.81	0.23	33.37	1.10678	23.02	9.91	21.35	15.36	20.7	14.144
1.025	18.45	12.3	0.615	2.554195285	36.26%	1.81%	54.39%	7.53%	0.40	4.92	0.24	34.17	1.09653	23.01	10.06	21.45	14.26	21.2	13.253
1.159	20.85	9.486	1.6668	1.926581946	27.95%	4.91%	61.46%	5.68%	0.35	3.8	0.65	38.62	1.10486	23.01	10.35	21.5	13.81	19.65	12.475
1.189	21.39	9.137	1.8406	1.844663689	26.70%	5.38%	62.52%	5.39%	0.34	3.66	0.71	39.62	1.10365	23.01	10.32	21.25	12.82	20.8	11.827
1.340	24.13	7.0225	2.798	1.369507996	19.88%	7.92%	68.32%	3.88%	0.28	2.81	1.08	44.68	1.10633	23.01	9.84	21.15	17.9	20.7	16.483
1.263	22.74	8.66	2.188	1.734649097	24.52%	6.19%	64.38%	4.91%	0.32	3.47	0.85	42.11	1.10787	23.02	10.22	21.1	15.655	20.3	14.31
1.159	20.86	10.1055	1.5324	2.061225893	29.24%	4.43%	60.37%	5.96%	0.36	4.05	0.59	38.64	1.10134	23.01	10.05	21.5	17.465	20.7	16.082
1.427	25.69	4.533	3.6264	0.817973202	13.08%	10.46%	74.10%	2.36%	0.20	1.81	1.41	47.57	1.10861	23.02	9.13	21.4	21.715	20.8	20.032
1.447	26.04	4.596	3.6768	0.829341459	13.08%	10.46%	74.10%	2.36%	0.20	1.84	1.43	48.23	1.10753	23.02	9.19	21.3	21.765	20.95	20.134
1.040	18.73	12.484	0.6242	1.765924935	37.15%	1.86%	55.73%	5.26%	0.27	5	0.24	34.68	1.05851	23.02	10.28	21.4	6.24	21.2	5.799
1.015	18.26	12.176	0.6088	0.760028841	38.28%	1.91%	57.42%	2.39%	0.12	4.87	0.24	33.82	1.07594	23.01	11.66	21	5.2	21.15	4.828
1.252	22.54	7.51	2.405	0.488293731	22.80%	7.30%	68.42%	1.48%	0.10	3.01	0.93	41.74	1.07428	23.01	11.08	21.3	11.06	20.55	10.156
1.235	22.22	7.898	2.2624	0.449316848	24.06%	6.89%	67.68%	1.37%	0.09	3.16	0.88	41.15	1.06393	23.02	11.18	21.2	9.77	20.8	9.013
1.138	20.48	9.8585	1.5178	1.763433038	29.32%	4.51%	60.92%	5.24%	0.31	3.95	0.59	37.93	1.02096	23.02	10.72	20.8	11.315	20.75	10.429
1.196	21.53	9.225	1.845	1.532517171	27.03%	5.41%	63.07%	4.49%	0.28	3.69	0.72	39.86	1.06819	23.02	11.11	20.9	10.46	20.7	9.632
1.430	25.75	4.5435	3.6348	0.406821218	13.23%	10.59%	74.99%	1.18%	0.10	1.82	1.41	47.68	1.05636	23.01	11.05	21.15	14.155	21.15	13.143
1.428	25.71	4.5375	3.63	0.321288614	13.27%	10.61%	75.18%	0.94%	0.08	1.82	1.41	47.62	1.04784	23.01	11.22	21.2	11.64	20.75	10.728